Faculdade de Engenharia da Universidade do Porto

Dynamic Analysis of a valve train system, used in a four stroke engine

João António dos Reis Nogueira

Working version

Dissertation of MIEM

Dissertation for a Master's Degree in Mechanical Engineering

Supervisor: Professor Doutor Jorge H. Seabra

Second Supervisor: Eng. César Ferreira

July 2014

Dynamic Analysis of a valve train system, used in a four stroke engine

João António dos Reis Nogueira

Dissertation for a Master's Degree in Mechanical Engineering

em09072@fe.up.pt

DEMec - Department of Mechanical Engineering

CETRIB - Section of Vibrations, Tribology and Industrial Maintenance

Faculdade de Engenharia da Universidade do Porto

Porto, Portugal

Abstract

The internal combustion engine (ICE) plays an important role in our society and much work is done into improving it's efficiency, power output and reliability. In the motorcycle world, two types of engine are being used: the two-stroke and the four-stroke engines. The latter requires the use of an auxiliary system to control the opening and closing of the valves - the valve train.

Traditionally, the valve train uses eccentric lobes to actuate rocker arms that open the intake and exhaust valves while the closing of the valves is done by the force of springs which are compressed during the opening of the valves.

The portuguese motorcycle manufacturer AJP Motos SA developed a new valve train - **InnerCam** - that promises the reliability and stability of more complex systems while retaining the smaller size and low gravity center of some simpler, yet less reliable, systems. Previously analysis work led to functioning prototypes that reveal the grand potential of the system. However, these tests also revealed an unidentified issue that caused a power loss in a small range of engine speeds. A new kinetic and dynamic analysis, as well as a vibration analysis on the system, are needed in order to identify the source of the power loss, mentioned above, that required to model the real mechanism into simpler systems that allow an easier approach and an expedite analysis without compromising the accuracy of the results.

This work revealed that the profiles for the valve displacement, velocity and acceleration are similar to the theoretical profiles required for the good engine operation, which helps to validate the InnerCam concept as a valid system with commercializing potential. The dynamic analysis performed also showed that the engine's acceleration isn't an influence to the system's dynamic balance, neither is the variable point of contact between the rollers and the cam path. However, this variation in the point of contact implies very sharp changes in rotational speed and direction, which may increase the rate of wear of these components' surfaces.

The vibration analysis was performed on the exhaust sub-system and it revealed that the resonance frequency of this system is well above the range of excitation frequencies that the system supports (from 2000 to 12000 rpm). This rules out resonance issues, such as the source of the power loss that was previously described.

Resumo

O motor de combustão interna (ICE) desempenha um papel importante na nossa sociedade e bastante trabalho tem sido feito para melhorar a sua eficiência, potência e durabilidade. No mundo do motociclismo, são utilizados dois tipos de motor: motores a dois tempos e motores a quatro tempos. Este último requer o uso de um sistema auxiliar para controlar a abertura e fecho das válvulas - o trem de válvulas. Tradicionalmente, o trem de válvula usa lóbulos excêntricos para acionar os braços que abrem as válvulas de admissão e de escape, enquanto o fecho das válvulas é feito pela força das molas que são comprimidas durante a abertura das válvulas.

O fabricante de motos português AJP Motos SA desenvolveu um novo trem de válvulas - **InnerCam** - que promete a durabilidade e estabilidade dos sistemas mais complexos, mantendo as pequenas dimensões e baixo centro de gravidade de alguns sistemas mais simples, mas menos fiáveis. O trabalho de análise anterior levou a protótipos que revelam o grande potencial do sistema em funcionamento. No entanto, estes testes também revelaram uma perda de potência anormal numa pequena gama de velocidades do motor. Uma nova análise cinemática e dinâmica, bem como a análise de vibrações sobre o sistema, foi necessária, no sentido de tentar explicar a perda de potência. Isto exigiu modelar o sistema em sistemas mais simples, que permitiram uma aproximação mais fácil e uma análise expedita sem comprometer a precisão dos resultados.

Este trabalho revelou que os perfis de deslocamento, velocidade e aceleração são semelhantes aos perfis teóricos necessários para o bom funcionamento do motor, o que ajuda a validar o conceito InnerCam como um sistema pertinente com potencial de comercialização. A análise dinâmica também mostrou que a aceleração do motor não influencia o equilíbrio dinâmico do sistema, nem o ponto de contato variável entre os pinos rolantes e a came. No entanto, esta variação no ponto de contacto implica mudanças muito agressivas na velocidade de rotação e sentido de rotação, que podem acelerar o desgaste das superfícies destes componentes.

A análise de vibrações foi realizada para o sub-sistema de escape e revelou que a frequência de ressonância deste sistema está situada bem acima da gama de frequências de excitação que o sistema tem de suportar (2000-12000 rpm). Isto elimina os problemas de ressonância, como a fonte de perda de energia descrita anteriormente.

Acknowledgements

I would like to acknowledge and express my sincere gratitude to some people without whom I wouldn't be able to present this thesis or even finish the master's degree.

First of all, I thank my parents, Antero e Isabel, for all the trust and continued support. I stand where I am thanks to them.

Secondly, I'd like to acknowledge my entire family, specially my uncle António, as well as Frederica Oliveira, for all the help and support for this thesis.

Thirdly, I'd like to express my greatest gratitude to the Prof. Jorge Seabra, Prof. José Dias Rodrigues and Eng. César Ferreira, that provided me the tools, guidance and patience for this thesis to be done. For this, I also thank all the staff at CETRIB who warmly welcomed as one of them.

Fourthly, I'd like to acknowledge and thank Pedro Noronha, Carlos Vieira, Diogo Moura, Mário Oliveira,Pedro Soares, Eduardo Moreira, João Mata, Salvador Costa, Ana Ribeiro, Ana Oliveira, Susana Costa, Raquel Camacho, Samuel Pinho, Daniel Laranjinha, Luísa Vieira, Hugo Carvalho, Daniel Freitas, Guaicaipuro Neves, Ricardo Martins, Marta Rolo, Leonor Madureira, Carlos Oliveira, Joana Coutinho, Marta Conceição, Inês Mesquita, Luísa Louro and all my friends who accompanied me to this day. You may never know how much you've helped me get here, but nevertheless, thank you.

Finally, I would like to thank AJP Motos SA for their collaboration and assistance for this thesis, as well as Faculdade de Engenharia da Universidade do Porto and all their staff for their contribution to this work.

João Nogueira

"Opportunity is missed by most people because it is dressed in overalls and looks like work."

Thomas A. Edison

Contents

List of Figures

Nomenclature

Symbol	Units	Description
a	m	Distance between points A and C
a'	m	Distance between points A' and C'
a_i^j	m/s^2	Acceleration of point i in the j direction
A	–	Exhaust rocker arm hole center point
A	–	Intake rocker arm hole center point
$\overline{AC}$	m	Displacement vector between points A and C
$\overline{A'C'}$	m	Displacement vector between points A' and C'
b	m	Distance between A and B
b'	m	Distance between A' and B'
B	–	Exhaust rocker arm-to-valve contact point
B'	–	Intake rocker arm-to-valve contact point
BDC	–	Bottom dead center
C	–	Exhaust roller center point
C'	–	Intake roller center point
DOHC	–	Double Overhead Camshaft layout
DOHV	–	Double Overhead Camshaft layout
F_i	N	Force applied
G_2	–	Exhaust rocker arm center of gravity position
G_2'	–	Intake rocker arm center of gravity position
G_3	–	Exhaust valve center of mass position
G_3'	–	Intake valve center of mass position
I	–	Exhaust point of contact between the roller and the cam path
I'	–	Intake point of contact between the roller and the cam path
I_{zz}, J	kg/mm^2	Moment of inertia according to the z rotational direction
k	N/m	Component's rigidity
K_i^j	N	Dynamic component of body i in the direction j
m	kg	Component's mass
M_i	$N \bullet m$	Component's torque (or rotational momentum) - for component i
O	–	Camshaft's center of mass position
OHV	–	Overhead Valve layout
OHC	–	Overhead Camshaft layout
PAO	–	Polyalphaolefin base oil
$\dot{Q}_i$	$kg \bullet m/s^2$	Quantity of acceleration for body i

Symbol	Units	Description
r	m	Distance between the points O and C
r'	m	Distance between the points O and C'
R_i^j	N	Reaction force applied in point i in the j direction
$\dot{r}$, $\dot{r'}$	m/s	First derivative of the function r and r', respectively
$\ddot{r}$, $\ddot{r'}$	m/s^2	Second derivative of the function r and r', respectively
SOHC	$-$	Single Overhead Camshaft layout
SOHV	$-$	Single Overhead Valve layout
T	s	Period of vibratory response
TDC	$-$	Top dead center
v_i^j	m/s	Velocity in point i in the j direction
α	rad	Angle between $\overrightarrow{OC}$ and the XX axis
α'	rad	Angle between $\overrightarrow{OC'}$ and the XX axis
$\dot{\alpha}$, $\dot{\alpha'}$	rad/s	First derivative of the function α and α', respectively
$\ddot{\alpha}$, $\ddot{\alpha'}$	rad/s^2	Second derivative of the function α and α', respectively
β	rad	Angle between $\overrightarrow{AB}$ and the XX axis
β'	rad	Angle between $\overrightarrow{A'B'}$ and the XX axis
β_0	rad	Angle between $\overrightarrow{AB}$ and the XX axis for the non-actuated cycle part
β_1	rad	Angle between $\overrightarrow{AC}$ and the YY axis for the non-actuated cycle part
β_0'	rad	Angle between $\overrightarrow{A'B'}$ and the XX axis for the non-actuated cycle part
β_1'	rad	Angle between $\overrightarrow{A'C'}$ and the YY axis for the non-actuated cycle part
$\dot{\beta}$, $\dot{\beta'}$	rad/s	First derivative of the function β and β', respectively
$\ddot{\beta}$, $\ddot{\beta'}$	rad/s^2	Second derivative of the function β and β', respectively
δ	m	Displacement from flexing
Δ	m	Valve lift (displacement)
$\dot{\Delta}$	m/s	First derivative of the function for valve lift displacement
$\ddot{\Delta}$	m/s^2	Second derivative of the function for valve lift displacement
γ	rad	Angle between $\overrightarrow{CI}$ and $\overrightarrow{OC}$
γ'	rad	Angle between $\overrightarrow{C'I'}$ and $\overrightarrow{OC'}$
$\dot{\gamma}$, $\dot{\gamma'}$	rad/s	First derivative of the function γ and γ', respectively
$\ddot{\gamma}$, $\ddot{\gamma'}$	rad/s^2	Second derivative of the function γ and γ', respectively
ω	rad/s	Rotational speed
ω_n	rad/s	Natural frequency of free vibratory response
Ω	rad/s^2	Rotational acceleration

Chapter 1

Introduction

On 2013, a new valve train system, the InnerCam, was proposed by AJP Motos SA and was analysed (both dynamically and tribologically) by former student and now engineer, César Ferreira.

This work and development was motivated by the need to implement a valve control system that should be more compact and very reliable at high engine speeds.

Using the data collected from this analysis, AJP Motos SA was able to solve a great set of problems presented by early systems, resulting in a working set of prototypes.

A dynamic analysis on this system was previously done, with a larger focus on the lubrication between surfaces and contact mechanics between components, resulting in few constructive changes that helped to reduce the wear between critical surfaces and improve the life cycle of the components.

The major constructive changes applied to the InnerCam consisted on thermal surface treatments, such as nitriding, applied to key components and the inclusion of upgraded lubrications circuits, which allowed to remove debris, improve the contact between bodies and significantly reduce wear in the system, improving the overall system life cycle.

This work led to working prototypes that revealed the potential to reduce fuel consumption and improve the power output of engines fitted with the InnerCam.

Although the newer prototypes are already reliable enough to be assembled in test motorcycles, a few problems were diagnosed during these tests. There seems to be an issue with the engine that is causing an unusual power loss in the engine. This power loss only happens between the 8000 and 10000 rpm (see appendix A). Since the only new factor in play is the new valve train system, an improved analysis was required to explain this power loss.

The goal of this dissertation is an improved and more precise dynamic analysis of the Innercam mechanism, resulting in kinematic and dynamic models for this valve train, in particular, and a vibration analysis of the system, as well. With this analysis, a better understanding of the theoretical behaviour of this system is expected, serving as a benchmark against experimental measures that may be done in the future.

The main contribution of this work will be a solid theoretical basis for the required dynamic behaviour of the InnerCam, helping to adjust the system real operation in order to improve the performance of the engine and, consequently, the entire motorcycle.

1.1 Dissertation Outline

On chapter 2, several types of valve train, as well as the functions of these parts in the operation of a four stroke engine, are presented.

On chapter 3, the InnerCam system is presented in detail.

On chapter 4, the mechanical analysis is presented. It consists on a kinematic and dynamic description (modelling) of the system as well as an analysis on the model results.

On chapter 5, a vibration analysis of the system is presented, continuing the analysis on chapter 4.

On chapter 6, the final one, the conclusions of this work are presented as well as suggestions for future work.

Chapter 2

The engine for the PR5

Before starting a detailed analysis of the valve train proposed by AJP Motos SA, it's important to overview the system where the valve train will be applied. The engine used for these motorcycles is a 4-stroke mono-cylinder gasoline engine with 4 valves with liquid cooling, manufactured by Zongshen, and employs a single over-head camshaft for the valve train system. This engine is the result of a joint venture between Zongshen and an European company. [1]

The main goal of AJP Motos SA is to replace this valve train system with the InnerCam system, resulting in a more powerful, compact and reliable engine, especially at higher speeds and accelerations.

The traditional spark-ignited 4-stroke engine is based on 4 phases that correspond to the filling and emptying of the cylinder. These phases have the following denomination:

- Intake stroke;
- Compression stroke;
- Power stroke;
- Exhaust stroke;

In the intake stroke, the intake poppet valve is opened (through the action of the valve train) allowing a mixture of air and fuel to enter the chamber. As soon as the piston reaches its bottom dead center(BDC), the intake poppet valve is closed and the compression stroke is initiated. Since the piston is fitted with sealing rings, there's no loss on matter between the bottom dead center and the top dead center (TDC), allowing to properly compress the air-fuel mixture. [2] [3]

As soon as the piston reaches its top dead center, the spark-plug ignites the air-fuel mixture, initiating the power stroke. In this stroke, the pressure and temperatures in the chamber reach very high values (tens of thousands of atmospheres of pressure and thousands of degrees Celsius). The energy generated from the explosion of the air-fuel mixture, allied to the big pressure differential, propels the piston and, consequently, the crankshaft, allowing to propel the rest of the pistons through their own intake and compression stroke, for example. [2][3]

As soon as the piston reaches its bottom dead center, the exhaust stroke is initiated and the exhaust poppet valves are opened, allowing the post-combustion gases to be expelled from the cylinder, clearing the cylinder for the new combustion cycle. For every combustion cycle, or 4-stroke cycle, it corresponds to 2 piston cycles. [3] [4]

These 4 strokes are further described in the figure 2.1.

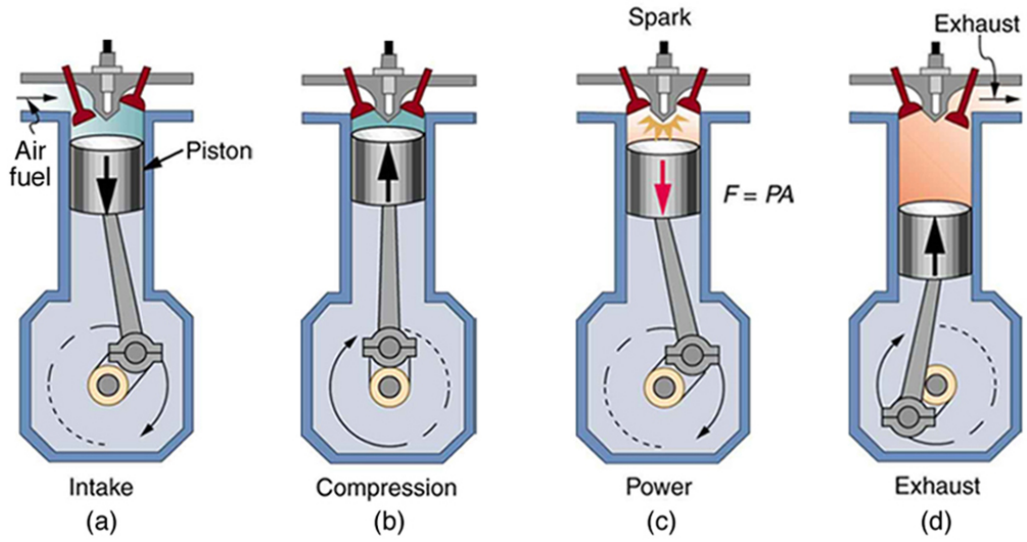

Figure 2.1: 4 stroke engine diagram, with separated strokes [5]

On a 4-stroke engine, a valve train is required in order to control the opening and closing of the valves, unlike the 2-stroke engines, in which the valves are controlled and actuated directly by the crankshaft. For an engine to work properly while maintaining low emissions, high power output and a low level of noise, it's imperative that every component of the engine works together with the rest of the system flawlessly. [2] [6] [7]

The opening and closing of the valves must be very precise and should directly depend on the 4 stroke cycle on the engine. On the next figure, an example of the valve lift defined for a 4 stroke cycle in an engine is presented (figure 2.2).

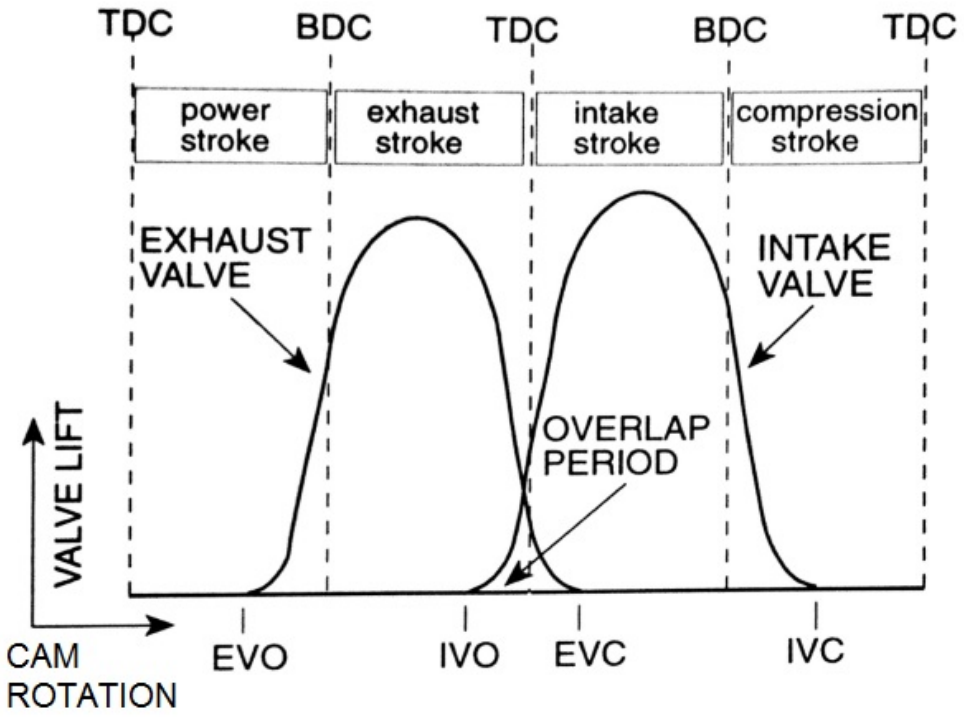

Figure 2.2: 4 stroke engine diagram, with separated strokes[2]

The capital relevance of the valve train system becomes obvious, since it allows to properly control the admission an exhaust on the engine and prevent any collisions between the pistons and the valves, preventing the engine's malfunction. In fact, the more developed the valve train is, the more efficient is the engine [2] [6].

2.1 Technical information about the engine

As previously presented, the engine fitted in the PR5 model - ZS177MM - is manufactured by the Chinese company Zongshen and was developed in collaboration with an European company [1].

According to the manufacturer, this engine, without any tune up from AJP Motos SA, develops 19 kW (aprox. 25,85 BHP) of power (at 9000 rpm). AJP Motos SA then modifies this engine, introducing an electronic fuel-injection system and a high performance exhaust pipe. With these tune ups, the engine can now develops 20,2 kW (aprox. 27,08 BHP) of power (at 8000 rpm), a respectable increase in power.

In terms of lubrication, the engine has 2 oil pumps, one for the gearbox lubrication and another for the rest of the system. It uses a polyalphaolefin (PAO) oil - ENI I-RIDE 20W50 supplied by ENI, as part of a partnership between AJP Motos SA and a Portuguese agent of ENI. Further technical specifications of the engine can be found in figure 2.3.

2.2 Valve Trains

Internal combustion engines require a cyclic supply of fresh air, as well as the removal of post-combustion gases. As seen above, the 4-stroke engines require the use of valve trains.

The valve train is required to:

1. Perform the opening and closing of the valves rapidly;
2. Clear the largest opening diameter;
3. Have a streamlined design in order to reduce pressure losses;
4. Ensure an effective sealing when the valves are closed;
5. Ensure good durability.

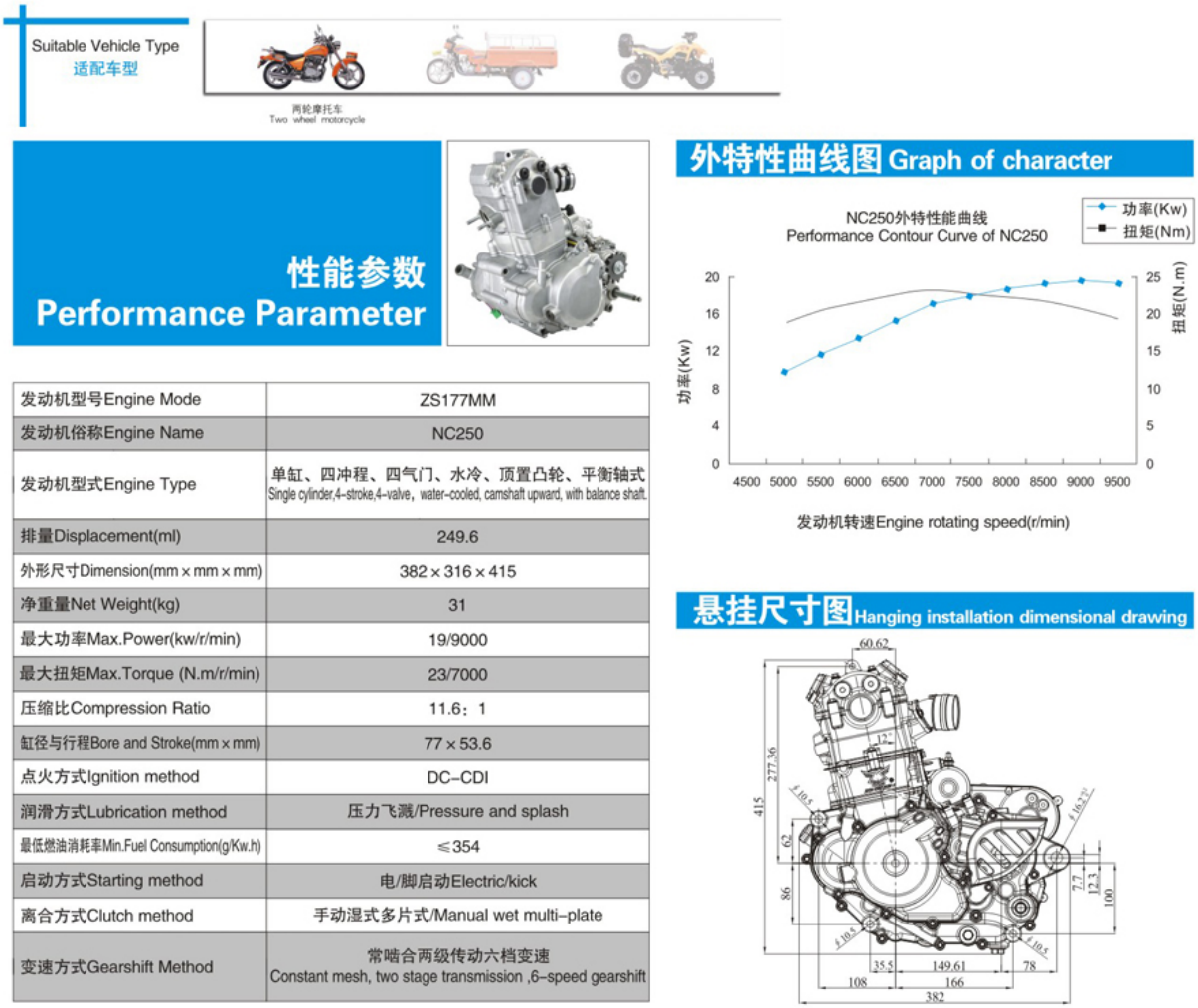

发动机型号Engine Mode	ZS177MM
发动机俗称Engine Name	NC250
发动机型式Engine Type	单缸、四冲程、四气门、水冷、顶置凸轮、平衡轴式 Single cylinder,4-stroke,4-valve，water-cooled, camshaft upward, with balance shaft.
排量Displacement(ml)	249.6
外形尺寸Dimension(mm × mm × mm)	382 × 316 × 415
净重量Net Weight(kg)	31
最大功率Max.Power(kw/r/min)	19/9000
最大扭矩Max.Torque (N.m/r/min)	23/7000
压缩比Compression Ratio	11.6：1
缸径与行程Bore and Stroke(mm × mm)	77 × 53.6
点火方式Ignition method	DC-CDI
润滑方式Lubrication method	压力飞溅/Pressure and splash
最低燃油消耗率Min.Fuel Consumption(g/Kw.h)	≤354
启动方式Starting method	电/脚启动Electric/kick
离合方式Clutch method	手动湿式多片式/Manual wet multi-plate
变速方式Gearshift Method	常啮合两级传动六档变速 Constant mesh, two stage transmission ,6-speed gearshift

Figure 2.3: Technical information of the standard engine [8]

The valve train is composed by the joint operation of poppet valves, their actuating parts (rocker arms, lobes, push rods, etc.), and the camshaft driven by the crankshaft's gear wheel (through a drive belt).

The design of a valve train will depend on:

1. The arrangement of the valves in the cylinder block (overhead valves or side valves, for example);

2. The geometry of the combustion chamber;

3. The arrangement of the valves and camshaft together;

4. The design of the camshaft and the rocker (one- or two-arm levers or lobe rockers, for example);
5. The number and type of springs;
6. The type of drive applied in the camshaft.

Only valve trains that can ensure a good gas exchange in the engine, both at low and high speeds, are currently used in the most modern engines. It's vital to maintain the optimal flow of matter (air and fuel mixture) in the engine, preferably in the entire range of speeds and accelerations of the engine. [6] [7] [2]

In order to make the valve train more rigid, it's advisable to position the camshaft the closest possible to the valves. This way, it's possible to reduce the flexing and compressing of the valve train components, reducing the vibrations in the system and the noise generated in the operation, and reduce the possibility of the tappets to jump of the cam as well [6].

Thus, valve trains with shorter push rods tend to have better behaviour at higher engine speeds - this is usually associated with overhead cam systems. [6]

It's also recommended to use highly rigid springs, in order to counter the effects of the larger forces of inertia at higher speeds of the engine and to prevent harmful phenomenons like "valve float" or "valve bounce". The "valve float" phenomenon happens when the closing of the valves is not synchronized. The "valve bounce" consists on the unintended movement of the valves thanks to their inertia combined with the resonance of the springs.

Any one of these phenomenons can impair the performance of the engine and even lead to serious damage of the valves (in case they slam of the piston, for example)[6].

2.2.1 State of the art

As it was previously presented, the valve train plays a vital role in the operation of a 4-stroke engine. It's this system that properly opens or closes de intake

and exhaust valves, allowing a proper mass flow control of fuel and air inside the combustion chamber. It's not surprising, then, to see many valve trains systems. There's a constant interest in the development of new valve trains that can boost the power output while reducing the noise and gas emissions of the engine, achieving that goal in the most compact way in order to further improve manoeuvrability and reduce weight.

There are many designs for the valve train and usually they're distinguished by the number of valves drives and the number and position of the camshafts.

2.2.1.1 Overhead Valves (OHV)

This is, probably, the most common type of 4-stroke engine produced. There are various options on the number of valves for each cylinder but the most common is the two valve system, one for intake and one for exhaust. This denomination derives from the fact that the valves are located above the combustion chamber. The actuation of the valves can be accomplished by the use of a single cam - Single Overhead Valves (SOHV) - or by the use of two cams - Double Overhead Valves (DOHV).

In figure 2.4, a SOHV valve train is displayed. It's possible to see that the actuation of the valves is done by the rocker arms that are, in their turn, actuated by the cams located in the single camshaft, next to the combustion cylinder.

2.2.1.2 Overhead Cam (OHC)

In this valve train design, the camshaft actuating the valves are located above the combustion chamber, just like the valves. If there's only one camshaft actuating both intake and exhaust valves, the system is called Single Overhead Cam (SOHC). If the system employs two camshafts, one for the intake valves and one for the exhaust valves, it's called Double Overhead Cam (DOHC). An example of this layout is presented of figure 2.5.

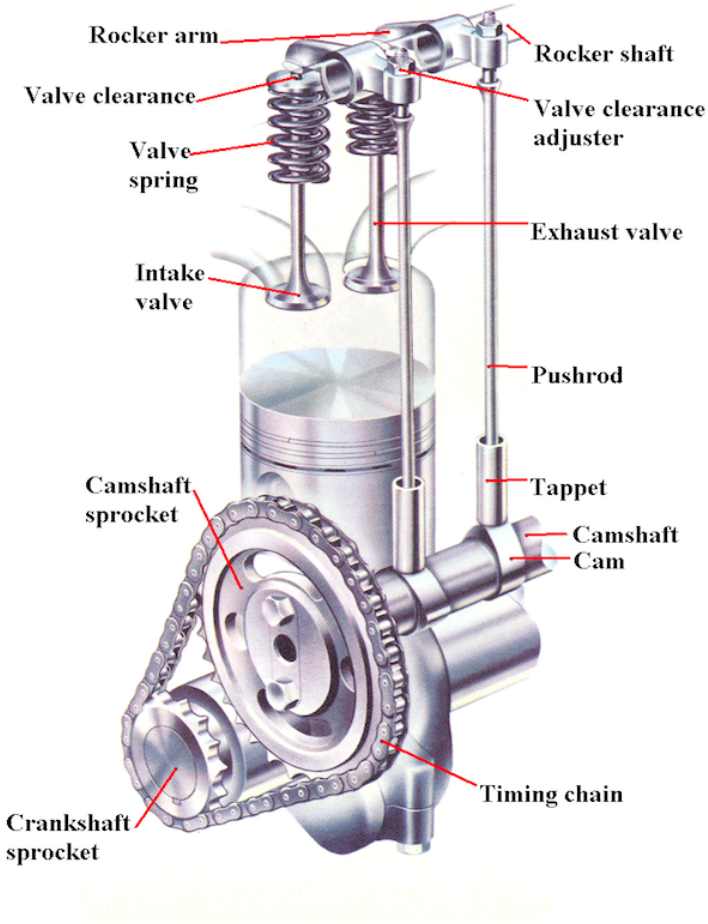

Figure 2.4: Example of a Single Overhead Valve system [9]

One good example of the SOHC system is the Honda Unicam (see figure 2.6). Developed by the japanese manufacturer Honda, this system relies on a single overhead cam for the actuation of both the intake and exhaust valves. This system has been applied to their dirt motorcycle line. [10]

In this system, the camshaft directly actuates the admission valves and the two exhaust valves are operated through low-friction roller rocker arms. A roller bearing on the rocker arms reduces the friction and wear, which allows for the cam lobes to be narrower, smaller and lighter than conventional rocker arms, contributing for a lighter engine.

This results in a much more compact, lighter, ideal for off-road bikes, in which the weight of the engine is an important fact to take into consideration since it directly affects the handling of the motorcycle. This system also improves the

breathing and the flow on the engines, resulting in great power output.

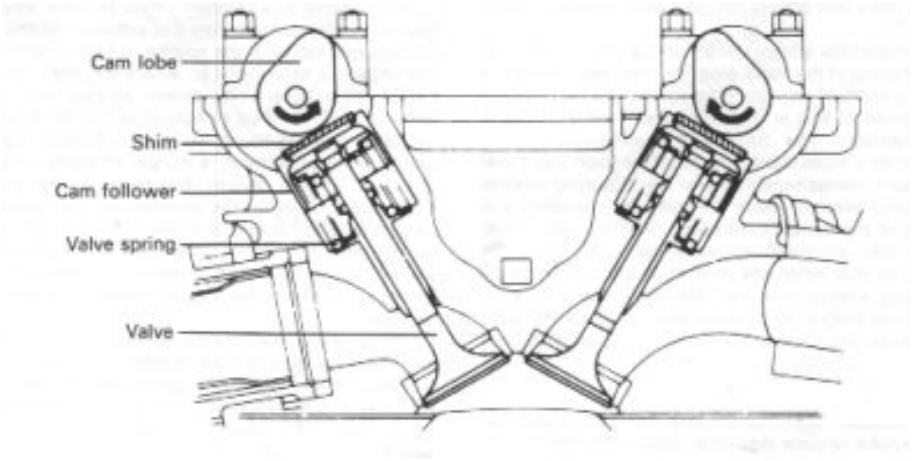

Figure 2.5: An example of a Double Overhead Cam valve train [11]

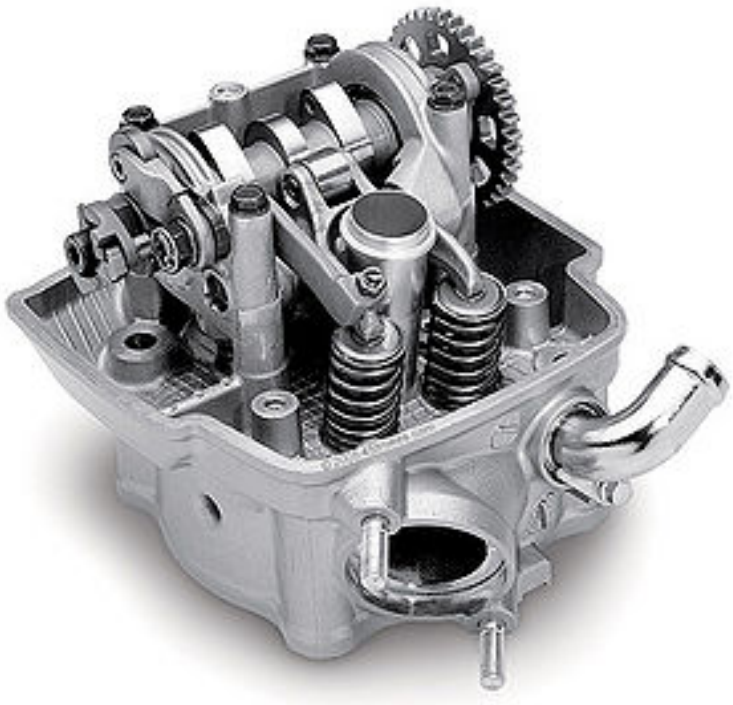

Figure 2.6: Honda Unicam engine. It's possible to see that only one camshaft, with two cam lobes, is used. [12]

2.2.1.3 Two Valve Side Engine

The two valve side engine, or flathead engine, is a valve train design that was used in the 1940's and 1950's and it was quite popular among the engine producers,

through the simplicity of the system. This valve train consists on placing both the admission and exhaust valves on the side of the combustion chamber, parallel to the chamber. Due to geometric limitations of this design, it wasn't possible to fit more than one intake valve and one exhaust valve. It's also visible in figure 2.7 that the bore in which all the air flow must pass to enter the chamber is small, limiting the breathing capabilities of the engine. This engine also suffered from low compression rates. All these design problems resulted in an engine with a low power output [2].

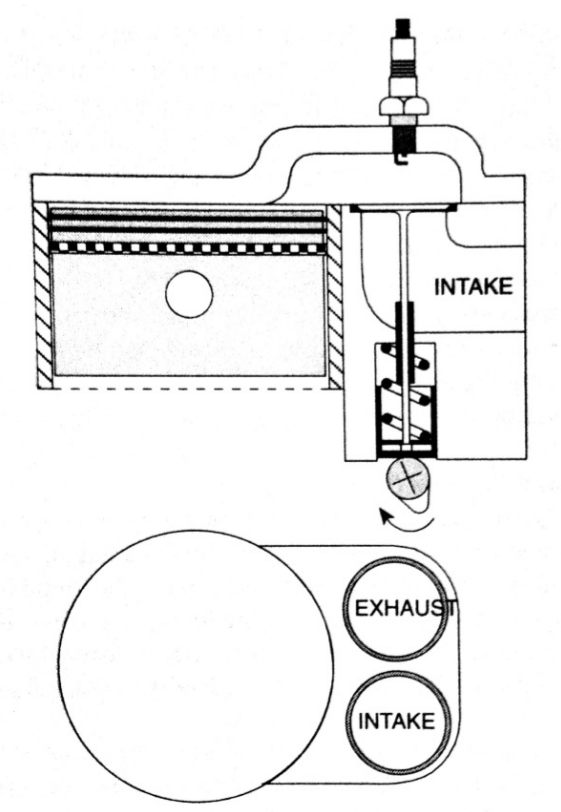

Figure 2.7: Two valve side engine example [2]

This type of engines had some advantages, such as the simplicity of the engines (which made it very easy to produce), their cheapness and compactness. It was also insensitive to lower-octane fuel, making it versatile, and had a good response at lower rotational speeds.

This type of engine was frequently applied in some cars - like the Ford Model T - and in motorcycles, especially in the 1950's Harley-Davidsons'. These bikes

became famous for the low-rev engines with good torque output, enabled by this engine design.

2.2.1.4 Four-Valve Pent-Roof Cylinder Head

This is currently the most used valve train and was first introduced in racing vehicles. Afterwards, the japanese motor industry started applying this design to their consumer vehicles [2].

This design sets itself apart by placing the valves in the side of a wedge (the pent-roof name comes from this characteristic), allowing for bigger valves and larger valve areas and, consequently, better breathing conditions of the engine. Additionally, there's a possibility to fit the spark plug on the center of the combustion chamber, allowing for equal flame paths from the spark plug to the sides of the chamber, resulting in a balanced explosion and application of the pressure resulting from the explosion [2] [7].

This design can be applied together an overhead valve system or an overhead cam system. Usually, the DOHC layout is used [2]. An example of this system (with the inclusion of a DOHC layout) is presented in the fig. 2.8.

2.2.1.5 Desmodromic Systems

A desmodromic valve is a reciprocating engine valve that is positively opened and closed by a cam and leverage system, rather than being closed only by a more conventional spring.

An engine using typical desmodromic valves has two cams and two actuators, each for positive opening and closing without a return spring. Although the closing of the valves is actuated by a cam, springs can still be applied in the system in order to hold the valves in their place during the closed time.

The desmodromic valves can take many mechanical forms, usually depending on the manufacturer.

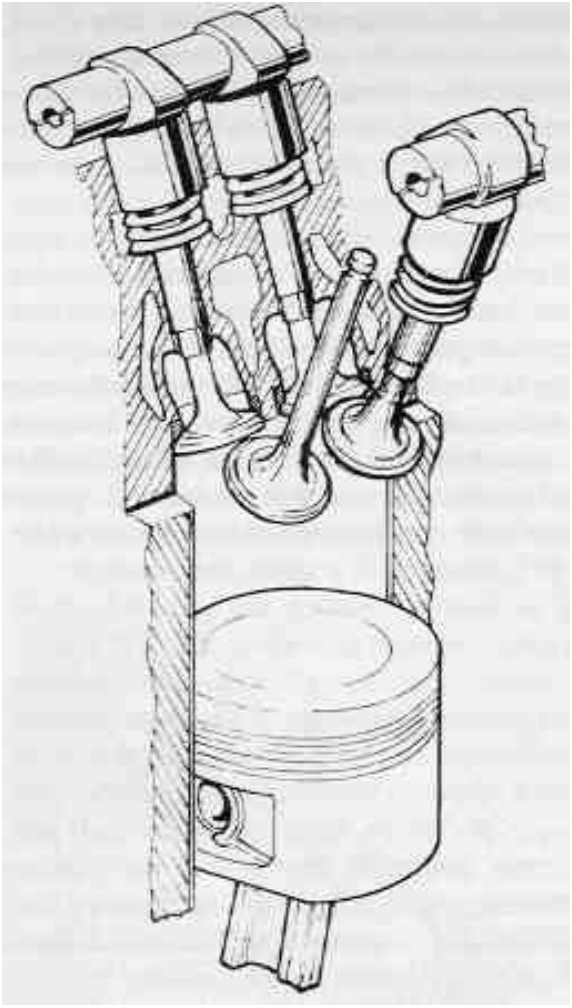

Figure 2.8: Example of a Four-Valve Pent-Roof Cylinder Head. [13]

This mechanism was inspired by the necessity to have a valve train that could work properly at high rotations, since the common valve spring system usually doesn't work properly at high speeds. In fact, when desmodromic systems were first applied, it was commom for the typical spring-valve engines to fail after some time because the springs broke due to the wear and fatigue.

At very high rotational speeds, it is required the use of very rigid and strong springs to avoid valve float. The use of such rigid springs leads to other problems. At high speeds, the acceleration of the valve train components can be very high, resulting in great inertia forces during the actuation of the poppet valves. This will eventually result in fatigue on the cam follower and add lubrication issues in the cam, increasing the friction losses in the valve train.

The desmodromic systems tries to solve these issues by decreasing the dependence on the spring-valve mechanism since the opening and closing of the valves is done by camshafts.

Thanks to this change, the cam is only required to supply the force to accelerate the valve train components, vastly reducing the friction at lower speeds. Valve float is also greatly reduced.

Although this concept dates back to the beginning of the internal combustion engine, the first use of the desmodromic valve was on a 1914 Delage. After that, the system was implemented on a 1922 Rolland-Pilain and on 1954 and 1991 Mercedes-Benz's.

Also, the Italian motorcycle manufacturer Ducati has been using desmodromic valve trains since 1955, becoming the trademark of their engines (see fig. 2.9).

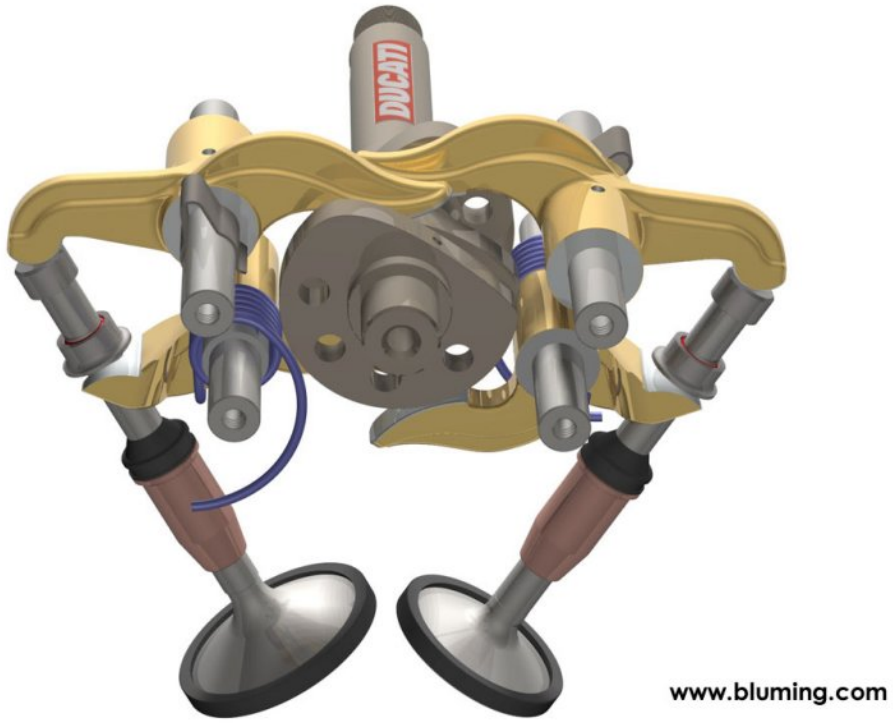

Figure 2.9: Desmodromic valve train used in Ducati motorcycles [14]

This system has, of course, their disadvantages. First of all, most of the issues detected in the more common sprung-valve trains can currently be solved with

some adjustments. This adjustments rendered technologies like valve adjustment, hydraulic tappets, push rods and valve float adjustment, obsolete.

Secondly, since this system depends on the use of one camshaft for the opening of the valves and another camshaft for the closing, as well as two rocker arms, this leads to a heavy system, adding inertia forces to the delicate dynamic equilibrium that is required.

Thirdly, this is a more expensive and complex system than the traditional spring-valves set.

This technology was often abandoned and recovered years after, each time proving his added value to the engine technology.

2.2.1.6 Alternative Systems

It is also important to refer some of the lesser known valve train designs. Some of them influenced the development of the most common ones, already addressed above, but there are also new solutions for the valve train result from the continuous effort to improve the engine and his inner mechanisms.

- **Sleeve Valves Engines**

  One of these alternative systems is the sleeve valves system.

  In this system, the pistons run in an inner sleeve that runs on an outer sleeve which, itself, runs in the cylinder bore.

  Each sleeve has intake and exhaust bores. When the inner and outer sleeves align the bores, the air flow can move to or from the cylinder, corresponding to the intake and the exhaust, respectively (see figure 2.10).

  For the sleeves to properly slide on one another, they must be flooded with lubricating oil. Since the sealing between the the oil of the sleeves and the intake/exhaust bores is very difficult to achieve, there was usually some contamination of the mass flow in the cylinder, resulting in exhaust gases

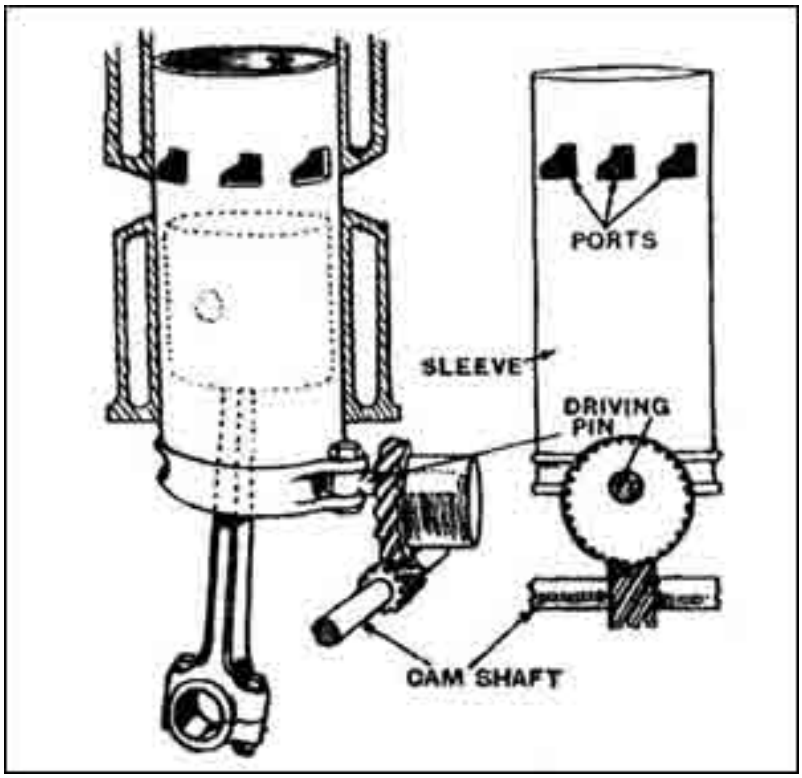

Figure 2.10: Example of a sleeve valve system [15]

with oil (followed by a blue smoke coming from the exhaust pipes of the engine) [7].

The system was very quiet and trouble-free, but the oil leakage and subsequent dark exhaust gases, allied with the development of the spring-valve systems (better sound isolation using damping valve covers, for example), made the sleeve valve system obsolete [7].

- **Camless Valve Engines**

  On the past few years, some manufacturers have been investigating the possibility of building engines without camshafts for the actuations, or even push rods, rocker arms and all the components of the typical valve train.

  The main advantages of these systems is their ability to infinitely control the valve timing, allowing an optimal volumetric efficiency through out the range of speeds in the engine. It also grants bigger power outputs, lower emissions and noise, and bigger fuel economy.

The different types of camless valve actuating systems that are being developed can be classified in two groups: electrohydraulic and electromechanical.

When it comes to electromechanical valve trains, there are several designs that are being trialled. Most developers are using the conventional poppet valve system but an alternative is a ball valve set up. Both use electromagnets in one way or another to open and close the valve.

The electromechanical poppet valve system uses an armature attached to the valve rod.The outside casing contains a magnetic coil that can be used to either attract or repel the armature and, therefore, opening or closing the valve.

Most early systems employed solenoid and magnetic attraction/repulsion actuating principals, using an iron or ferromagnetic armature. These types of armatures limited the performance of the actuator because they resulted in a variable air gap, causing variations on the magnetic force. In order to maintain high forces on the armature as the lift of the valves increases, a higher current is employed in the coils of such devices. This increased current leads to higher energy losses in the system and a non-linear behaviour that makes it difficult to obtain adequate performance. The result of this is that most of such designs have high seating velocities (the initial opening and the end of the closing of valves is very fast and creates an impact between the surfaces) and the system cannot vary the amount of valve lift.

The electromechanical valve actuators of the latest poppet valve design eliminate the iron or ferromagnetic armature by replacing it with a current-carrying armature coil. Combining the effects of a generated magnetic field along with the direction of the current passing through the armature coil, it allows to fully control the opening and closing of the valves, eliminating the variation of magnetic force as function of the lift (the main problem with the original eletromechanical valve actuators) [16] [17].

The ability of the electromechanical valve actuator to generate force in either direction and to vary the amount of force applied to the armature in either

direction is an important advantage of this design. It allows, for example, to vary the speed of opening and closing valves, granting a greater control over the behaviour of the engine through out its various speeds. This method can also be used to slow the valve in order to reduce the seating velocity, thereby reducing wear as well as the resulting noise [16] [17].

Originally created for the Apollo space program, the electrohydraulic valve actuator works by sending pressurised hydraulic fluid to the engine valve to move it open or closed [16].

In general terms, the latest designs of electrohydraulic valves are based on poppet valves that are moveable between a first and a second position. It uses a source of pressurised hydraulic fluid and a hydraulic actuator coupled to the poppet valve. The motion between a first and second position is the response to the flow of the pressurised hydraulic fluid. An electrically operated hydraulic valve controls the flow of the pressurised hydraulic fluid to the hydraulic actuator. The use of engine oil as the hydraulic fluid simplifies and lowers the cost of the design by removing the need for a separate hydraulic system [16].

A R&D company for the supercar manufacturer Koenigsegg has recently unveiled a prototype of their take on the camless engine, in which the actuation of the valves is done by pneumatic actuators [18].

2.2.2 Typical kinematic profiles for valve trains

In order to fully understand the kinematic and dynamic properties of the InnerCam, it's advisable to first look at some information available about current systems being used. There has been plenty of work done in order to determine the lift profile, as well as the velocities and accelerations profiles for the same valve train which lead to some lift position, velocity and acceleration profiles.

Although the valve train systems developed already to this day greatly differ from one another (from a mechanical point of view), the lift's position, velocity and

acceleration profiles are usually very similar to the profiles shown above, since these profiles were designed to improve the efficiency of the engine.

This grants a benchmark for the profiles that need to be determined for the current Innercam system.

It's interesting to analyse the fast variation of acceleration (presented in figure 2.11) in the movement of the valves. This can lead to high inertial forces that may impair the dynamic behaviour of the valve train.

Of course the kinematic profiles of real systems differ from the theoretic profiles.

It's expected that the Innercam system generates lift position, velocity and acceleration profiles similar to the ones already presented.

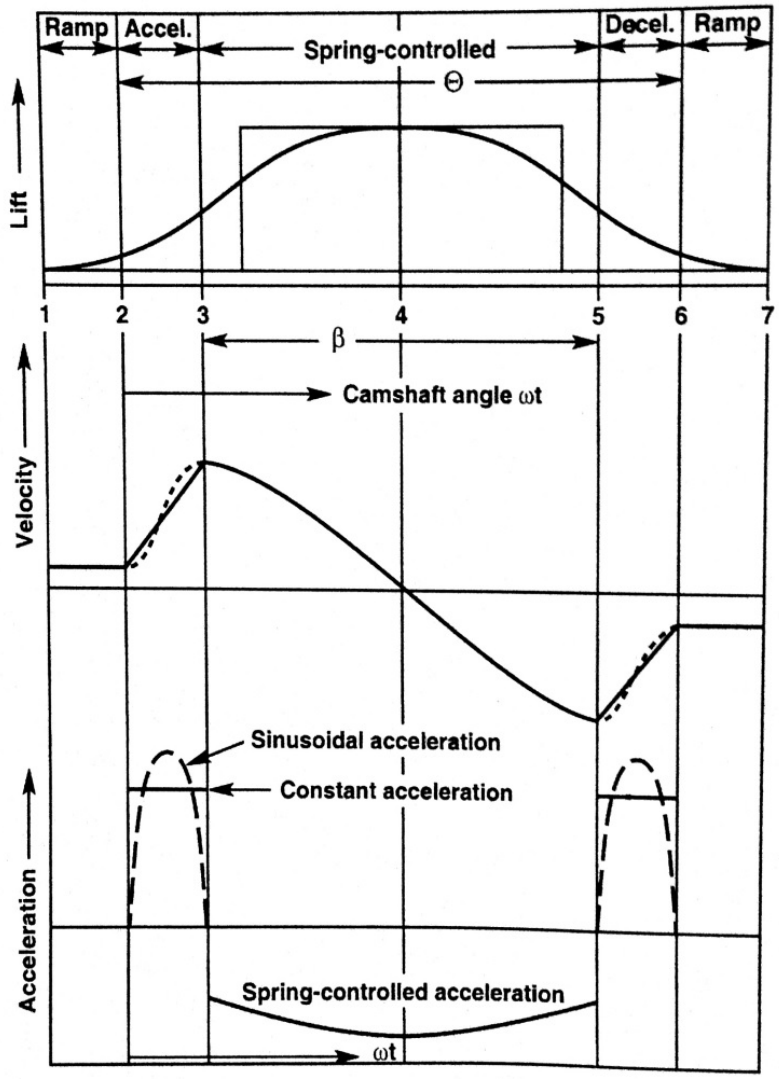

Figure 2.11: Theoretical lift profile, velocities and accelerations of the valves. In the dotted lines, it shows the common real kinematic behaviour instead of the theoretical behaviour. [7]

Chapter 3

InnerCam

The InnerCam system is a valve train mechanism introduced by AJP Motos SA, a portuguese motorcycle manufacturer specialized on off-road bikes. Since the PR5 is the flagship of the AJP Motos SA motorcycles, there's a high demand from the costumers and professional racers for a more powerful motorcycle, in order to give the competitive edge they always require.

Before proposing a new valve train, there were some few trials on other solutions that could improve the engine. First, they tried to increase the engine revolution per minute by altering the electronic central unit as well as adding an electronic fuel injection system. Although they improved the power output, they found some durability issues in the standard valve train used at the time.

The standard engine uses a single overhead cam in its valve train (SOHC), which performs well at lower speeds and allows for a compact engine. Actually, the greatest strength of the PR5 is its manoeuvrability; besides, the compact engine with a low center of gravity is one of the main reasons for the good handling of the motorcycle.

One of the solutions was to adapt the engine from a SOHC to a DOHC, since the DOHC engines perform well at high engine speeds. However, since the DOHC valve train is larger and more complex, this would result in a bigger engine, compromising the manoeuvrability of the PR5.

The other solution is to create a new valve train system that is just as compact as the standard valve train and could offer the same level of performance that the DOHC engines provide. Since AJP Motos SAis a small manufacturer, without the ability to produce their own engines and the engine is provided by an european-chinese joint venture, the new valve train must be compatible with the standard engine and must be designed in order to fit in this engine.

The valve train proposed is based on the SOHC design present in the original engine, with several modifications on the valves, rocker arms, springs and camshaft.

As shown in the figure 3.1, the new camshaft has two inner cams, one for the actuation of the admission valves and one for the actuation of the exhaust valves. In order to further reduce the size of the engine and improve the dynamic behaviour, new rocker arms were made for this system. Each rocker arm will move 2 valves for the admission sub-system and 2 valves for the exhaust valves. To further reduce the inertia forces in the system (improving the kinematic and dynamic behaviour of the valve train), a new set of lighter valves were installed. Two springs maintain an upward force on the valves, guaranteeing the seal required for the engine to work properly when the valves are closed.

When the cam follower reaches the non-circular trajectory, it forces the rotation of the rocker arms, causing, in turn, the opening of the valves. At low speeds, the springs can force the valves to close, as soon as the rocker arm can rotate anti-clockwise when the cam trajectory allows it. At higher speeds, though, the inertia of the components is too high and the springs alone can't close the valves and push the rocker arm into the resting position. So, the inner surface of the cam will perform the rotation of the rocker arm into its resting position, leaving the springs to only move the valves, guaranteeing the sealing required for the engine to work properly. This allows the usage of lighter springs, since it's not required a great stiffness given that, at higher speeds, the springs only need to move the valves. As the inertia is significantly lower than the one corresponding to regular engines, it's less likely to occur the "valve bounce" phenomenon.

The cam features two paths for two cam followers simultaneously, allowing to control de admission and exhaust with only one cam. This is a completely new

Figure 3.1: Innercam valve train - schematic representation (springs are not represented).

component and its production is made exclusively by AJP Motos SA. The camshaft is machined from a single block of steel which is, afterwards, submitted to a thermal treatment different from the one applied in the original camshaft. The steel is provided by the portuguese company F. Ramada (see appendix B for the full technical sheet of the steel and the appendix C for the report on the thermal treatment applied). Its chemical composition is presented in table 3.1.

Table 3.1: Chemical composition of the steel used to manufacture the camshaft

C	Si	Mn	Cr	Mo	Ni
0.34%	<= 0.40%	0.65%	1.50%	0.22%	1.50%

The first version of the camshaft feature a flawed design. The edges between the circular path and the non-circular path were too aggressive, resulting in very high accelerations deriving from the sudden changes in direction. The newer

prototypes display a smoother path, reducing the extreme variations in velocity and acceleration, reducing the wear on the cam and the cam follower (see figure 3.2).

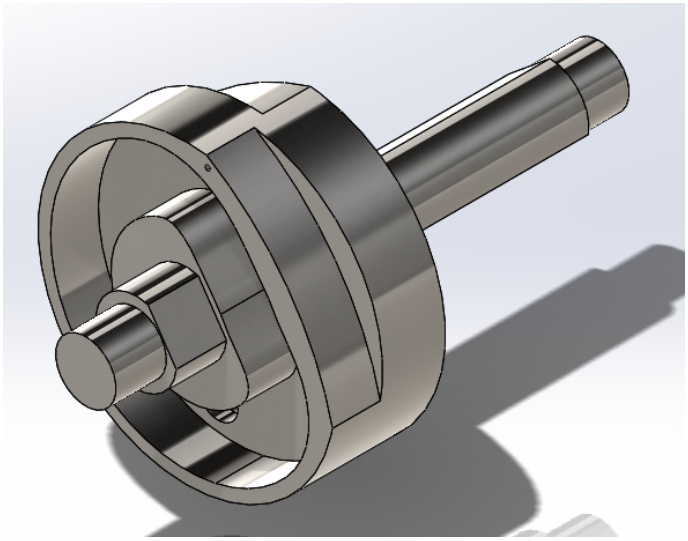

Figure 3.2: Innercam Camshaft.

The new rocker arms feature an entire new design, incorporating a cam follower that is assembled in the respective cam path (see figure 3.4). This cam follower consists on a roller mounted in the rocker arm, which rotates from the contact between the roller and the cam. The cam follower forces the movement of the rocker arm as a function of the position of the cam. If the cam follower is in the non-circular path defined in the cam (see figure 3.5), the roller (and subsequently the rocker arm) will rotate around its support, causing the actuation of the valves.

The new rocker arm also features the tuning bolts found on the original rocker arms. This tuning bolts allow to adjust the free space between the rocker arm and the valves. This open space must be determined with great care in order to account for dimensional variations from thermal expansion and wear on the components. If the spacing is too short, it may lead to problems such as, for example: the valves can open too soon and close too late leading to dangerous accumulations of heat; the valves may not close entirely, allowing for exhaust gases and flames to fire back into the intake valves. If, on the other hand, the spacing is to big, it may cause the valves to open later and close earlier than they should,

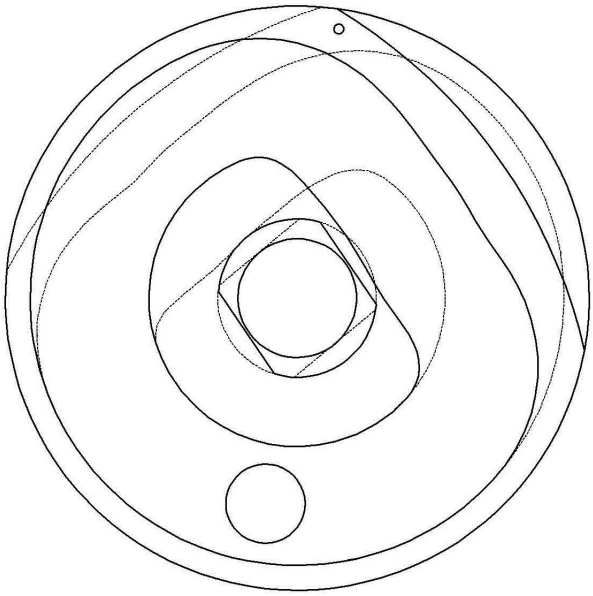

Figure 3.3: Innercam camshaft's cam paths. The inner path (dotted lines) corresponds to the exhaust sub-system.

compromising the amount of fuel mixture in the chamber and thus reducing the performance of the engine.

The springs currently used in the Innercam system are provided by a North American company, and these are the same springs currently used on the Yamaha YZF 250. They are characterized by a rigidity of 25400 N/m and are assembled with a 2 mm of pre-deformation. This allows a positive force from the spring, maintaining the valves closed and sealed in the normal, non-actuated, behaviour of the valve train.

Since the new valve train is considerably different from the original one (the camshaft, for example, is significantly larger than the factory camshaft), a new cylinder head must be fabricated in order to house the new system. This new cylinder head was manufactured by sand casting, and it already includes de admission and exhaust ducts.

AJP Motos SA also provided some numeric values of the valves' lift as a function of the rotation of the camshaft (see figure 3.5), allowing to determine lift profile generated by the Innercam system. The dots corresponds to the values given by

AJP Motos SA. These values also allows to determine the basic geometric relations for the system, which are presented in the next chapter.

By comparing the lift profiles generated by the Innercam (figure 3.5) and the theoretical lift profiles discussed in the chapter 2 (see figures 2.2 and 2.11), we can see that the new system develops similar lift profiles and is able to generate the distinct exhaust lift profile and intake lift profile.

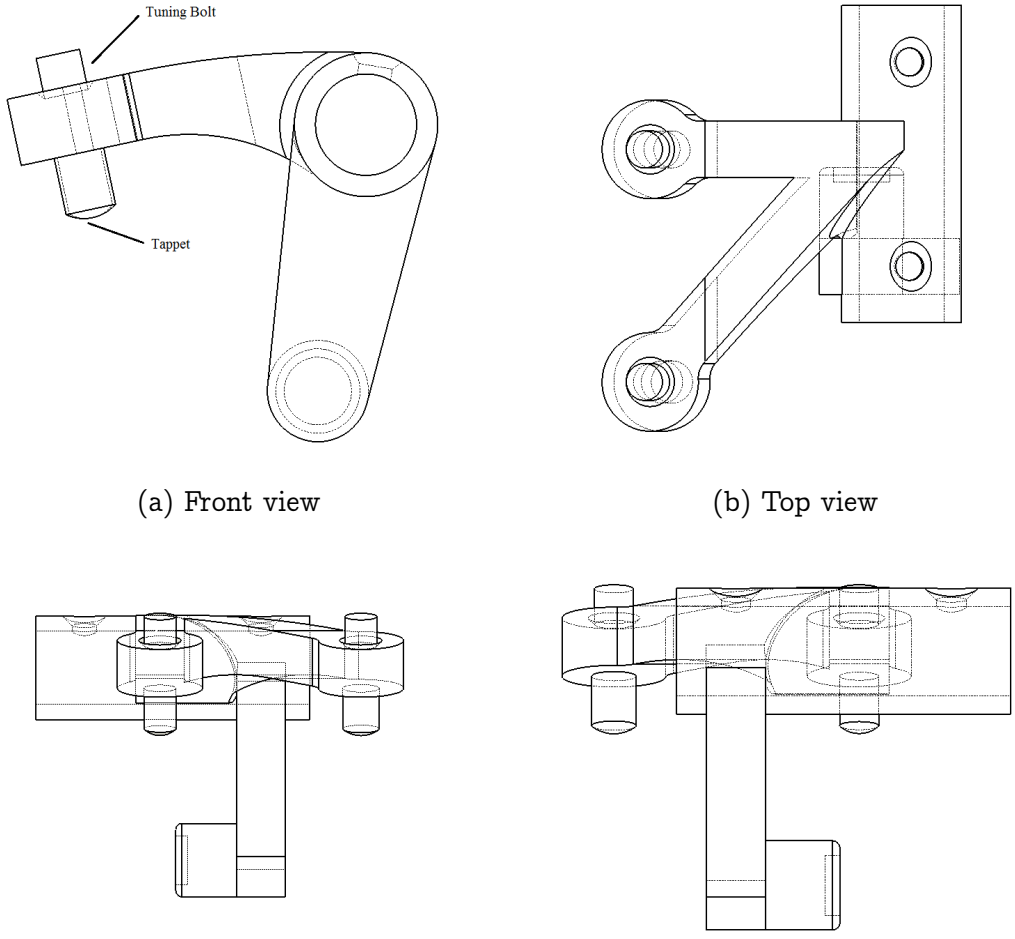

(a) Front view (b) Top view

(c) Left view (d) Right view

Figure 3.4: Rocker arm - schematic rendering.

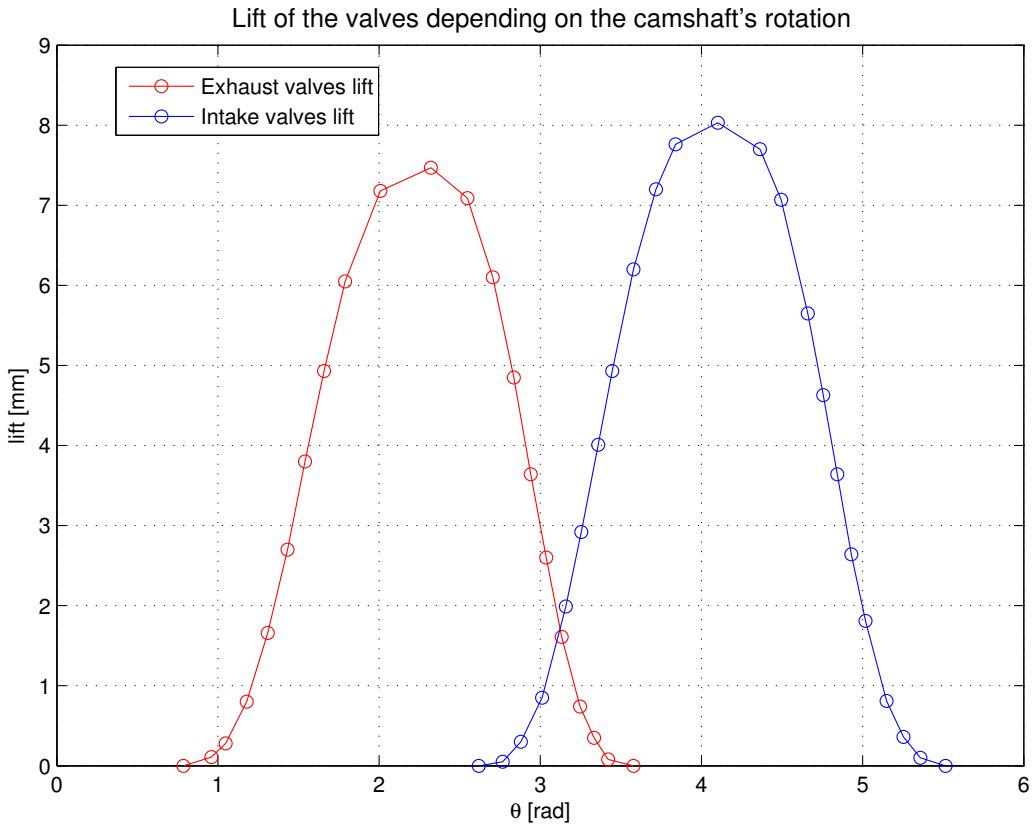

Figure 3.5: Lift profiles measured through valve timing by AJP Motos SA

Chapter 4

Dynamic Analysis

It's possible to simplify the system that is being analysed into a 2D mechanism. This can be achieved since there are no movements along the ZZ axis, or any rotations along any other axis but the ZZ axis.

We can simplify it further by separating the admission and exhaust sub-systems. These sub-systems are identical and are actuated depending on the cam rotation. Regarding the function of the valve trains system, the opening and closing of the intake valves must occur in a different part of the combustion cycle as the opening and closing of the exhaust valves, as explained on chapters 2 and 3.

One more possible simplification is to consider the mass of the set valve-spring as a single mass, considering the mass of the spring as a part of the valve's mass - all placed in the valve's initial center of gravity. Although it's common to not consider the weight of springs in some dynamic analysis, this can only be done when the weight of the springs, in comparison to the weight of the other components, is very small.

In this system, the weight of the springs is comparable to the rest of the components of the Innercam, so, the weight of the springs must be taken into account in the kinematic and dynamic analysis of the system.

4.1 Exhaust sub-system

The exhaust sub-system can be defined by the following schematics (see figure 4.1 for the non-actuated exhaust sub-system and the fig. 4.2 for the actuated exhaust sub-system):

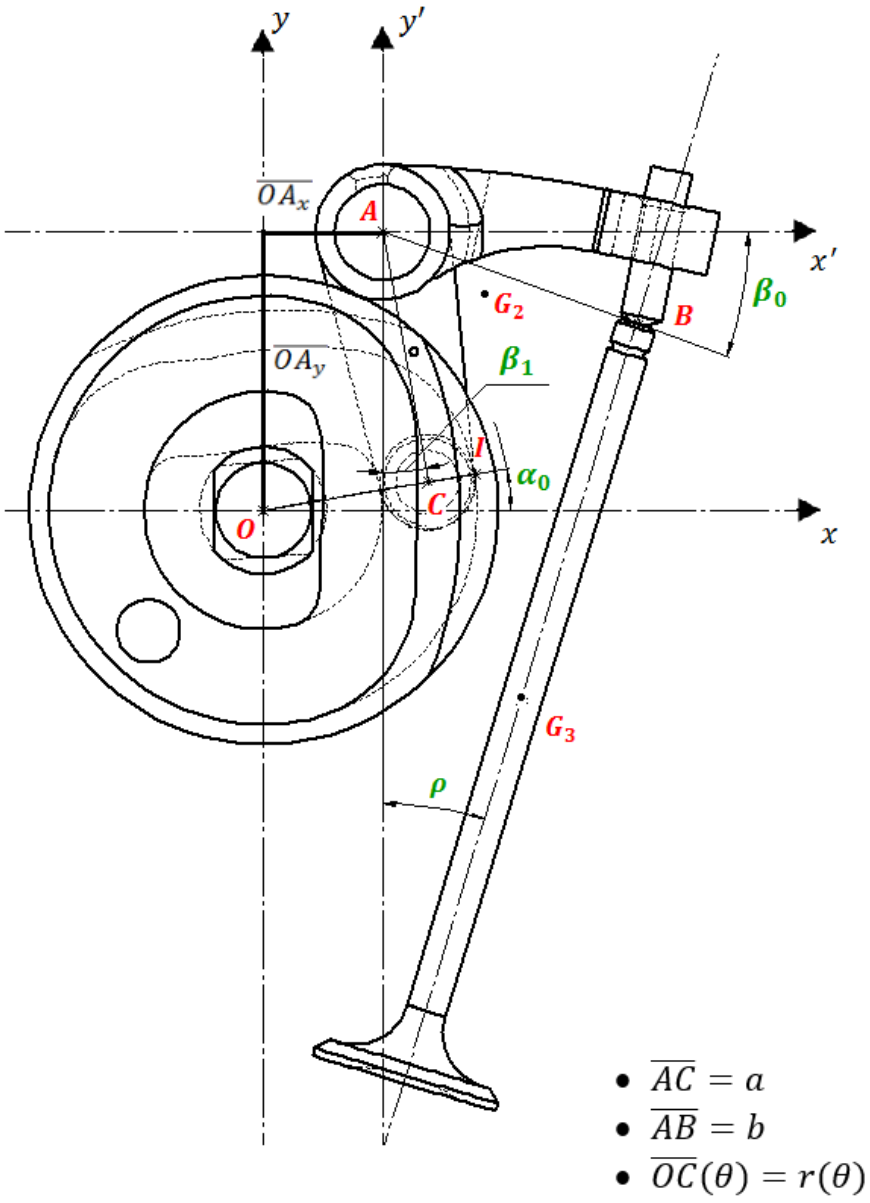

Figure 4.1: Exhaust sub-system schematics - position for non-actuated rocker arm

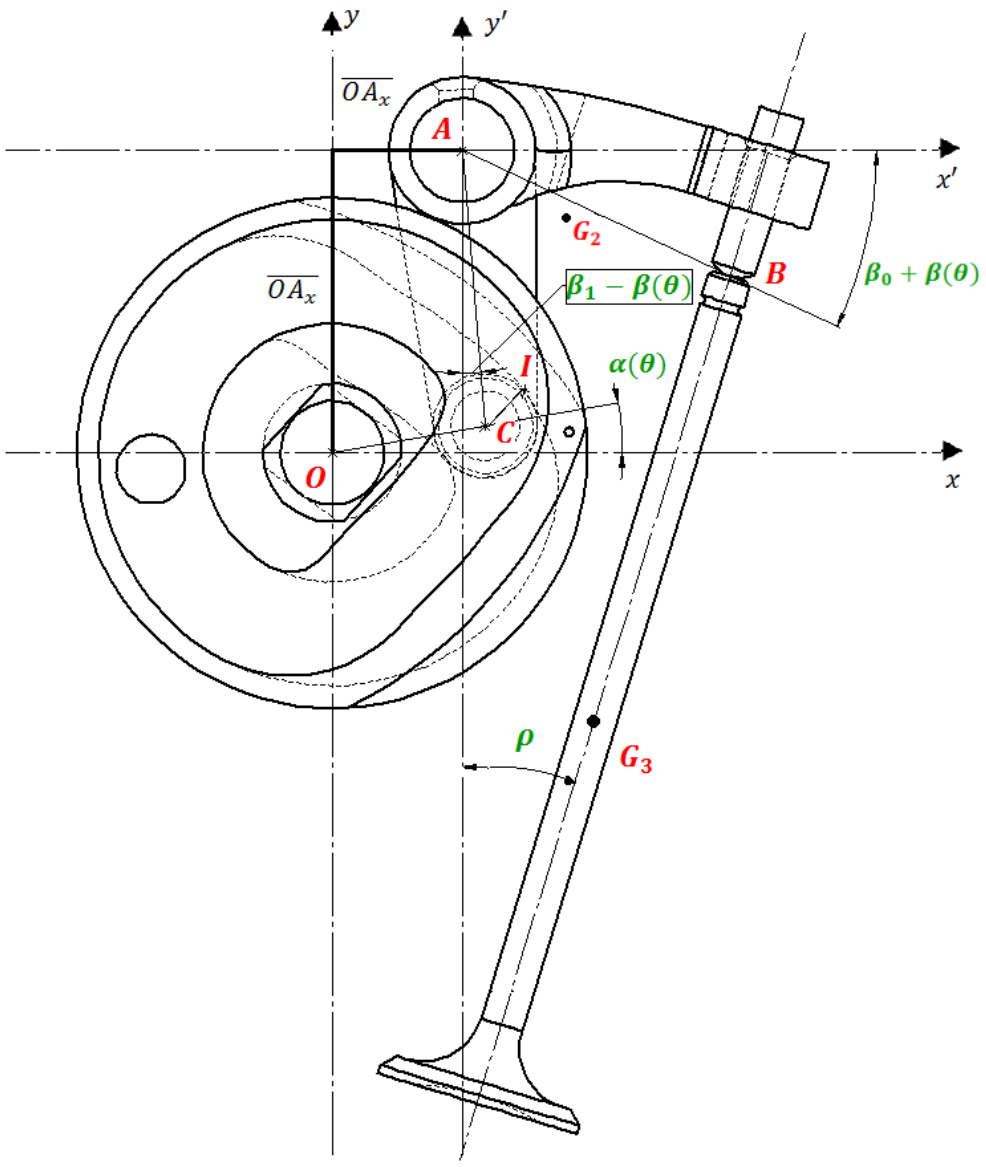

Figure 4.2: Exhaust sub-system schematics - position for actuated rocker arm

4.1.1 Geometric Properties

Considering the geometry of the exhaust sub-system, we can determine the geometric relations between the lift (Δ) and the remaining variables "r" (distance between the point O and C), α (the angle between "r" and the xx axis) and β (the angle of rotation of the rocker arm). The variable a and b correspond to the distance between the point A and C and the distance between the point A and B, respectively.

$$\Delta\cos\rho = b\sin(\beta+\beta_0) - b\sin(\beta_0); \tag{4.1}$$

$$\overline{OA_y} = r\sin(\alpha) + a\cos(\beta_1-\beta); \tag{4.2}$$

$$\overline{OA_x} = r\cos(\alpha) + a\sin(\beta_1-\beta); \tag{4.3}$$

It was given access to a set of $\Delta(\theta)$ points (through a valve timing analysis performed by AJP), allowing to determine an analytical expression using numeric regression. Since the curve is similar to a Gaussian curve, it was used a Gaussian regression as well as a polynomial regression. The gaussian equations offer a better numeric approximation when compared to the polynomial equations. Therefore, the following work was done using gaussian equations to describe $\Delta(\theta)$.

Using the numeric expressions of $\Delta(\theta)$ and the geometric relations displayed above, we can calculate the value of $\beta, \dot{\beta}$ and $\ddot{\beta}$, using equation 4.1, and the values of r, $\dot{r}$, $\ddot{r}$ and α, $\dot{\alpha}$, $\ddot{\alpha}$, using equations 4.2 and 4.3.

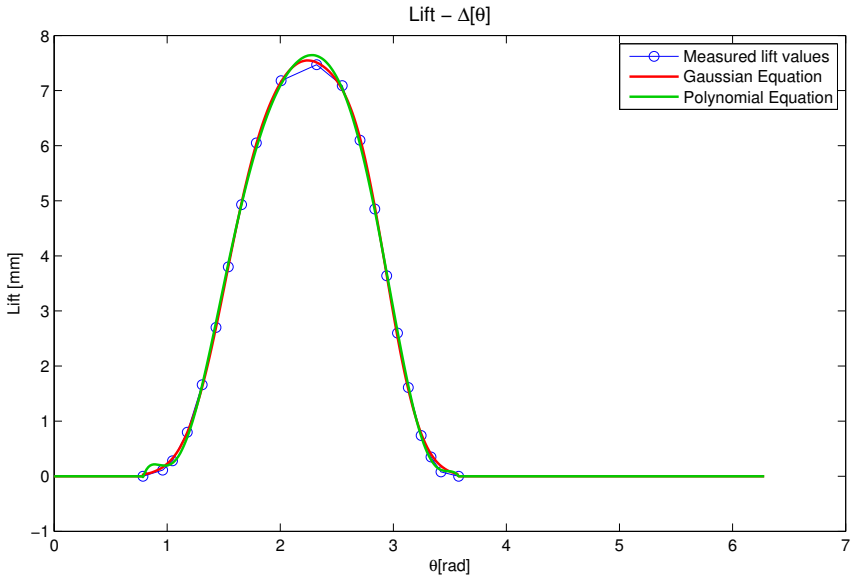

Figure 4.3: $\Delta(\theta)$ - Discrete values given by AJP Motos SA

4.1.2 Kinematics

We can define the displacement, velocities and accelerations for point C, using the following expressions,

- **Body 1 - Cam**

$$\overrightarrow{\omega_{10}} = \begin{Bmatrix} 0 \\ 0 \\ \dot{\theta} \end{Bmatrix}; \qquad \overrightarrow{\Omega_{10}} = \begin{Bmatrix} 0 \\ 0 \\ \ddot{\theta} \end{Bmatrix}; \tag{4.4}$$

$$\overrightarrow{OC_{10}} = \begin{Bmatrix} r\cos(\alpha) \\ r\sin(\alpha) \\ 0 \end{Bmatrix}; \tag{4.5}$$

$$\overrightarrow{v_{C10}} = \dot{\overrightarrow{OC_{10}}} = \begin{Bmatrix} \dot{r}\cos(\alpha) - r\dot{\alpha}\sin(\alpha) \\ \dot{r}\sin(\alpha) + r\dot{\alpha}\cos(\alpha) \\ 0 \end{Bmatrix}; \tag{4.6}$$

$$\overrightarrow{a_{C10}} = \dot{\overrightarrow{v_{C10}}} = \begin{Bmatrix} \ddot{r}\cos(\alpha) - 2\dot{r}\dot{\alpha}\sin(\alpha) - r\ddot{\alpha}\sin(\alpha) - r\dot{\alpha}^2\cos(\alpha) \\ \ddot{r}\sin(\alpha) + 2\dot{r}\dot{\alpha}\cos(\alpha) + r\ddot{\alpha}\cos(\alpha) - r\dot{\alpha}^2\sin(\alpha) \\ 0 \end{Bmatrix}; \tag{4.7}$$

- **Body 2 - Rocker Arm**

  Considering the rocker arm as the reference, we can obtain the following expressions:

$$\overrightarrow{\omega_{20}} = \begin{Bmatrix} 0 \\ 0 \\ -\dot{\beta} \end{Bmatrix}; \qquad \overrightarrow{\Omega_{20}} = \begin{Bmatrix} 0 \\ 0 \\ -\ddot{\beta} \end{Bmatrix}; \tag{4.8}$$

$$\overrightarrow{AC_{20}} = \begin{Bmatrix} a\sin(\beta_1 - \beta) \\ -a\cos(\beta_1 - \beta) \\ 0 \end{Bmatrix}; \tag{4.9}$$

$$\overrightarrow{v_{C20}} = \dot{\overrightarrow{AC_{20}}} = \begin{Bmatrix} -a\dot{\beta}\cos(\beta_1 - \beta) \\ -a\dot{\beta}\sin(\beta_1 - \beta) \\ 0 \end{Bmatrix}; \tag{4.10}$$

$$\overrightarrow{a_{C20}} = \dot{\overrightarrow{v_{C20}}} = \begin{Bmatrix} -a\ddot{\beta}\cos(\beta_1-\beta) - a\dot{\beta}^2\sin(\beta_1-\beta) \\ -a\ddot{\beta}\sin(\beta_1-\beta) + a\dot{\beta}^2\cos(\beta_1-\beta) \\ 0 \end{Bmatrix}; \tag{4.11}$$

Since point C is common to both bodies 1 and 2 (there's no relative displacement between the two bodies in this point), $\overrightarrow{v_{C20}}$ must be equal to $\overrightarrow{v_{C10}}$. The same principle is applicable to the accelerations ($\overrightarrow{a_{C20}} = \overrightarrow{a_{C10}}$).

This can be used as a method to verify the kinematic equations determined as well as to verify the generation of r, α and β.

Using the same reference (point A) and the same method applied before, we obtain the following expressions for point B:

$$\overrightarrow{AB_{20}} = \begin{Bmatrix} b\cos(\beta+\beta_0) \\ -b\sin(\beta+\beta_0) \\ 0 \end{Bmatrix}; \tag{4.12}$$

$$\overrightarrow{v_{B20}} = \dot{\overrightarrow{AB_{20}}} = \begin{Bmatrix} -b\dot{\beta}\sin(\beta+\beta_0) \\ -b\dot{\beta}\cos(\beta+\beta_0) \\ 0 \end{Bmatrix}; \tag{4.13}$$

$$\overrightarrow{a_{B20}} = \dot{\overrightarrow{v_{b20}}} = \begin{Bmatrix} -b\ddot{\beta}\sin(\beta+\beta_0) - b\dot{\beta}^2\cos(\beta+\beta_0) \\ -b\ddot{\beta}\cos(\beta+\beta_0) + b\dot{\beta}^2\sin(\beta+\beta_0) \\ 0 \end{Bmatrix}; \tag{4.14}$$

Using the SolidWorks®^{TM}tools available in the InnerCam schematics, it's possible to determine the precise location of the center of mass in all the bodies that belong to the InnerCam. This way, we can also determine the

kinematic properties on the center of mass in bodies 2 and 3 (the center of mass in body 1 is the origin of our referential).

$$\overrightarrow{AG2_{20}} = \begin{Bmatrix} \overline{AG2}\cos(\beta+\beta_2) \\ -\overline{AG2}\sin(\beta+\beta_2) \\ 0 \end{Bmatrix}; \tag{4.15}$$

$$\overrightarrow{v_{G2_{20}}} = \dot{\overrightarrow{AG2_{20}}} = \begin{Bmatrix} -\overline{AG2}\dot{\beta}\sin(\beta+\beta_2) \\ -\overline{AG2}\dot{\beta}\cos(\beta+\beta_2) \\ 0 \end{Bmatrix}; \tag{4.16}$$

$$\overrightarrow{a_{G2_{20}}} = \dot{\overrightarrow{v_{G2_{20}}}} = \begin{Bmatrix} -\overline{AG2}\ddot{\beta}\sin(\beta+\beta_2) - \overline{AG2}\dot{\beta}^2\cos(\beta+\beta_2) \\ -\overline{AG2}\ddot{\beta}\cos(\beta+\beta_2) + \overline{AG2}\dot{\beta}^2\sin(\beta+\beta_2) \\ 0 \end{Bmatrix} \tag{4.17}$$

- **Body 3 - Valve**

$$\overrightarrow{OG3_{30}} = \begin{Bmatrix} OG_{30}^x - \Delta\sin(\rho) \\ OG_{30}^y - \Delta\cos(\rho) \\ 0 \end{Bmatrix}; \tag{4.18}$$

$$\overrightarrow{v_{G3_{30}}} = \dot{\overrightarrow{OG3_{30}}} = \begin{Bmatrix} -\dot{\Delta}\sin(\rho) \\ -\dot{\Delta}\cos(\rho) \\ 0 \end{Bmatrix}; \tag{4.19}$$

$$\overrightarrow{a_{G3_{30}}} = \dot{\overrightarrow{v_{G3_{30}}}} = \begin{Bmatrix} -\ddot{\Delta}\sin(\rho) \\ -\ddot{\Delta}\cos(\rho) \\ 0 \end{Bmatrix}; \tag{4.20}$$

- **Body 4 - Roller**

$$\overrightarrow{\omega_{40}} = \begin{Bmatrix} 0 \\ 0 \\ \dot{\gamma} \end{Bmatrix}; \qquad \overrightarrow{\Omega_{40}} = \begin{Bmatrix} 0 \\ 0 \\ \ddot{\gamma} \end{Bmatrix}; \tag{4.21}$$

$$\overrightarrow{AC_{40}} = \overrightarrow{AC_{10}} = \overrightarrow{AC_{20}}; \tag{4.22}$$

$$\overrightarrow{v_{C_{40}}} = \overrightarrow{v_{C_{10}}} = \overrightarrow{v_{C_{20}}}; \tag{4.23}$$

$$\overrightarrow{a_{C_{40}}} = \overrightarrow{a_{C_{10}}} = \overrightarrow{a_{C_{20}}}; \tag{4.24}$$

It is also required to define the position of the point of contact between the cam and the roller - point I. Usually, the point of contact between these 2 bodies is located on the outer cam path, due to the spring force. For the purposes of this calculations, it's considered the outer point of contact.

$$\overrightarrow{OI_{10}} = \begin{Bmatrix} r\cos(\alpha) + \overline{CI}\cos(\alpha+\gamma) \\ r\sin(\alpha) + \overline{CI}\sin(\alpha+\gamma) \\ 0 \end{Bmatrix} \tag{4.25}$$

Since the angle γ is yet to be defined, we can calculate it by determining the angle between the perpendicular line to a secant constructed by the points $\overrightarrow{OI_{10}}(i+1)$ and $\overrightarrow{OI_{10}}(i-1)$ (see figure 4.4), and the horizontal referential. By doing so, we are able of calculate the angle gamma for $i-2$ points. The first and last value of gamma are determined by a linear extrapolation of the remaining values.

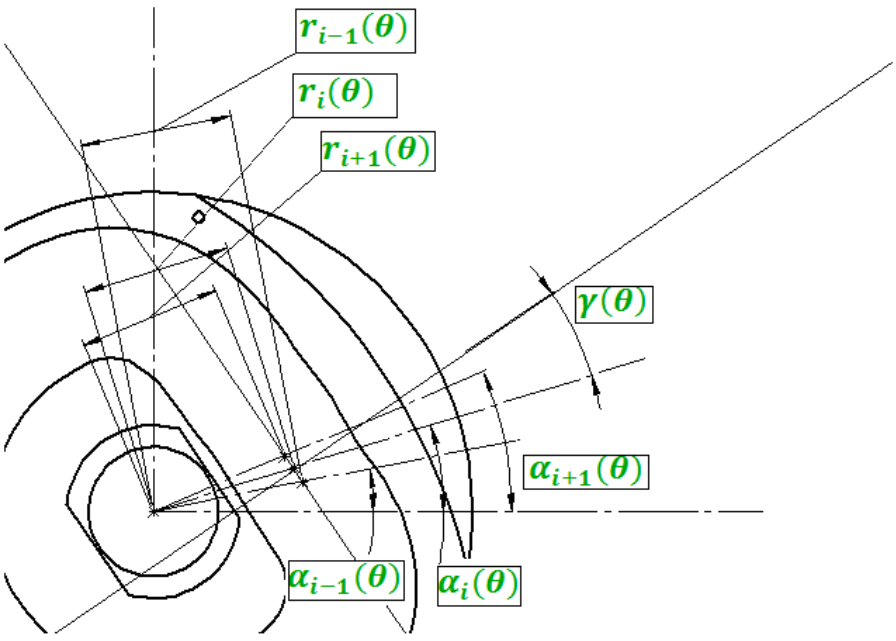

Figure 4.4: Process of calculating the angle γ

Now that we have all the values of *gamma* defined, we can apply the same numeric regressions to this variable, allowing us to determine the expressions for γ, $\dot{\gamma}$ and $\ddot{\gamma}$.

4.1.3 Dynamics

In order to determine the dynamic expressions for this system, it's first required to properly determine the mass and inertia properties of each body, in order to fully define the dynamic equations.

Using the SolidWorks®^{TM}tools available, we can obtain the various values of mass and inertia, presented below:

- $m_1 = 0,3285$ kg
- $m_2 = 0,1280$ kg
- $m_3 = 0,0247 \times 2 + 0,0131 \times 2$ kg (considering the weight of the springs)
- $m_4 = 0,0049$ kg
- Moments of Inertia - Cam

$$\begin{bmatrix} 186.809 & -0.123 & 0.22 \\ -0.123 & 187.122 & -0.106 \\ 0.022 & -0.106 & 96.955 \end{bmatrix} kg \bullet mm^2 \tag{4.26}$$

- Moments of Inertia - Rocker Arm

$$\begin{bmatrix} 55.46 & 4.61 & -9.99 \\ 4.61 & 47.31 & -15.38 \\ -9.99 & -15.38 & 42.31 \end{bmatrix} kg \bullet mm^2 \tag{4.27}$$

- Moments of Inertia - Valve

$$\begin{bmatrix} 48.351 & 14.393 & 0 \\ 14.393 & 5.672 & 0 \\ 0 & 0 & 57.750 \end{bmatrix} kg \bullet mm^2 \tag{4.28}$$

- Moments of Inertia - Roller

$$\begin{bmatrix} .10051 & 0 & 0 \\ 0 & .10051 & 0 \\ 0 & 0 & .124.3 \end{bmatrix} kg \bullet mm^2 \tag{4.29}$$

The main goal is to determine the correct expression for the equation of motion of the complete, rigid system. In order to do so, we can either analyse each body separately or analyse the whole system at once.

Analysing the whole system at once would give us only 3 equations and more than 3 unknown variables, so, it's still required to analyse some bodies separately, in order to define some of the unknown variables.

If we analyse each body separately, we will obtain 3 equations (in a 2D problem) for each body (2 equations for the forces equilibrium and 1 equation for the momentum equilibrium). This will give us 12 equations in total, more than enough to fully define all the forces and momentums actuating in the system.

Analysing the cam, we obtain the following free-body diagram, accompanied by their dynamic equilibrium equations:

- **Body 1 - Cam**

$$\sum \overrightarrow{F_1} = \dot{\overrightarrow{Q_1}} \Leftrightarrow \begin{Bmatrix} 0 \\ -m_1 g \\ 0 \end{Bmatrix} + \begin{Bmatrix} F_N \cos(\alpha+\gamma) \\ F_N \sin(\alpha+\gamma) \\ 0 \end{Bmatrix} + \begin{Bmatrix} -F_T \sin(\alpha+\gamma) \\ F_T \cos(\alpha+\gamma) \\ 0 \end{Bmatrix} + \begin{Bmatrix} R_O^x \\ R_O^y \\ 0 \end{Bmatrix} = \overrightarrow{0} \Leftrightarrow \tag{4.30}$$

$$\begin{cases} R_O^x = F_T \sin(\alpha+\gamma) - F_N \cos(\alpha+\gamma) & (4.31) \\ R_O^y = m_1 g - F_T \cos(\alpha) - F_N \sin(\alpha+\gamma) & (4.32) \end{cases}$$

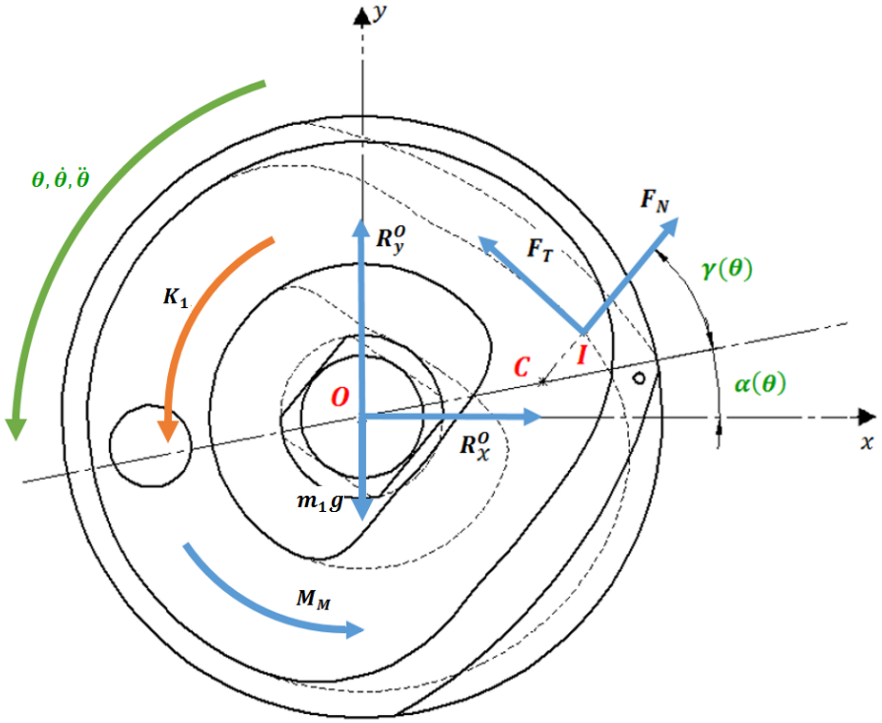

Figure 4.5: Free body diagram of the camshaft

$$\sum \overrightarrow{M_1} = \overrightarrow{K_O^1} \Leftrightarrow \begin{Bmatrix} \overline{OI_x} \\ \overline{OI_y} \\ 0 \end{Bmatrix} \times \begin{Bmatrix} F_N \cos(\alpha+\gamma) \\ F_N \sin(\alpha+\gamma) \\ 0 \end{Bmatrix} + \\ + \begin{Bmatrix} \overline{OI_x} \\ \overline{OI_y} \\ 0 \end{Bmatrix} \times \begin{Bmatrix} -F_T \sin(\alpha+\gamma) \\ F_T \cos(\alpha+\gamma) \\ 0 \end{Bmatrix} + \begin{Bmatrix} 0 \\ 0 \\ Mm \end{Bmatrix} = \overrightarrow{K_O^1} \Leftrightarrow \tag{4.33}$$

$$\Leftrightarrow Mm = I_{zz}\ddot{\theta} - F_T[OI_x \cos(\alpha+\gamma) + OI_y \sin(\alpha+\gamma)] - \\ - F_N[OI_x \sin(\alpha+\gamma) - OI_y \cos(\alpha+\gamma)]; \tag{4.34}$$

Applying the same principle for the rest of the bodies, we can obtain the diagrams presented next.

- **Body 2 - Rocker Arm**

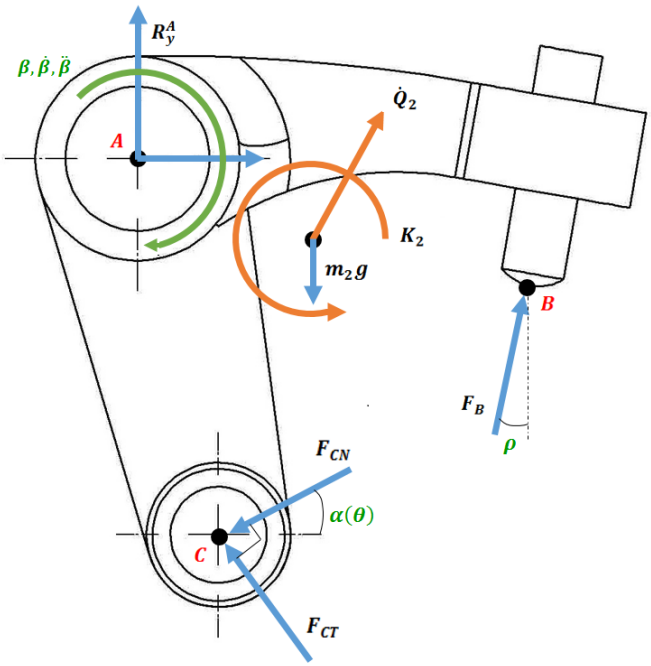

Figure 4.6: Free body diagram of the exhaust rocker arm

For the forces described in the free body diagram of the rocker arm (fig. 4.6), we obtain the following equations:

$$\sum \overrightarrow{F_2} = \dot{\overrightarrow{Q_2}} \Leftrightarrow \begin{Bmatrix} -F_{CN}\cos(\alpha) \\ -F_{CN}\sin(\alpha) \\ 0 \end{Bmatrix} + \begin{Bmatrix} -F_{CT}\sin(\alpha) \\ F_{CT}\cos(\alpha) \\ 0 \end{Bmatrix} + \begin{Bmatrix} F_B\sin(\rho) \\ F_B\cos(\rho) \\ 0 \end{Bmatrix} + \\ + \begin{Bmatrix} 0 \\ -m_2 g \\ 0 \end{Bmatrix} + \begin{Bmatrix} R_A^x \\ R_A^y \\ 0 \end{Bmatrix} = m2 \begin{Bmatrix} a_{G2}^x \\ a_{G2}^y \\ 0 \end{Bmatrix} \tag{4.35}$$

$$\begin{cases} R_A^x = m_2 a_{G2}^x + F_{CN}\cos(\alpha) - F_{CT}\sin(\alpha) - F_B\sin(\rho) & (4.36) \\ R_A^y = m_2(a_{G2}^y + g) + F_{CN}\sin(\alpha) + F_{CT}\cos(\alpha) - F_B\cos(\rho) & (4.37) \end{cases}$$

$$\sum \overrightarrow{M_2} = \overrightarrow{K_A^2} \Leftrightarrow \begin{Bmatrix} a\sin(\beta_1-\beta) \\ -a\cos(\beta_1-\beta) \\ 0 \end{Bmatrix} \times \begin{Bmatrix} -F_{CN}\cos(\alpha) \\ -F_{CN}\sin(\alpha) \\ 0 \end{Bmatrix} + \\ + \begin{Bmatrix} a\sin(\beta_1-\beta) \\ -a\cos(\beta_1-\beta) \\ 0 \end{Bmatrix} \times \begin{Bmatrix} F_{CT}\sin(\alpha) \\ -F_{CT}\cos(\alpha) \\ 0 \end{Bmatrix} + \begin{Bmatrix} \overline{AG_2^x} \\ \overline{AG_2^y} \\ 0 \end{Bmatrix} \times \begin{Bmatrix} 0 \\ -m_2 g \\ 0 \end{Bmatrix} + \\ + \begin{Bmatrix} b\cos(\beta+\beta_0) \\ -b\sin(\beta+\beta_0) \\ 0 \end{Bmatrix} \times \begin{Bmatrix} F_B\sin(rho) \\ F_B\cos(rho) \\ 0 \end{Bmatrix} = \overrightarrow{K_{G2}^2} + \overrightarrow{AG_2} \times \dot{\overrightarrow{Q_2}} \tag{4.38}$$

- **Body 3 - Valve**

  For the valve, a different coordinate system was used, parallel to the orientation of the valve, in order to simplify the equilibrium equations (see figure 4.7).

$$\sum \overrightarrow{F_3} = \dot{\overrightarrow{Q_3}} \Leftrightarrow F_K - m_3 g\cos(\rho) - F_B = -m_3\ddot{\Delta} \tag{4.39}$$

$$F_K = k(\Delta + \delta_{pre-tension}) \tag{4.40}$$

$$F_B = F_K + m_3\ddot{\Delta} - m_3 g \tag{4.41}$$

$$\sum \overrightarrow{M_3} = \overrightarrow{K_{G3}} \Leftrightarrow \overrightarrow{0} = \overrightarrow{0} \tag{4.42}$$

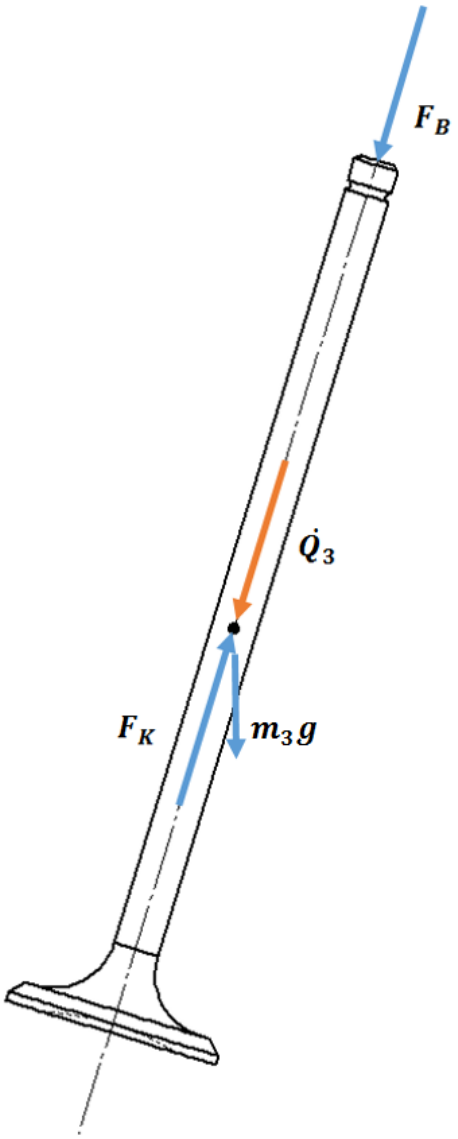

Figure 4.7: Free body diagram of the exhaust valve

- **Body 4 - Roller**

  For the roller, it's used the same coordinate system as in the cam and rocker arm (see figure 4.8).

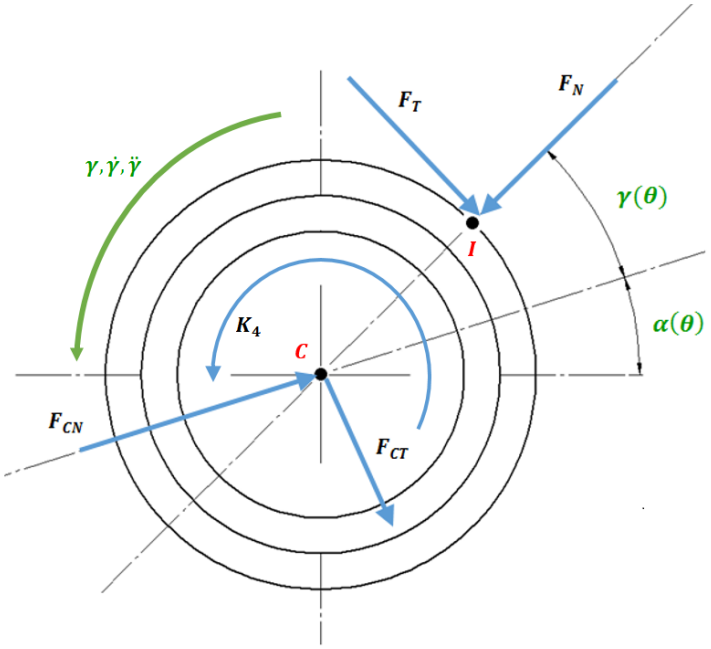

Figure 4.8: Free body diagram of the exhaust cam follower / roller

$$\sum \overrightarrow{F_4} = \dot{\overrightarrow{Q_4}} \Leftrightarrow \begin{Bmatrix} F_{CN}\cos(\alpha) \\ F_{CN}\sin(\alpha) \\ 0 \end{Bmatrix} + \begin{Bmatrix} F_{CT}\sin(\alpha) \\ -F_{CT}\cos(\alpha) \\ 0 \end{Bmatrix} + \begin{Bmatrix} -F_N\cos(\alpha+\gamma) \\ -F_N\sin(\alpha+\gamma) \\ 0 \end{Bmatrix} + \\ + \begin{Bmatrix} F_T\sin(\alpha+\gamma) \\ -F_T\cos(\alpha+\gamma) \\ 0 \end{Bmatrix} = m4 \begin{Bmatrix} a_C^x \\ a_C^y \\ 0 \end{Bmatrix} \tag{4.43}$$

$$\begin{cases} F_{CN}\cos(\alpha) + F_{CT}\sin(\alpha) - F_N\cos(\alpha+\gamma) + F_T\sin(\alpha+\gamma) = m_4 a_c^x & (4.44) \\ F_{CN}\sin(\alpha) - F_{CT}\cos(\alpha) - F_N\sin(\alpha+\gamma) - F_T\cos(\alpha+\gamma) = m_4 a_c^y & (4.45) \end{cases}$$

$$\sum \overrightarrow{M_4} = \overrightarrow{K_C^4} \Leftrightarrow \begin{Bmatrix} \overline{CI}\cos(\alpha+\gamma) \\ \overline{CI}\cos(\alpha+\gamma) \\ 0 \end{Bmatrix} \times \begin{Bmatrix} -F_N\cos(\alpha+\gamma) \\ -F_N\sin(\alpha+\gamma) \\ 0 \end{Bmatrix} + \\ + \begin{Bmatrix} \overline{CI}\cos(\alpha+\gamma) \\ \overline{CI}\cos(\alpha+\gamma) \\ 0 \end{Bmatrix} \times \begin{Bmatrix} F_T\sin(\alpha+\gamma) \\ -F_T\cos(\alpha+\gamma) \\ 0 \end{Bmatrix} = Izz^4\ddot{\gamma} \tag{4.46}$$

$$F_T = \frac{-Izz^4\ddot{\gamma}}{\overline{CI}} \tag{4.47}$$

We end up with 11 equation. While 10 of them allow us to define every force that are currently unknown (4.31, 4.32, 4.36, 4.37, 4.38, 4.44, 4.45, 4.40, 4.41, 4.70), the remaining one is the equation of motion (4.34), or the equation that describes the movement of the whole system, considering it rigid.

- **Complete System - Validation**

  For validation purposes, we can analyse the whole system at once (see figure 4.9), in order to verify the equation of movement obtained by the analysis of each body separately. For this purpose, only the forces exterior to the sub-system are considered.

$$\sum \overrightarrow{F_{sys}} = \dot{\overrightarrow{Q_{sys}}} \tag{4.48}$$

$$\begin{Bmatrix} R_O^x \\ R_O^y \\ 0 \end{Bmatrix} + \begin{Bmatrix} R_A^x \\ R_A^y \\ 0 \end{Bmatrix} + \begin{Bmatrix} 0 \\ -(m_1+m_2+m_4)g \\ 0 \end{Bmatrix} + \begin{Bmatrix} F_K\sin(\rho) \\ F_K\cos(\rho) \\ 0 \end{Bmatrix} = \dot{\overrightarrow{Q_1}} + \dot{\overrightarrow{Q_2}} + \dot{\overrightarrow{Q_3}} + \dot{\overrightarrow{Q_4}} \tag{4.49}$$

Since the body 1 has only a rotational movement, the quantity of acceleration of the cam is null. The body 3 (valve) only has a translational movement,

hence the dynamic momentum of this body is equal to 0, further simplifying the equilibrium equations for the system.

$$\sum \overrightarrow{M_{sys}} = \overrightarrow{K_{sys}} \Leftrightarrow \tag{4.50}$$

$$\Leftrightarrow \begin{Bmatrix} \overline{OA_x} \\ \overline{OA_y} \\ 0 \end{Bmatrix} \times \begin{Bmatrix} R_A^x \\ R_A^y \\ 0 \end{Bmatrix} + \begin{Bmatrix} r\cos(\alpha) \\ r\sin(\alpha) \\ 0 \end{Bmatrix} \times \begin{Bmatrix} 0 \\ -m_4 g \\ 0 \end{Bmatrix} + \begin{Bmatrix} \overline{OG_x^3} \\ \overline{OG_y^3} \\ 0 \end{Bmatrix} \times \begin{Bmatrix} F_K \sin(\rho) \\ F_K \cos(rho) - m_3 g \\ 0 \end{Bmatrix} + \\ + \begin{Bmatrix} \overline{OG_x^2} \\ \overline{OG_y^2} \\ 0 \end{Bmatrix} \times \begin{Bmatrix} 0 \\ -m_2 g \\ 0 \end{Bmatrix} + \begin{Bmatrix} 0 \\ 0 \\ M_m \end{Bmatrix} = \sum \overrightarrow{K_i} \tag{4.51}$$

With these equations, we now have the proper tools to evaluate the kinematic and dynamic properties of the system, allowing us to determine the points that are more susceptible to greater velocities, accelerations and forces.

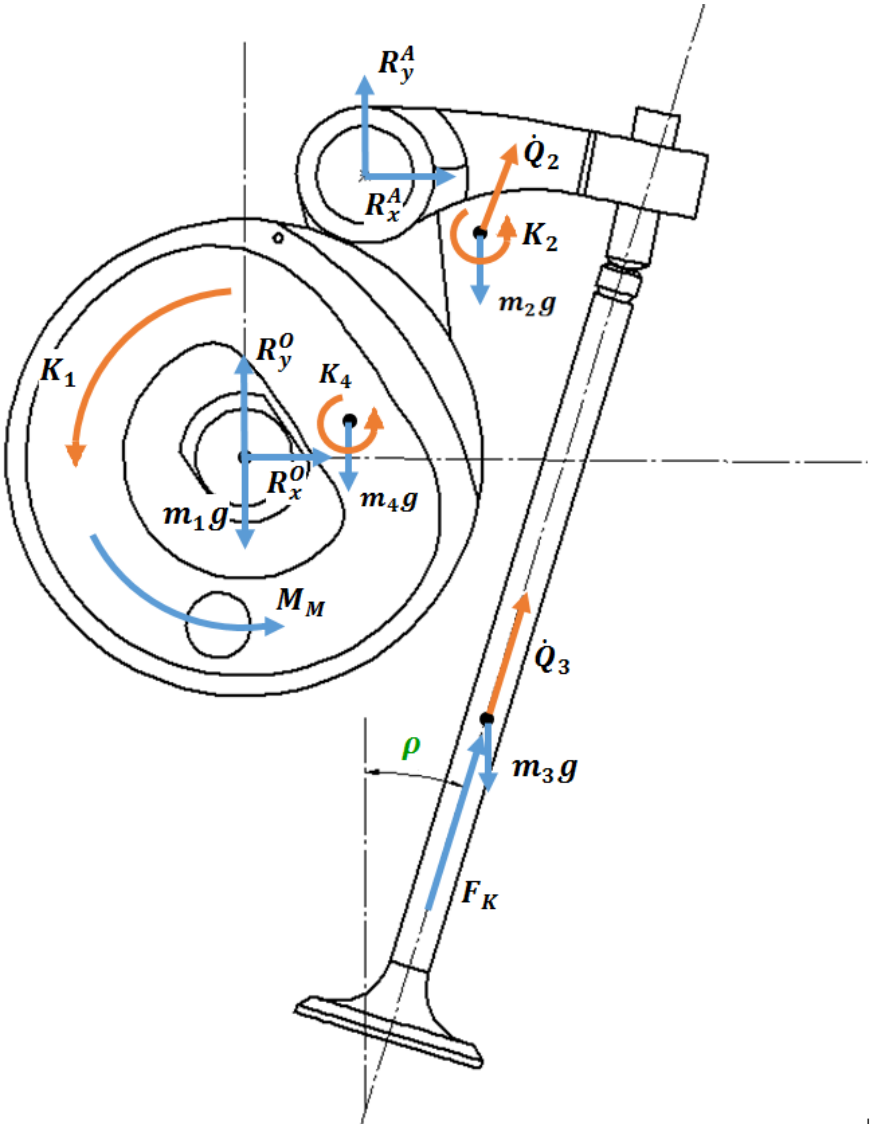

Figure 4.9: Free body diagram of the exhaust sub-system

4.2 Intake sub-system

For the intake sub-system, the same principles from the last chapter are applicable. Since the pathway that controls the intake valves is different from the pathway that controls the exhaust valves, different lift profiles are expected, as well as a new dynamic behaviour. The intake sub-system can be defined by the following schematics (see figure 4.10 for the non-actuated intake sub-system and figure 4.11 for the actuated intake sub-system):

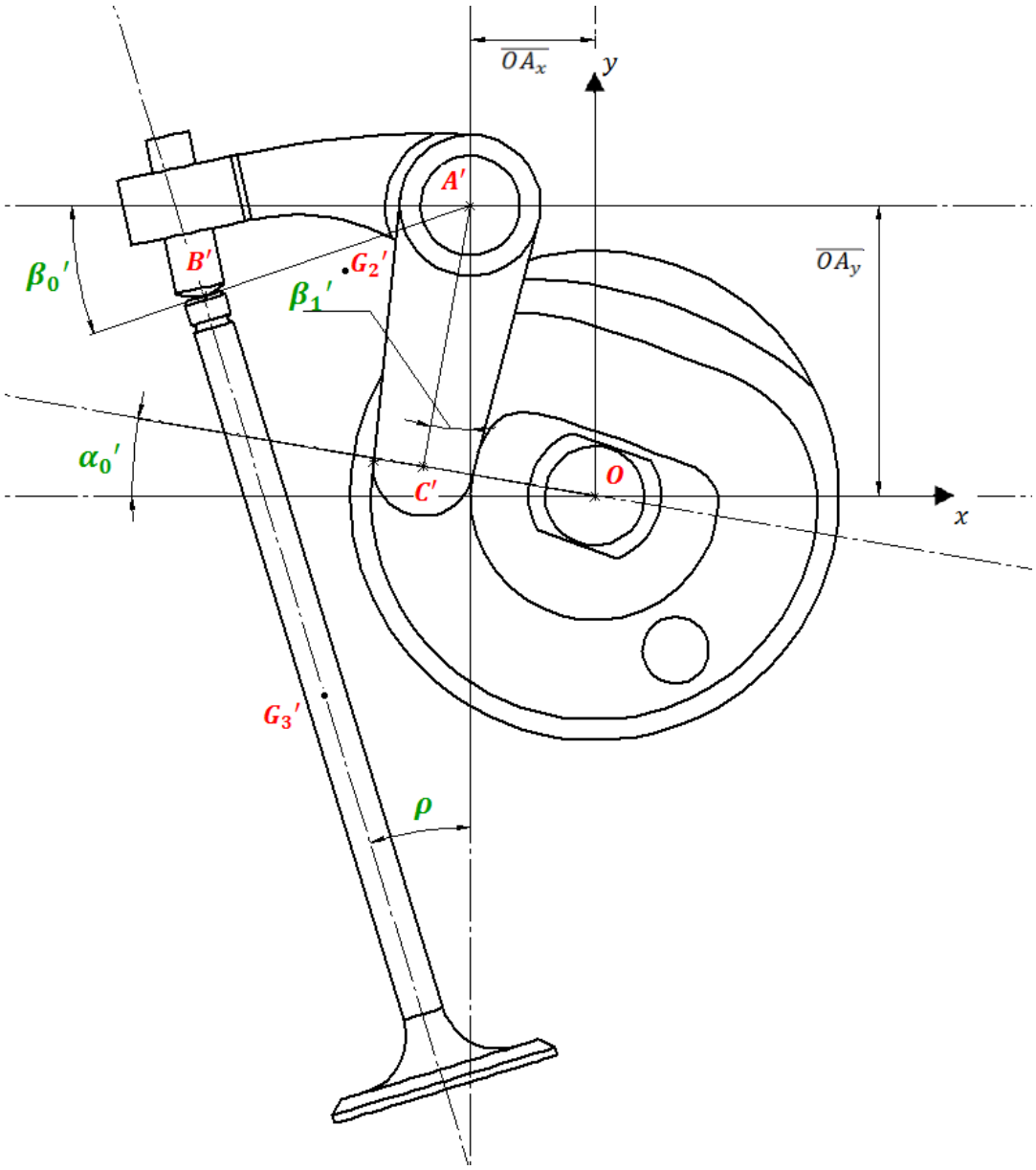

Figure 4.10: Schematic representation of the intake sub-system non-actuated

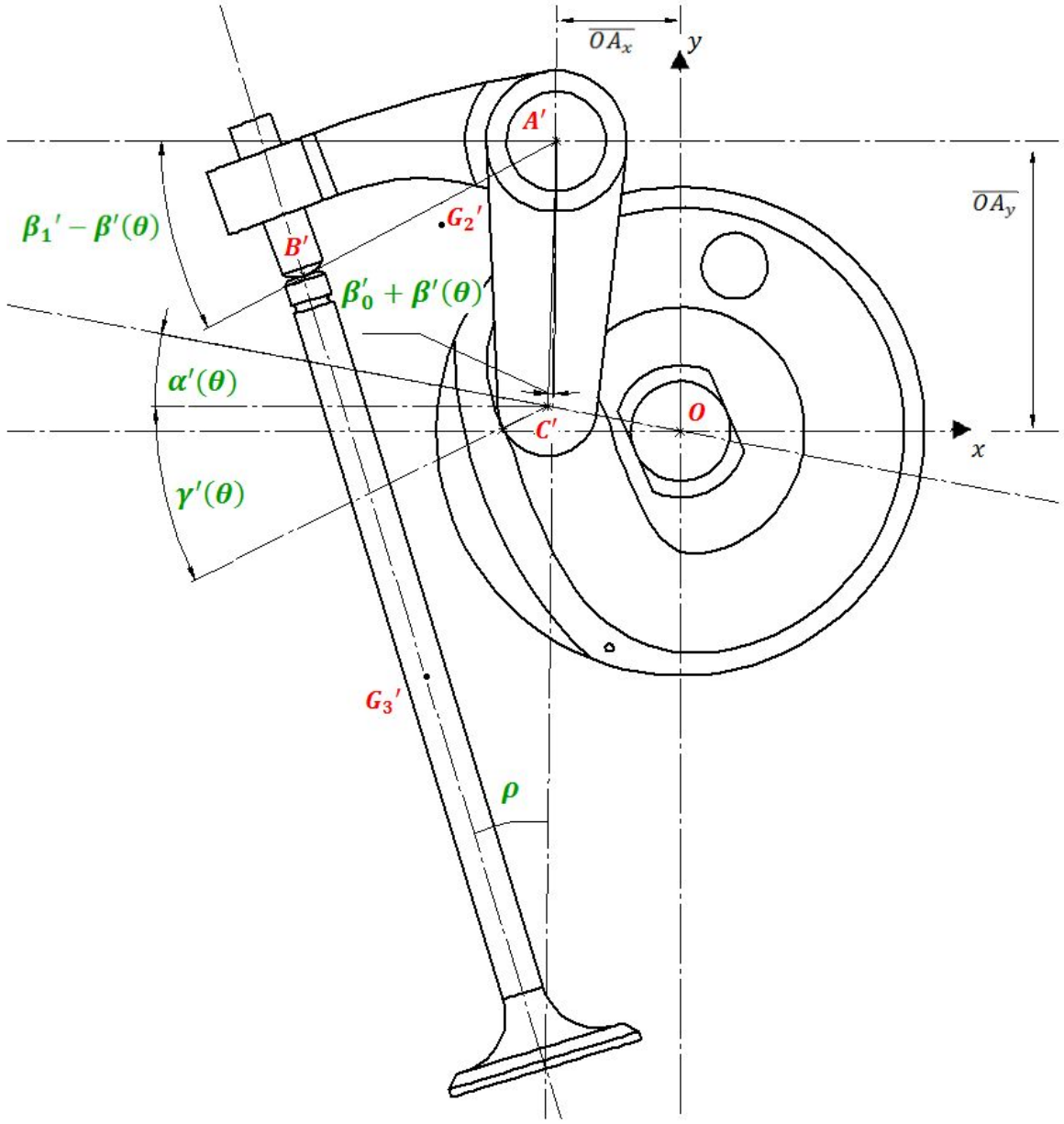

Figure 4.11: Schematic representation of the intake sub-system actuated

4.2.1 Geometric properties

For the intake sub-system, the same approach as the one applied in the exhaust sub-system was used, with the only difference being the coordinates of the relevant point in this sub-system.

4.2.2 Kinematics

The kinematic properties for this sub-system will reflect the different position of the subsystem, regarding the coordinate system that was previously adopted. Besides, these properties are expected to be in the same order of magnitude as the kinematic properties calculated for the exhaust sub-system, since the design (and therefore, all the geometric relations between points) is the same. The points in this sub-system will follow the same lettering rule applied in the exhaust sub-system, with the addition of an apostrophe in each point, in order to distinguish each sub-system.

In order to avoid repeating the same equations and principles applied in the previous sub-chapter, we will only present the displacement vectors (in order to show the main differences between the two sub-systems) and relevant equations that differ from the approach taken in the analysis of the exhaust sub-system.

$$\overrightarrow{\omega_{10}} = \begin{Bmatrix} 0 \\ 0 \\ \dot{\theta} \end{Bmatrix}; \qquad \overrightarrow{\Omega_{10}} = \begin{Bmatrix} 0 \\ 0 \\ \ddot{\theta} \end{Bmatrix}; \tag{4.52}$$

$$\overrightarrow{OC'_{10}} = \begin{Bmatrix} -r'\cos(\alpha') \\ r'\sin(\alpha') \\ 0 \end{Bmatrix}; \tag{4.53}$$

$$\overrightarrow{\omega_{20}} = \begin{Bmatrix} 0 \\ 0 \\ \dot{\beta} \end{Bmatrix}; \qquad \overrightarrow{\Omega_{20}} = \begin{Bmatrix} 0 \\ 0 \\ \ddot{\beta} \end{Bmatrix}; \tag{4.54}$$

$$\overrightarrow{A'C'_{20}} = \begin{Bmatrix} -a\sin(\beta - \beta_1) \\ -a\cos(\beta - \beta_1) \\ 0 \end{Bmatrix}; \tag{4.55}$$

$$\overrightarrow{A'B'_{20}} = \begin{Bmatrix} -b\cos(\beta' + \beta_0) \\ -b\sin(\beta + \beta_0) \\ 0 \end{Bmatrix}; \tag{4.56}$$

4.2.3 Dynamics

Before calculating the forces that are applied in this sub-system, we first need to determine the mass and inertia properties of the components of the sub-system.

Although this system is very similar to the exhaust system, their greater differences lie in the mass and inertia properties, as it can be verified by the following values:

- $m_1 = 0,3285$ kg
- $m_2 = 0,1280$ kg
- $m_3 = 0,0247 \times 2 + 0,0131 \times 2$ kg (considering the weight of the springs)
- $m_4 = 0,0049$ kg
- Moments of Inertia - Cam

$$\begin{bmatrix} 186.809 & -0.123 & 0.22 \\ -0.123 & 187.122 & -0.106 \\ 0.022 & -0.106 & 96.955 \end{bmatrix} kg \bullet mm^2 \tag{4.57}$$

- Moments of Inertia - Rocker Arm

$$\begin{bmatrix} 39.991 & -6.21 & -6.92 \\ -6.21 & 45.39 & -3.31 \\ -6.92 & -3.31 & 43.34 \end{bmatrix} kg \bullet mm^2 \tag{4.58}$$

- Moments of Inertia - Valve

$$\begin{bmatrix} 48.351 & 14.393 & 0 \\ 14.393 & 5.672 & 0 \\ 0 & 0 & 52.752 \end{bmatrix} kg \bullet mm^2 \tag{4.59}$$

- Moments of Inertia - Roller

$$\begin{bmatrix} .066914 & -.01569 & 0 \\ -.01569 & .02038 & 0 \\ 0 & 0 & .05838 \end{bmatrix} kg \bullet mm^2 \tag{4.60}$$

It's important to note the differences between the inertia matrices of the intake and exhaust rocker arms. The intake rocker arm has lower inertia values. This is important to reduce the inertial forces caused by the higher lift values.

4.3 Model Results

Since all kinematic and dynamic equations are fully defined, it's possible to obtain the graphics showing the variation of position, velocities and accelerations, as well as the variation of the forces generated within the system. These graphics were generated for various engine velocities, corresponding to the lower, medium and higher regime of the engine.

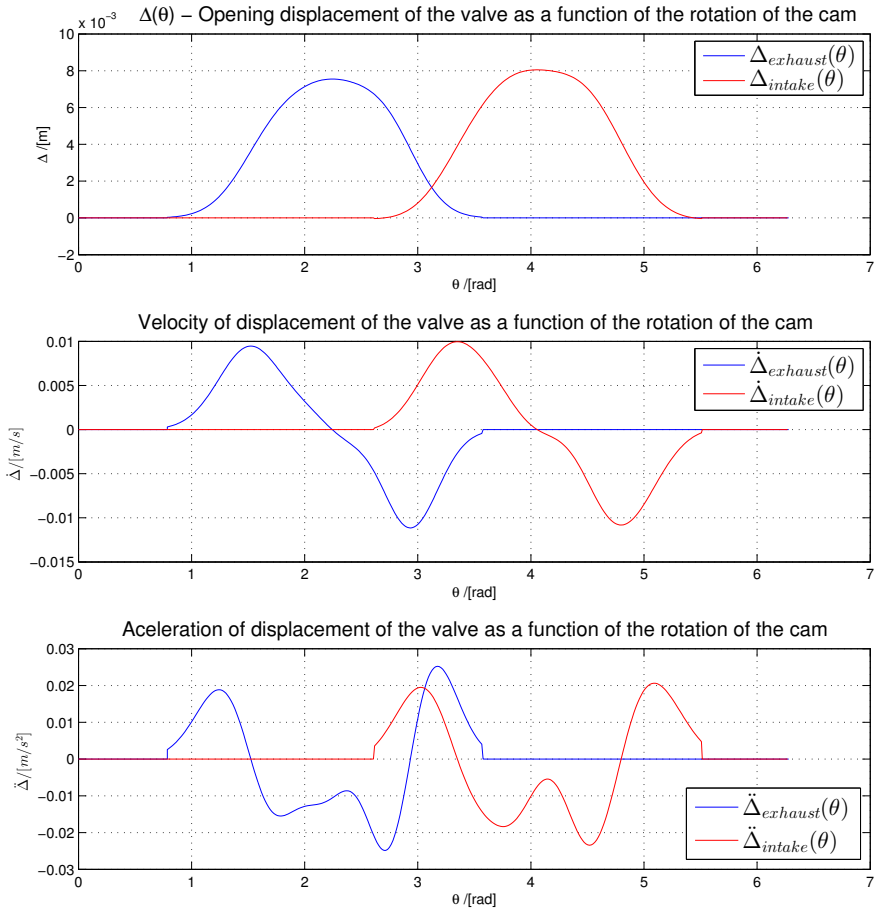

Figure 4.12: Lift (Δ, $\dot{\Delta}$, $\ddot{\Delta}$) profiles for the exhaust sub-system (engine at 12000 rpm)

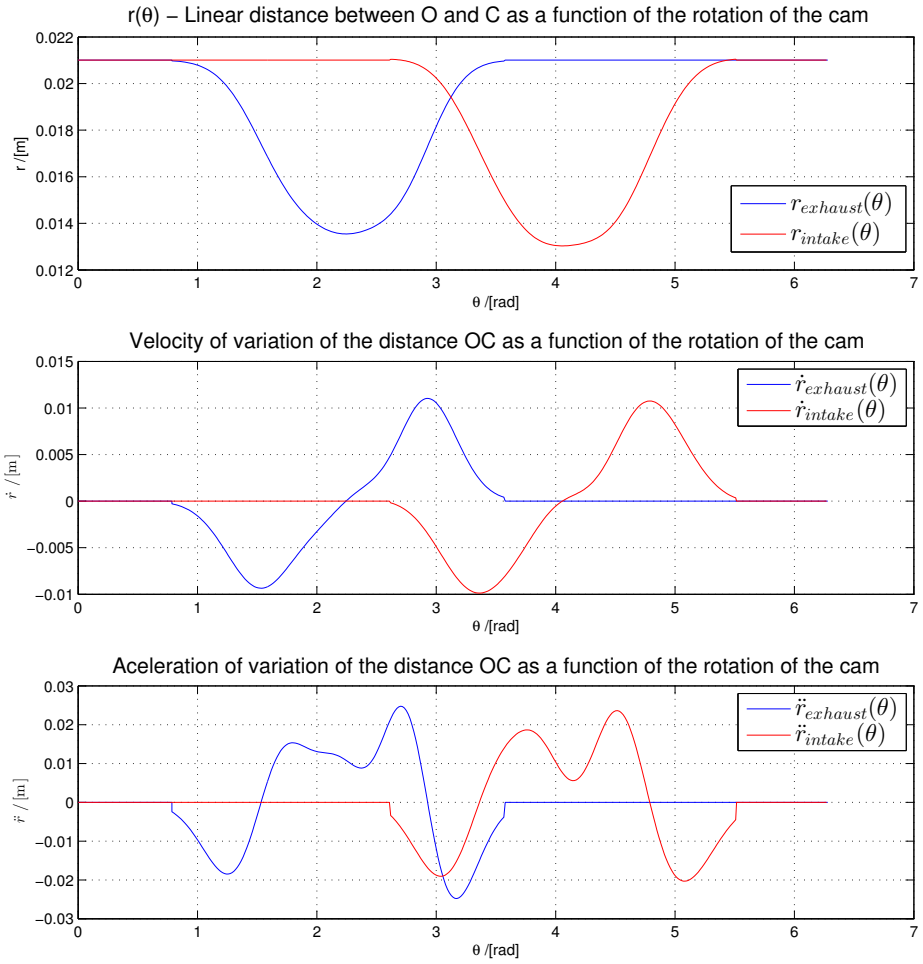

Figure 4.13: r, $\dot{r}$, $\ddot{r}$ profiles for the exhaust sub-system (engine at 12000 rpm)

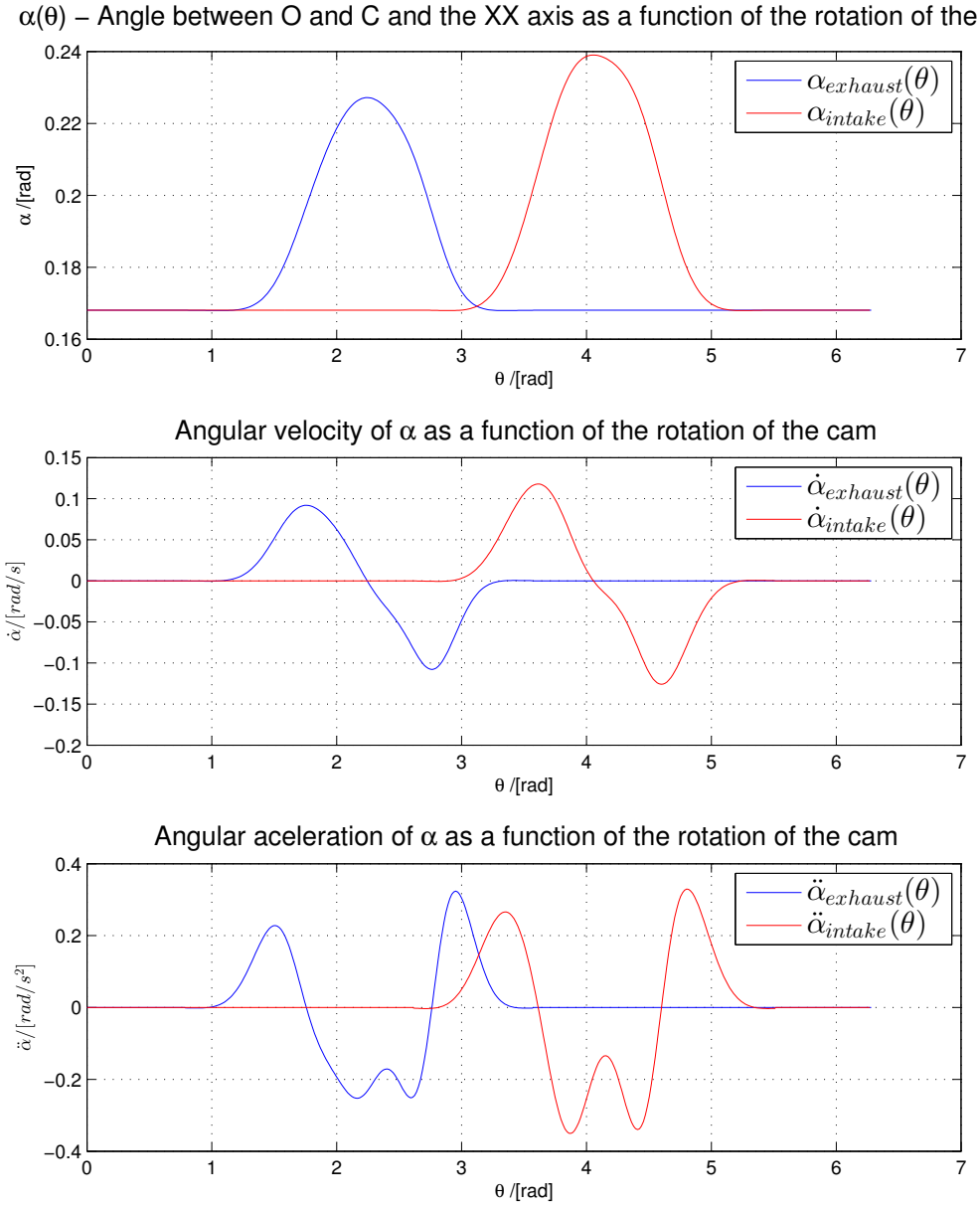

Figure 4.14: α, $\dot{\alpha}$, $\ddot{\alpha}$ profiles for the exhaust sub-system (engine at 12000 rpm)

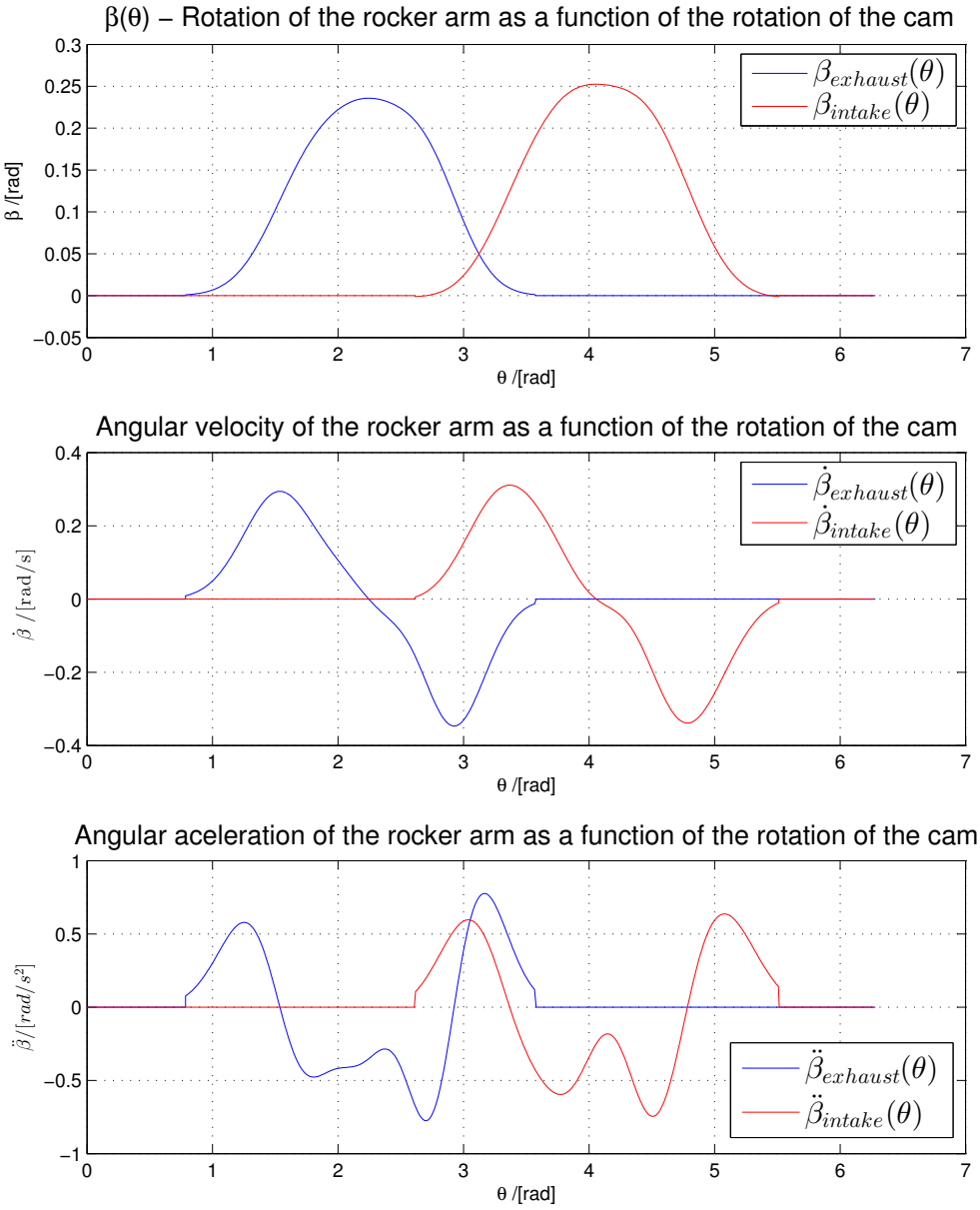

Figure 4.15: β, $\dot{\beta}$, $\ddot{\beta}$ profiles for the exhaust sub-system (engine at 12000 rpm)

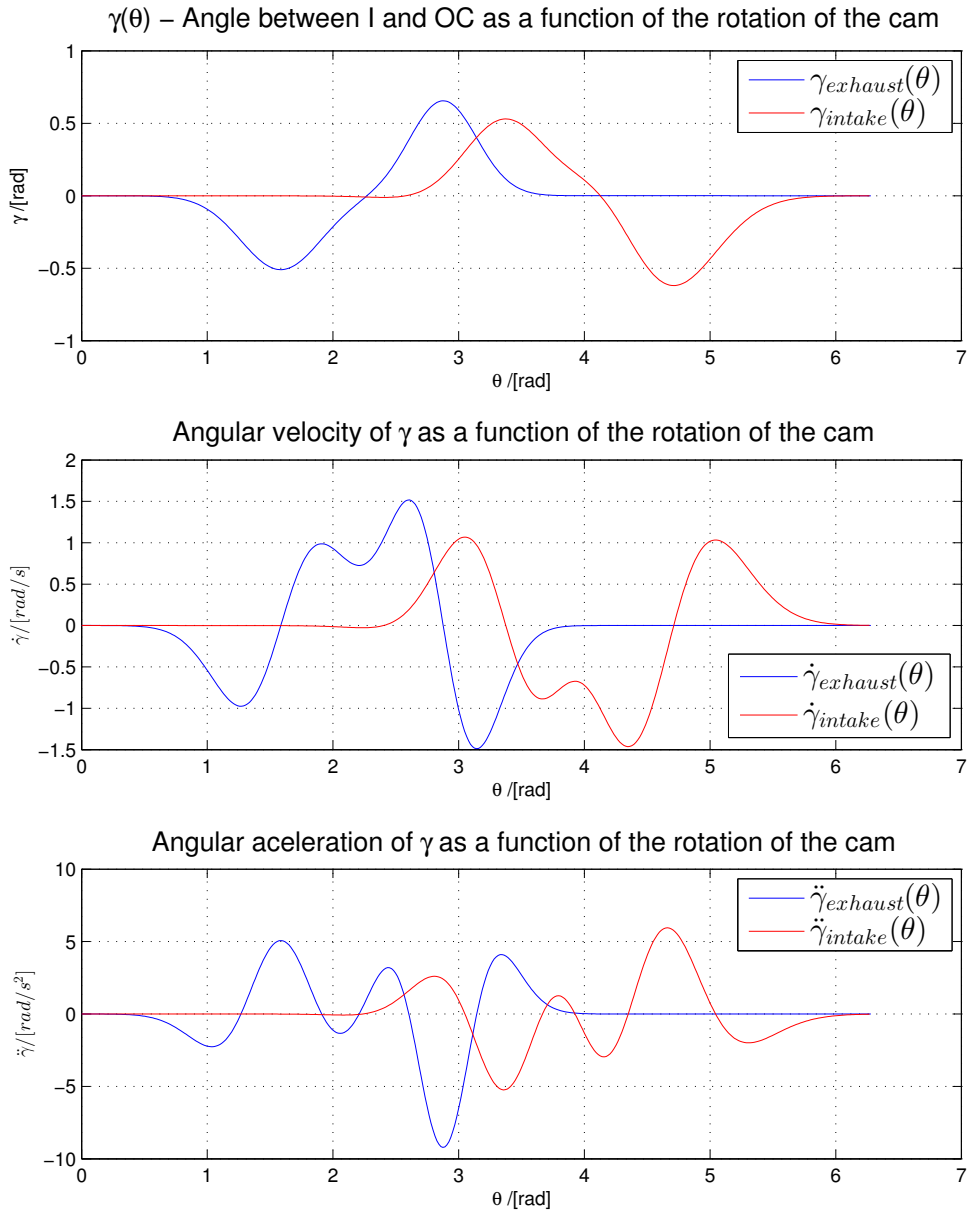

Figure 4.16: γ, $\dot{\gamma}$, $\ddot{\gamma}$ profiles for the exhaust sub-system (engine at 12000 rpm)

4.3.1 Exhaust Sub-system

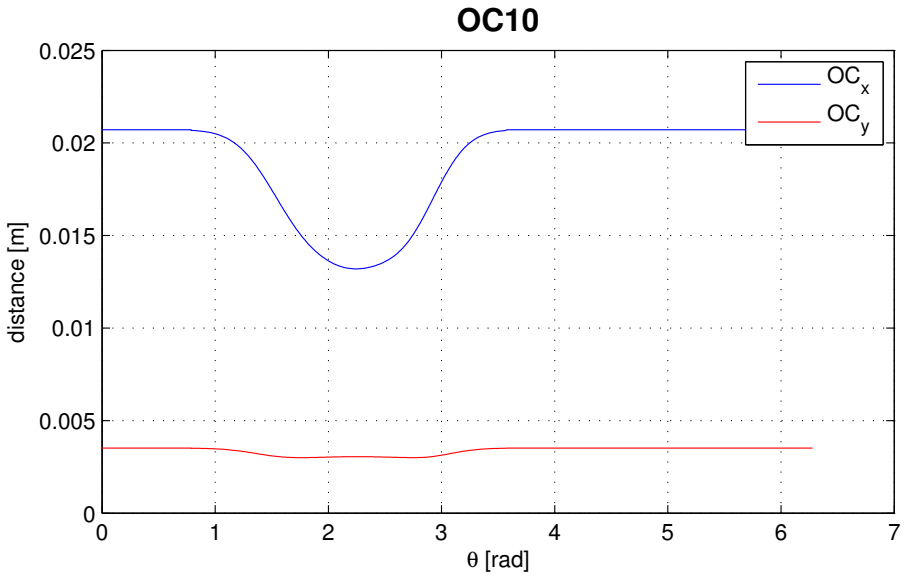

Figure 4.17: $\overrightarrow{OC_{10}}$ profile for the exhaust sub-system

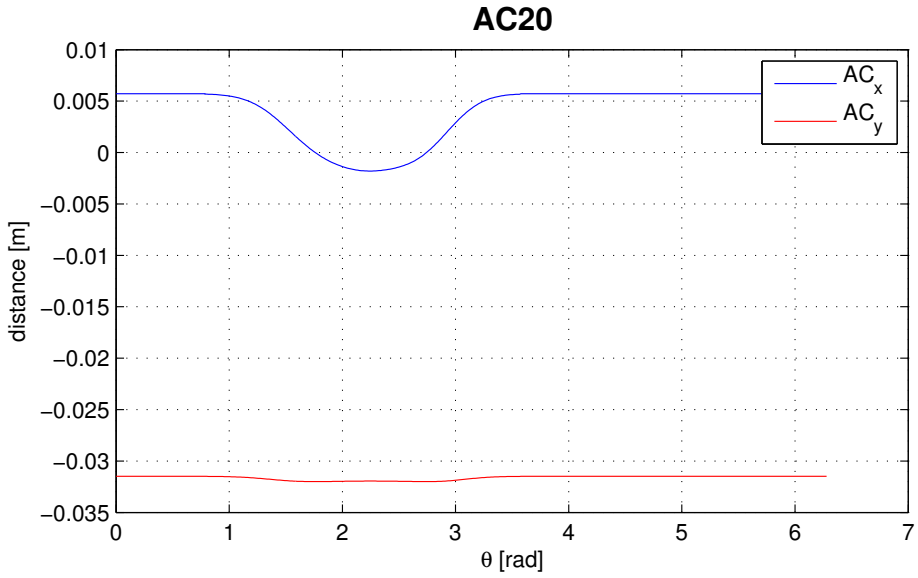

Figure 4.18: $\overrightarrow{AC_{20}}$ profile for the exhaust sub-system

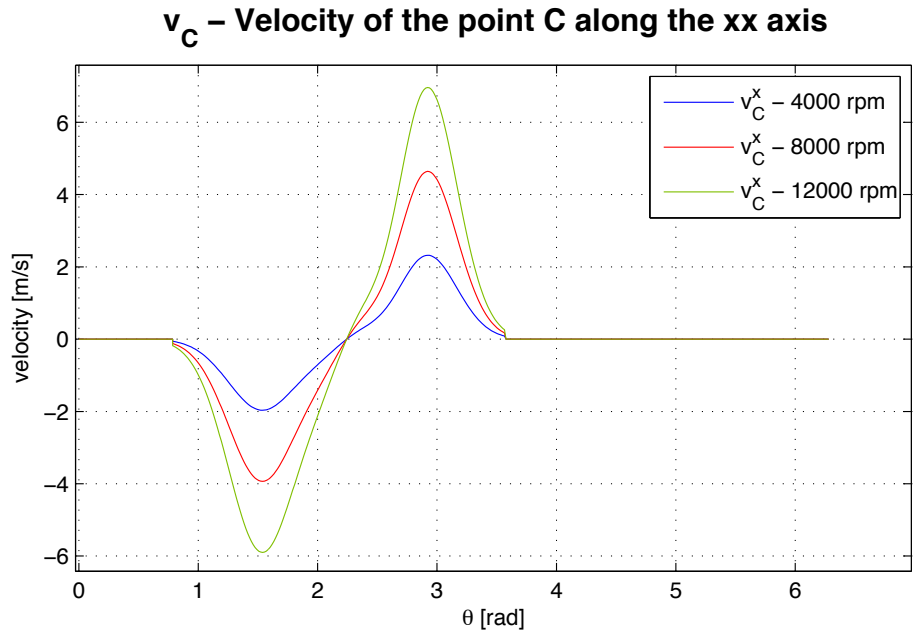

Figure 4.19: $\overrightarrow{v_{C10}^{x}} = \overrightarrow{v_{C20}^{x}}$ profile for the exhaust sub-system at various engine speeds

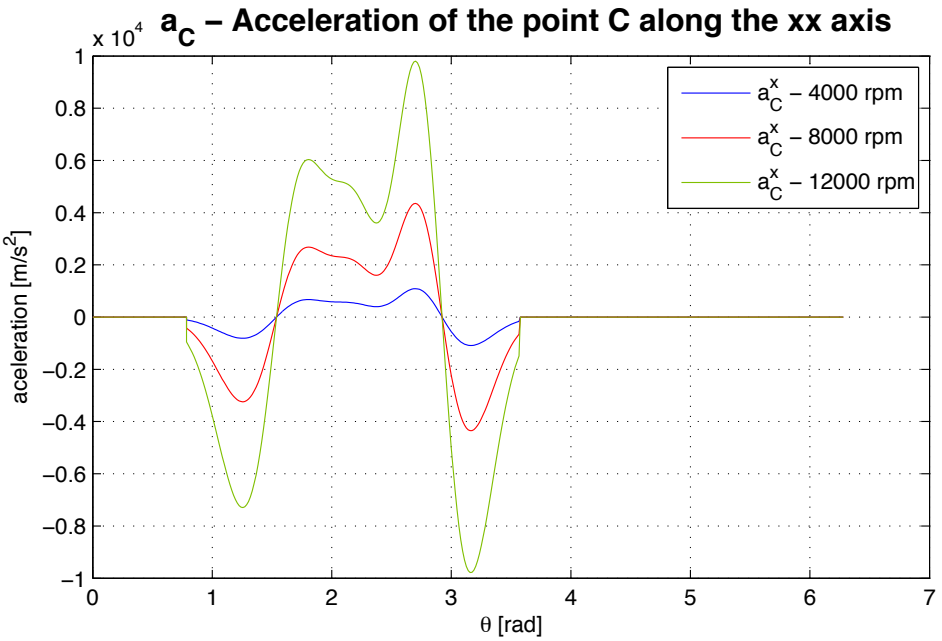

Figure 4.20: $\overrightarrow{a_{C10}^{x}} = \overrightarrow{a_{C20}^{x}}$ profile for the exhaust sub-system at various engine speeds

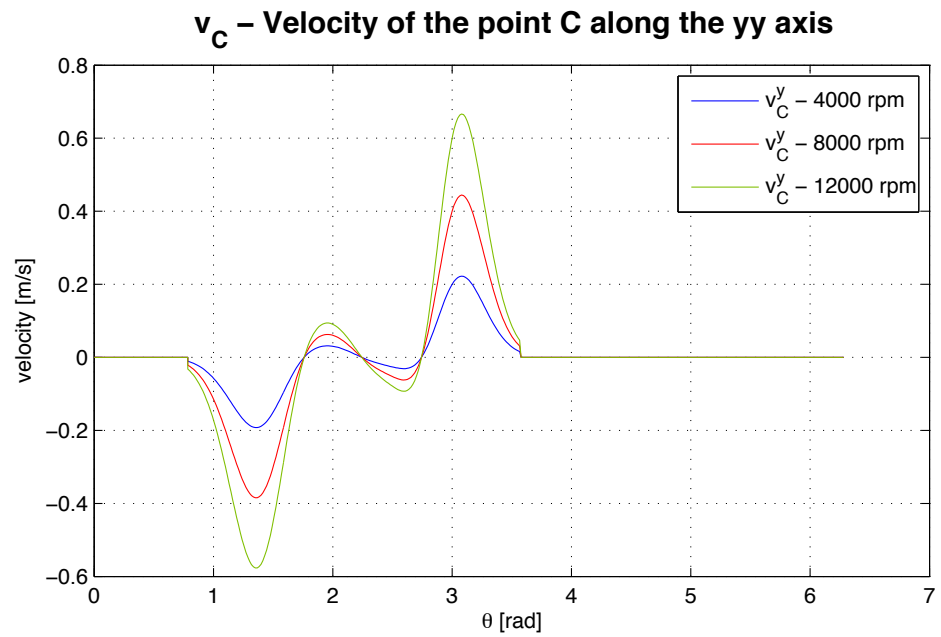

Figure 4.21: $\overrightarrow{v_{C_{10}^y}} = \overrightarrow{v_{C_{20}^y}}$ profile for the exhaust sub-system at various engine speeds

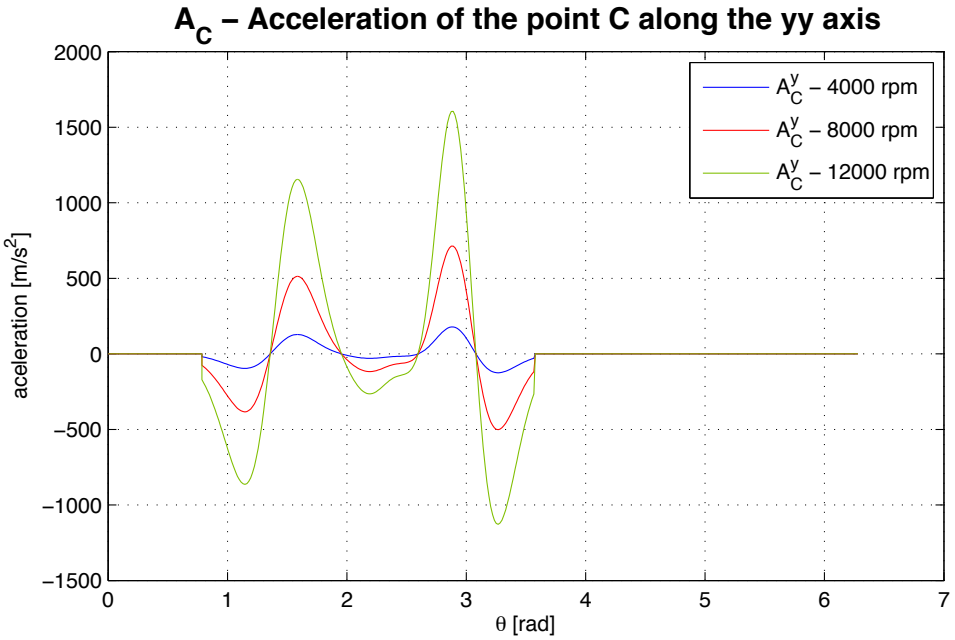

Figure 4.22: $\overrightarrow{a_{C_{10}^y}} = \overrightarrow{a_{C_{20}^y}}$ profile for the exhaust sub-system at various engine speeds

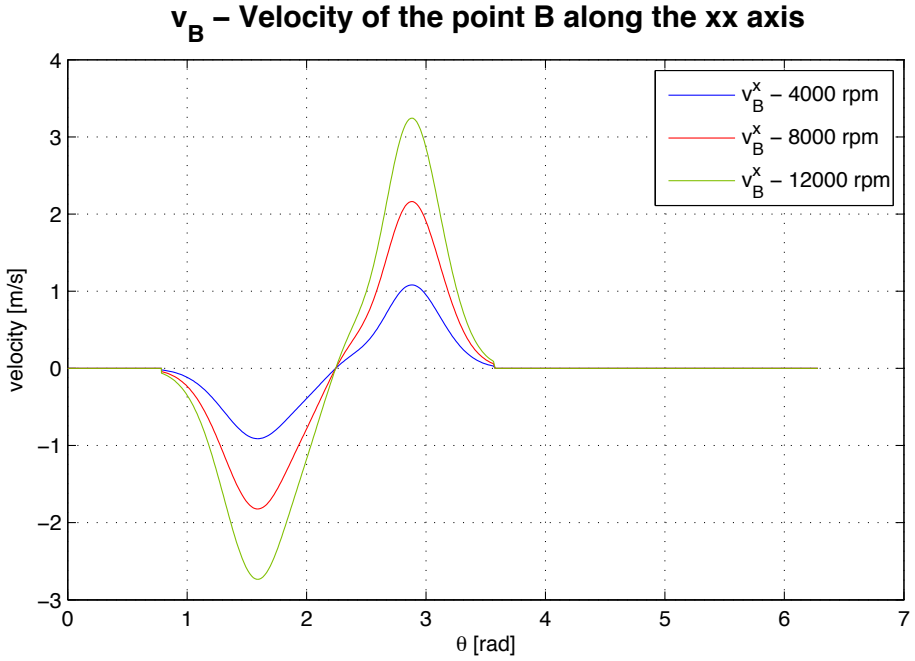

Figure 4.23: $\overrightarrow{v_{B_{20}^x}}$ profile for the exhaust sub-system at various engine speeds

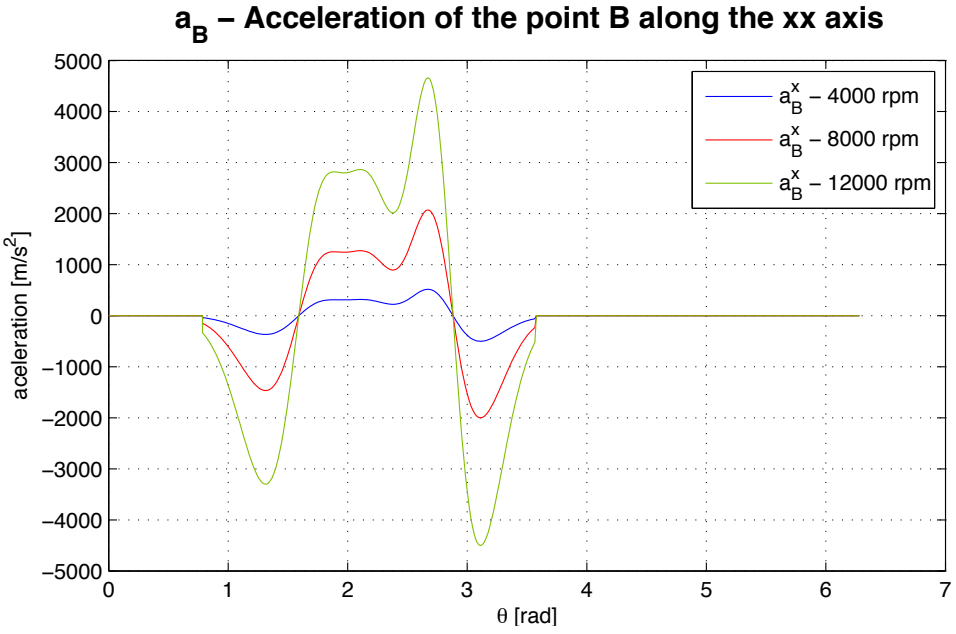

Figure 4.24: $\overrightarrow{a_{B_{20}^x}}$ profile for the exhaust sub-system at various engine speeds

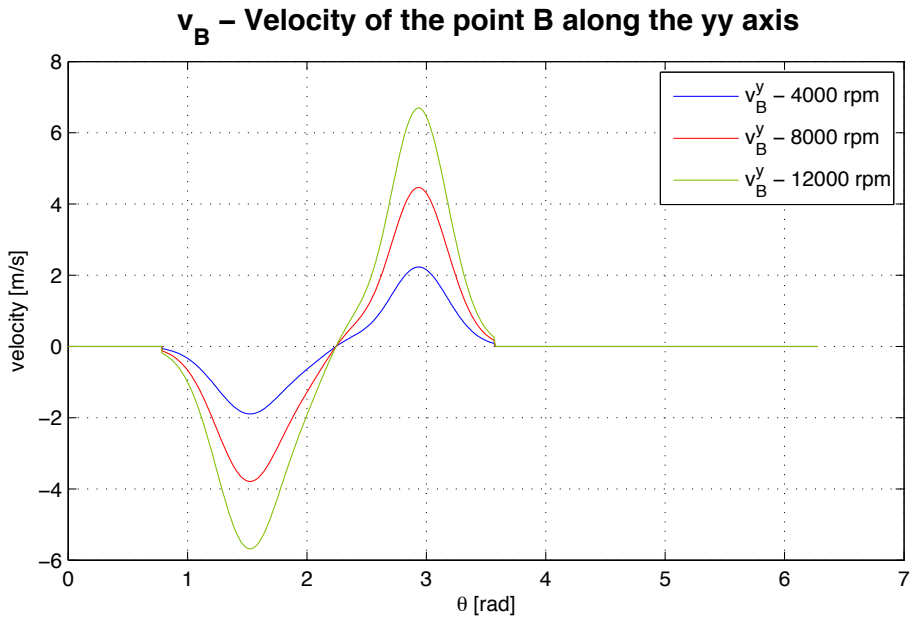

Figure 4.25: $\overrightarrow{v_{B_{20}}^{y}}$ profile for the exhaust sub-system at various engine speeds

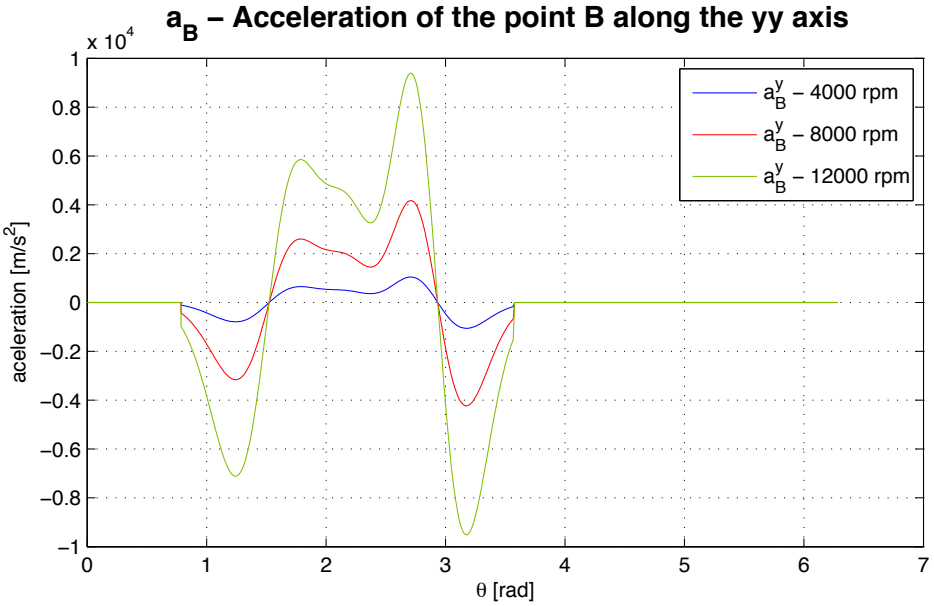

Figure 4.26: $\overrightarrow{a_{B_{20}}^{y}}$ profile for the exhaust sub-system at various engine speeds

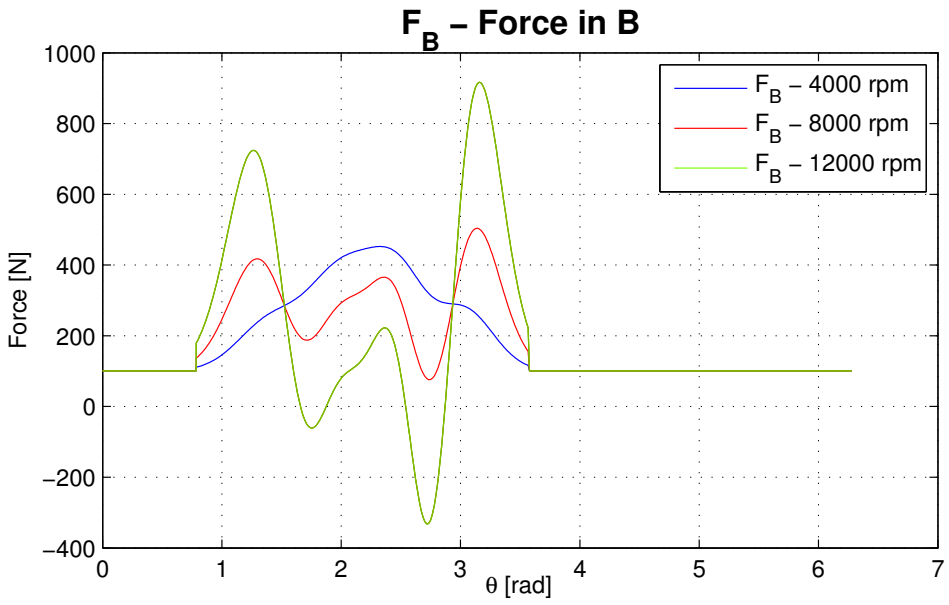

Figure 4.27: $\overrightarrow{F_B}$ profile for the exhaust sub-system at various engine speeds

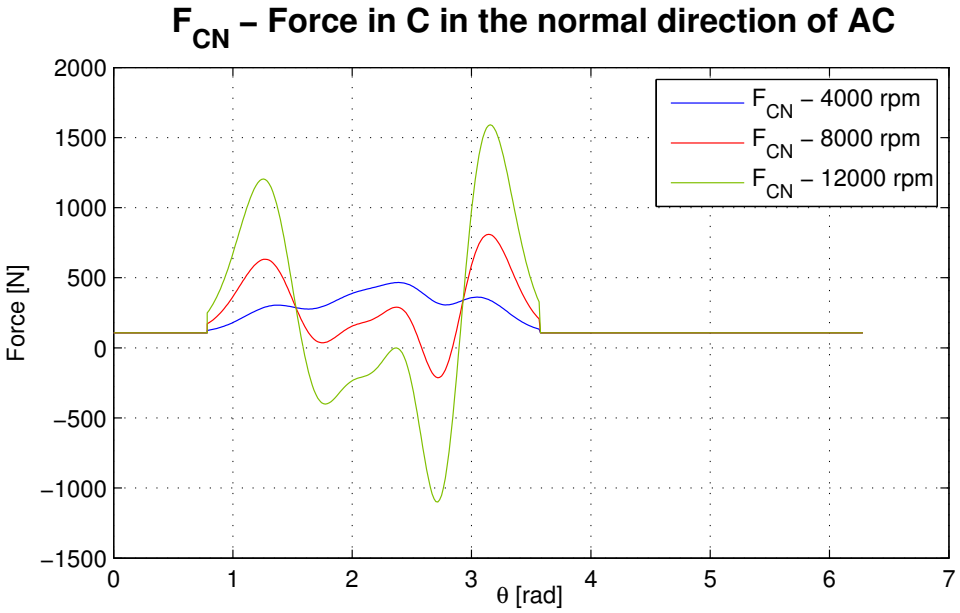

Figure 4.28: $\overrightarrow{F_{CN}}$ profile for the exhaust sub-system at various engine speeds

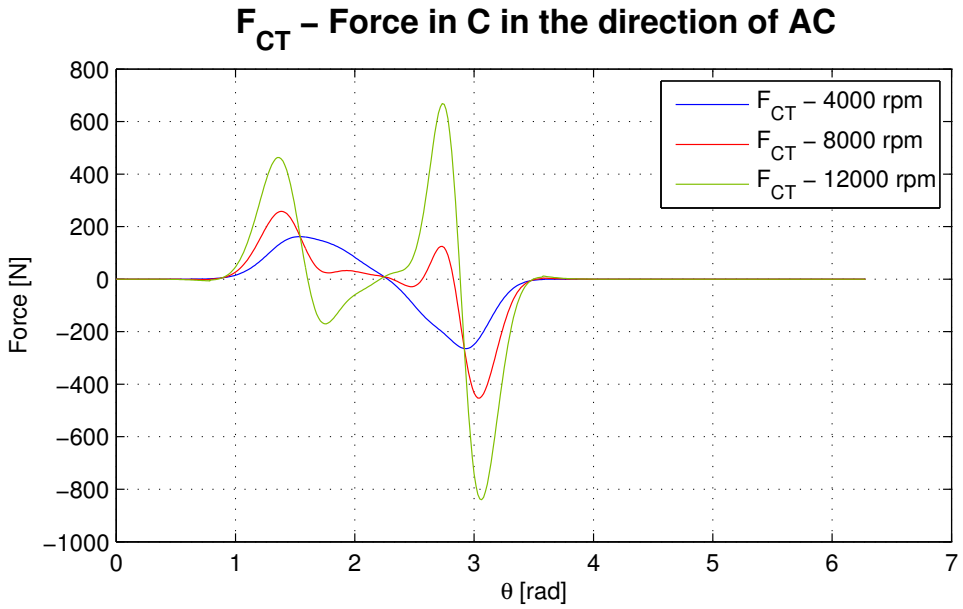

Figure 4.29: $\overrightarrow{F_{CT}}$ profile for the exhaust sub-system at various engine speeds

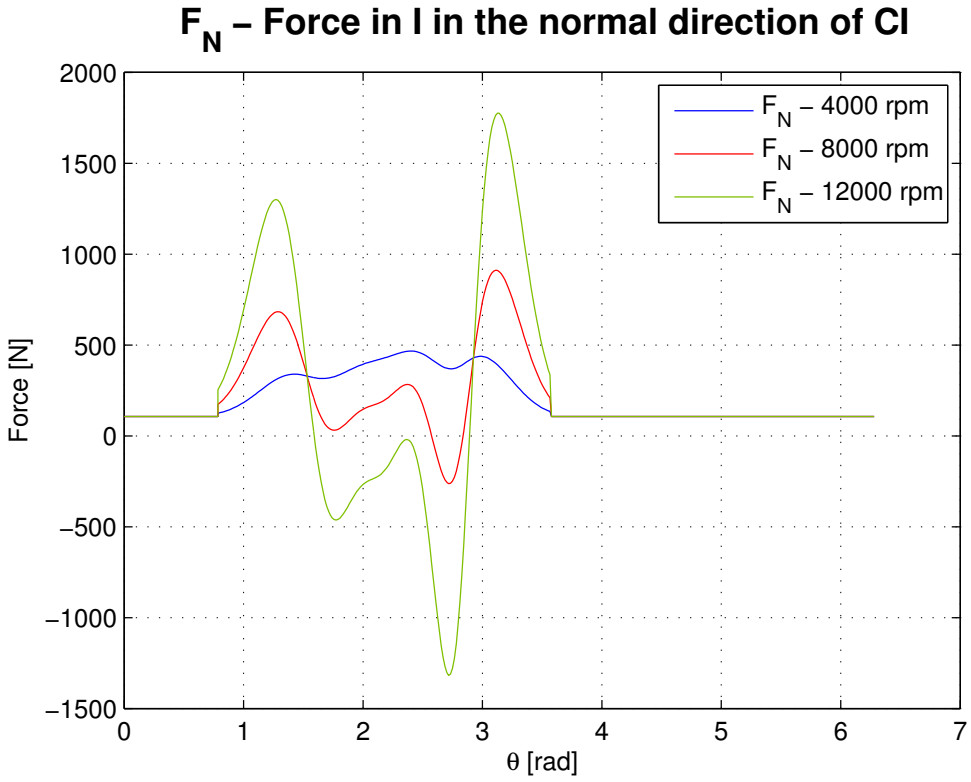

Figure 4.30: $\overrightarrow{F_N}$ profile for the exhaust sub-system at various engine speeds

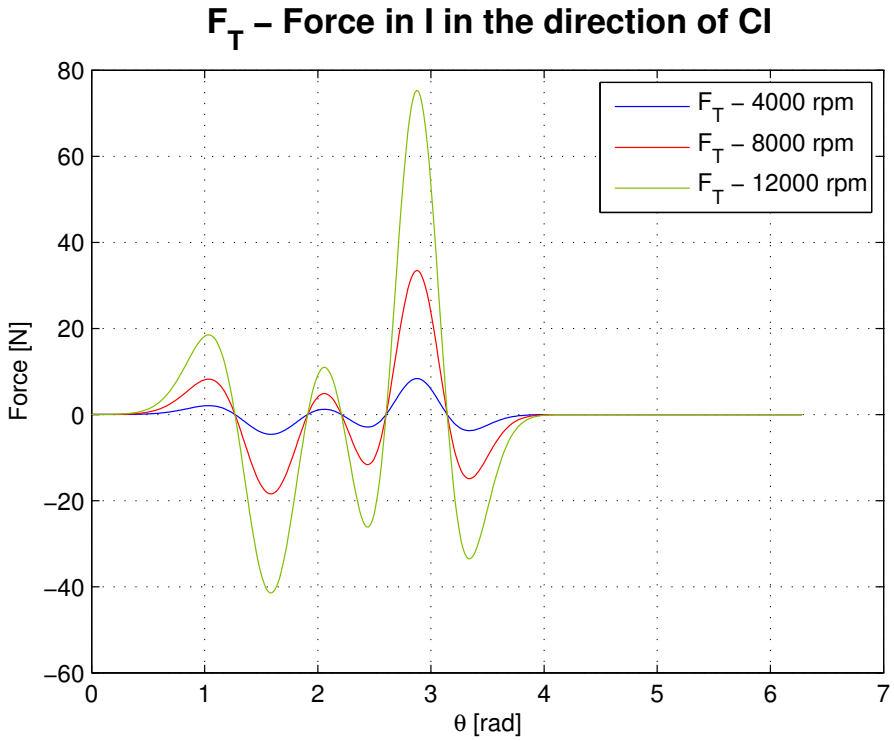

Figure 4.31: $\overrightarrow{F_T}$ profile for the exhaust sub-system at various engine speeds

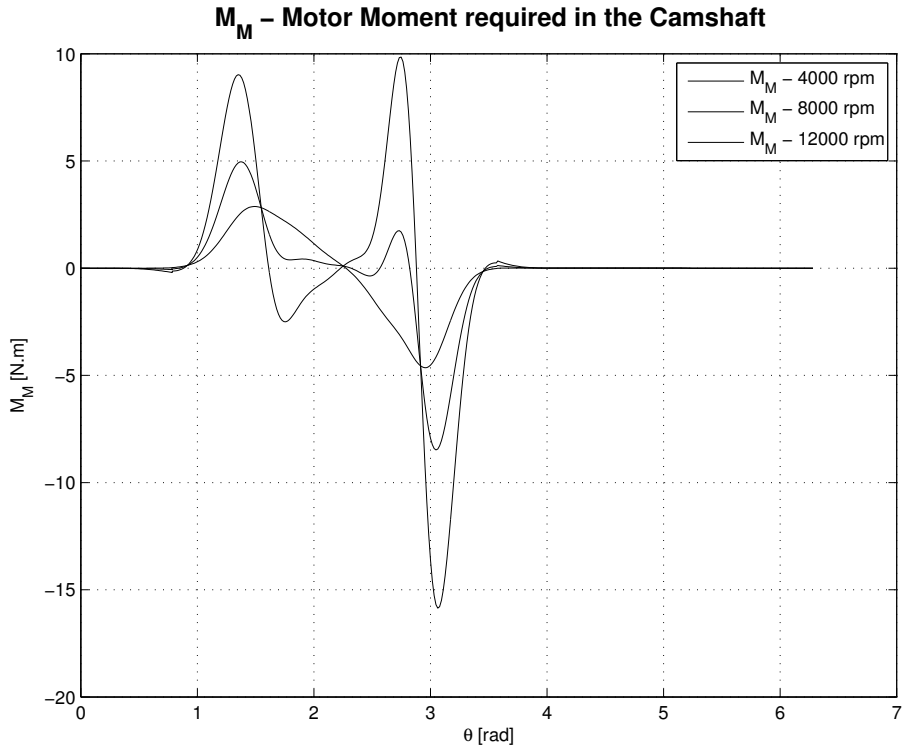

Figure 4.32: $\overrightarrow{M_m}$ profile for the exhaust sub-system at various engine speeds

4.3.2 Intake Sub-system

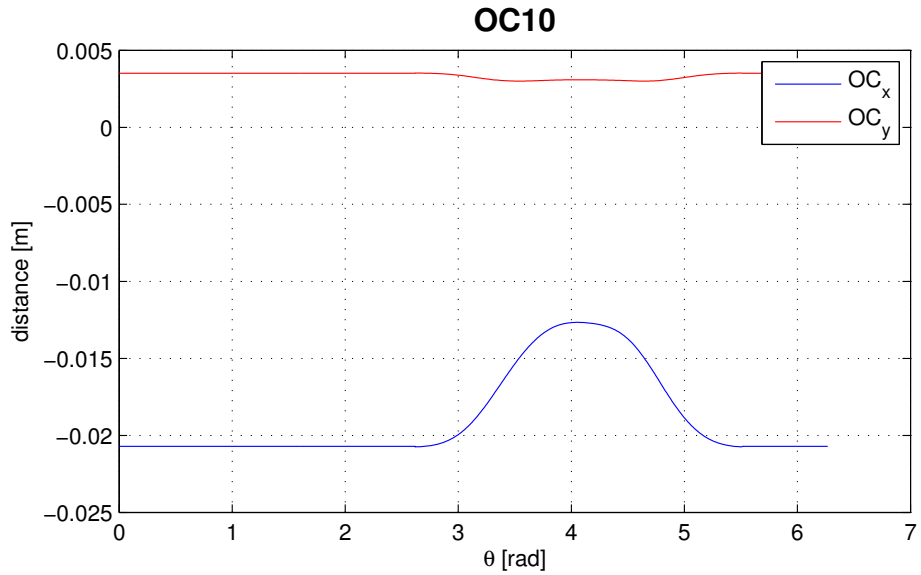

Figure 4.33: $\overrightarrow{OC_{10}}$ profile for the intake sub-system

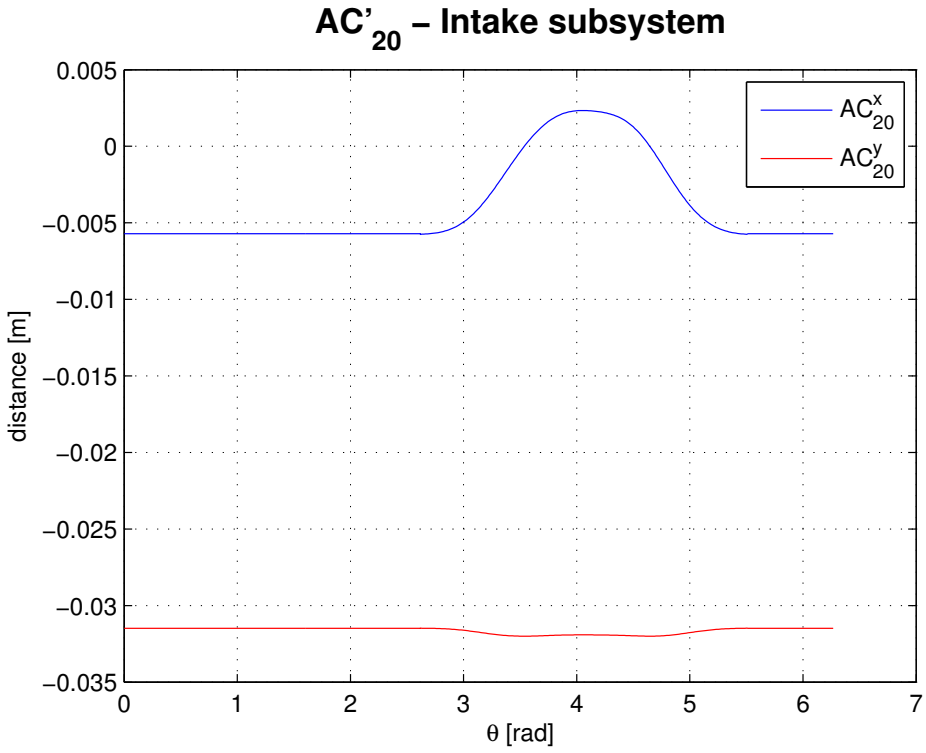

Figure 4.34: $\overrightarrow{AC_{20}}$ profile for the exhaust sub-system

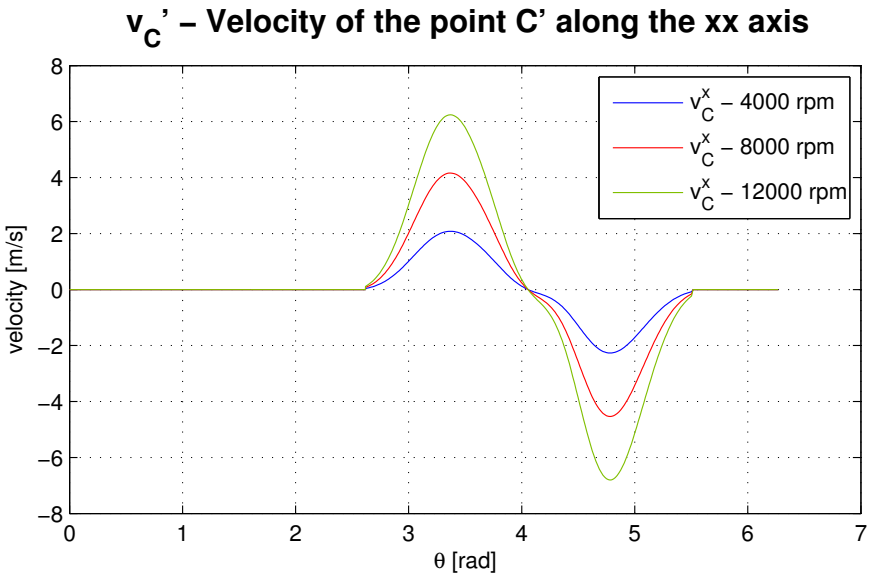

Figure 4.35: $\overrightarrow{v_{C10}^{x}} = \overrightarrow{v_{C20}^{x}}$ profile for the intake sub-system at various engine speeds

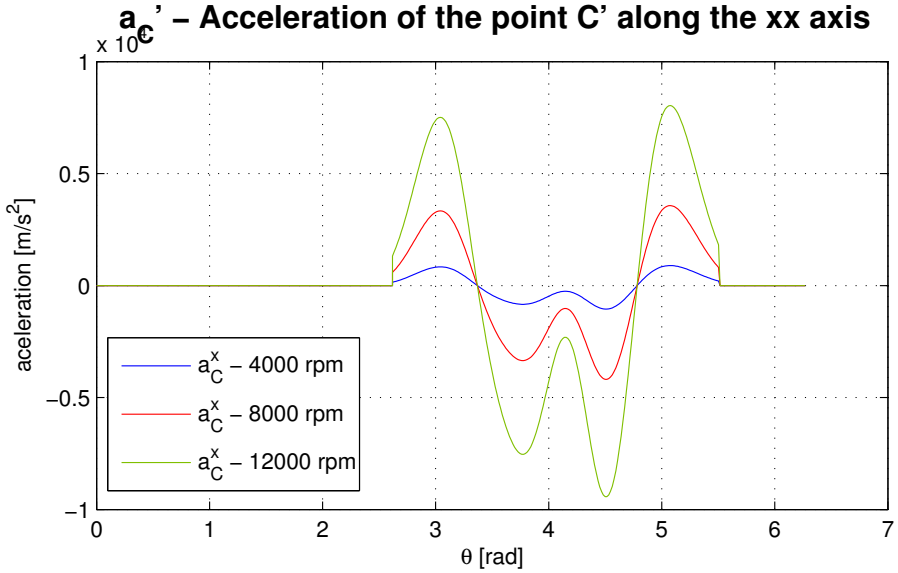

Figure 4.36: $\overrightarrow{a_{C10}^{x}} = \overrightarrow{a_{C20}^{x}}$ profile for the intake sub-system at various engine speeds

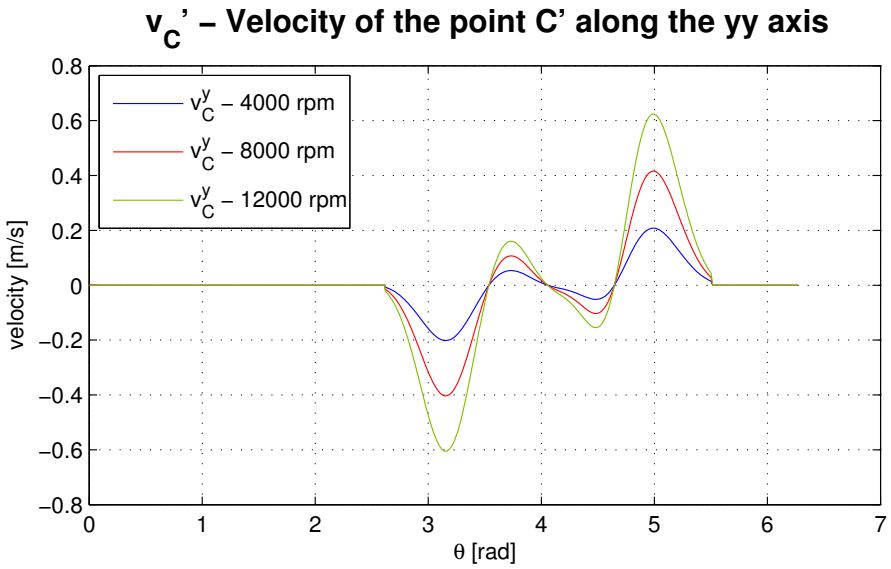

Figure 4.37: $\overrightarrow{v_{C'_{10}}^{y}} = \overrightarrow{v_{C'_{20}}^{y}}$ profile for the intake sub-system at various engine speeds

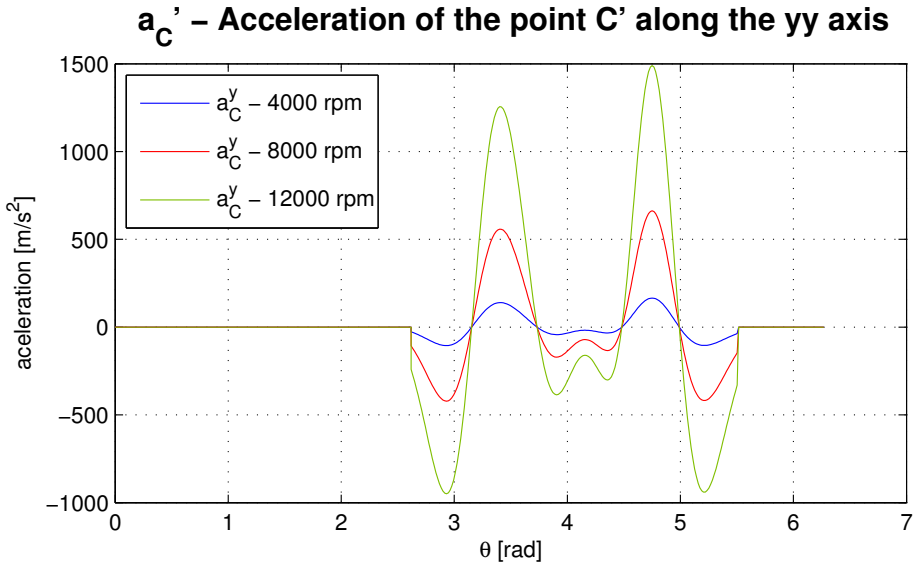

Figure 4.38: $\overrightarrow{a_{C'_{10}}^{y}} = \overrightarrow{a_{C'_{20}}^{y}}$ profile for the intake sub-system at various engine speeds

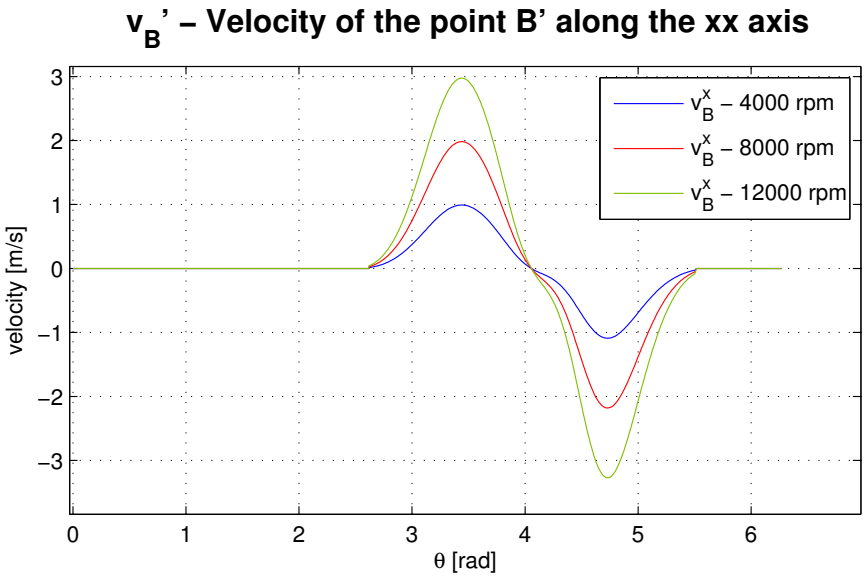

Figure 4.39: $\overrightarrow{v_{B'_{20}}^{x}}$ profile for the intake sub-system at various engine speeds

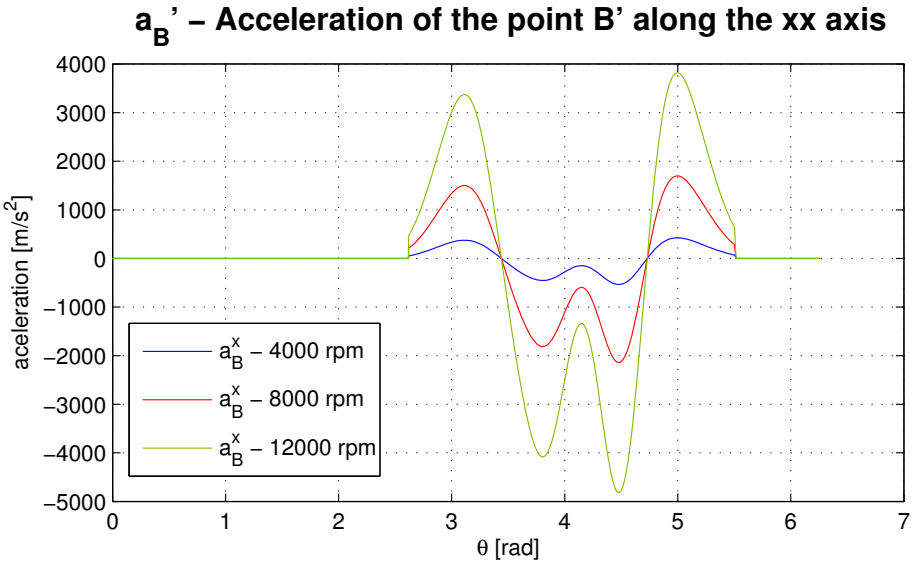

Figure 4.40: $\overrightarrow{a_{B'_{20}}^{x}}$ profile for the intake sub-system at various engine speeds

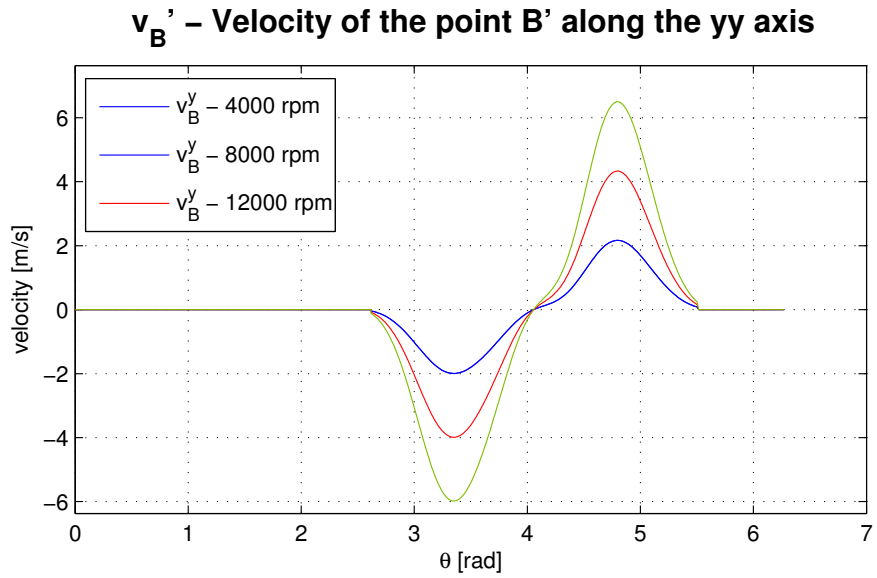

Figure 4.41: $\overrightarrow{v_{B'_{20}}^{y}}$ profile for the intake sub-system at various engine speeds

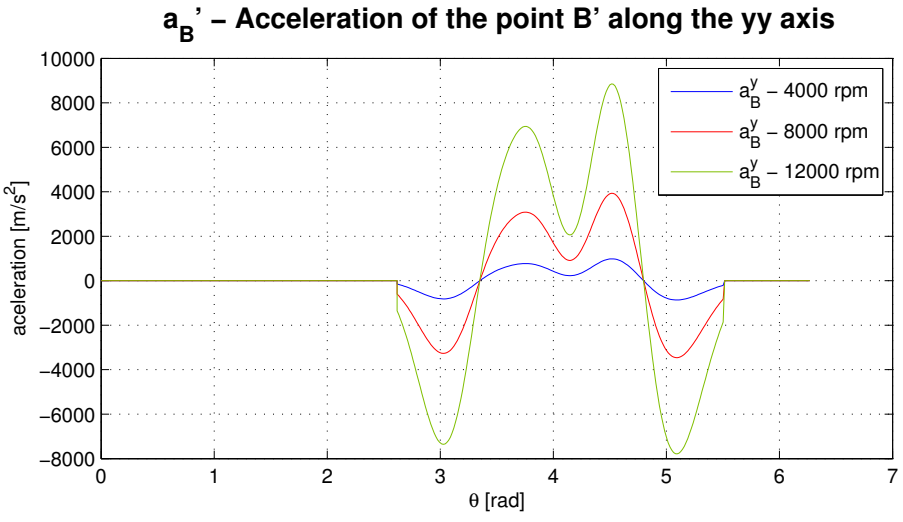

Figure 4.42: $\overrightarrow{a_{B'_{20}}^{y}}$ profile for the intake sub-system at various engine speeds

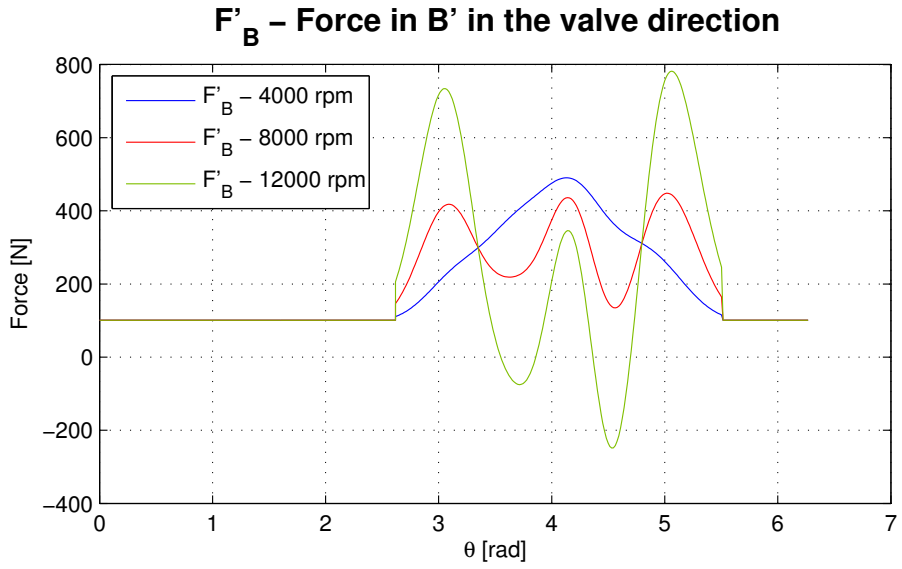

Figure 4.43: $\overrightarrow{F_B}$ profile for the intake sub-system at various engine speeds

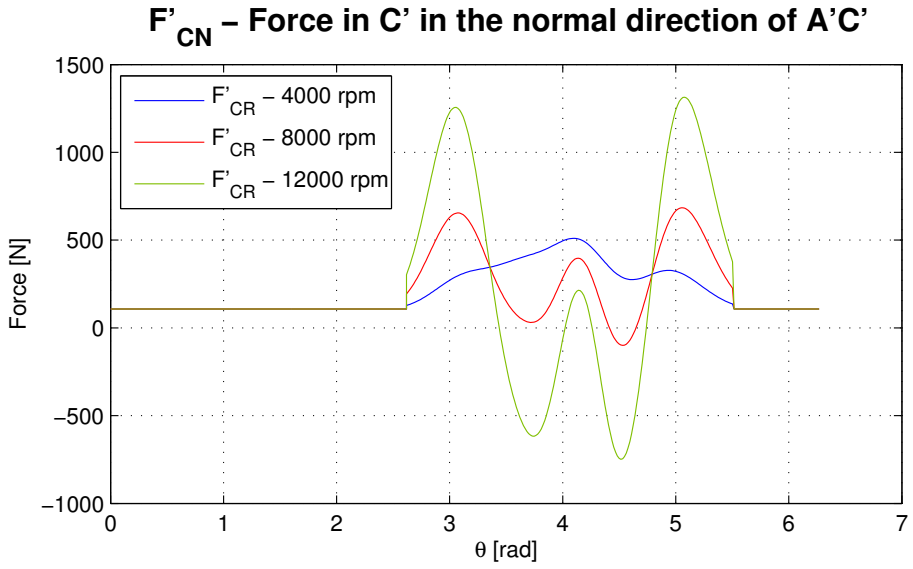

Figure 4.44: $\overrightarrow{F_{CN}}$ profile for the intake sub-system at various engine speeds

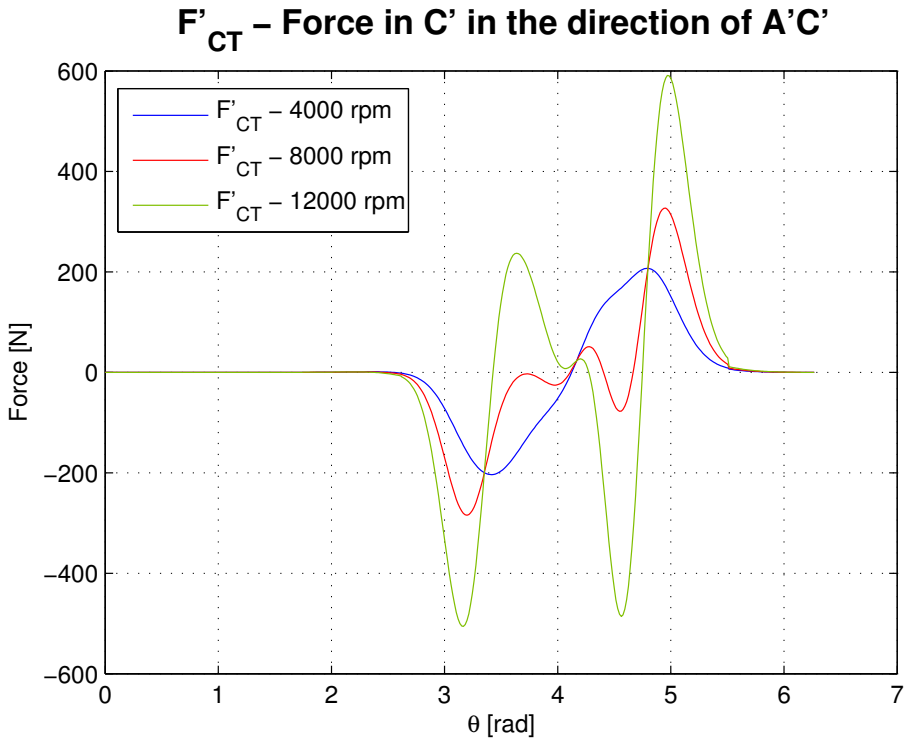

Figure 4.45: $\overrightarrow{F_{CT}}$ profile for the intake sub-system at various engine speeds

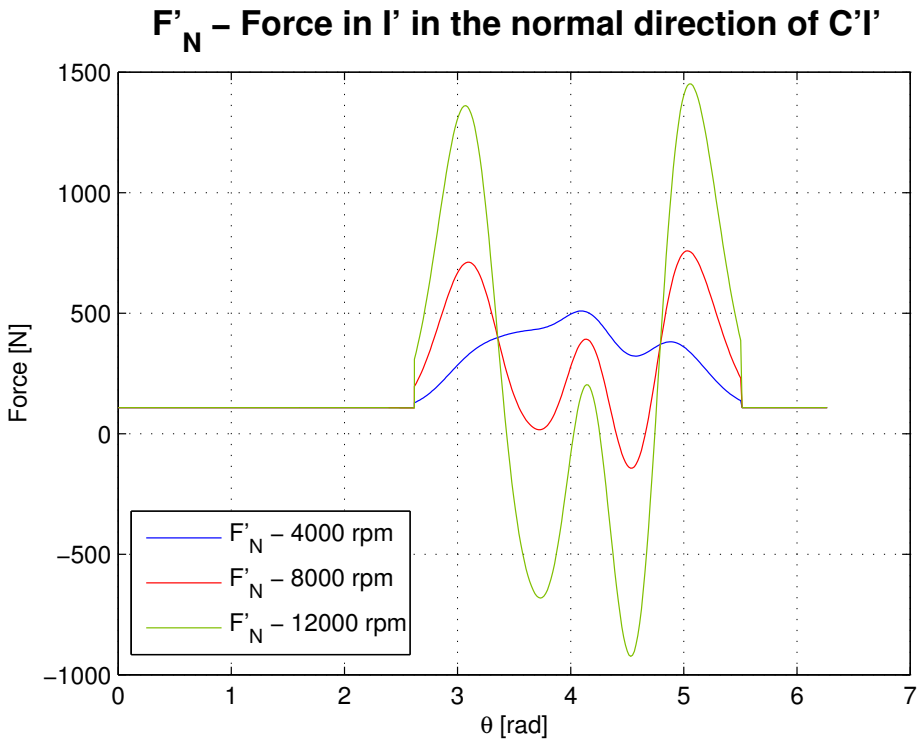

Figure 4.46: $\overrightarrow{F_N}$ profile for the intake sub-system at various engine speeds

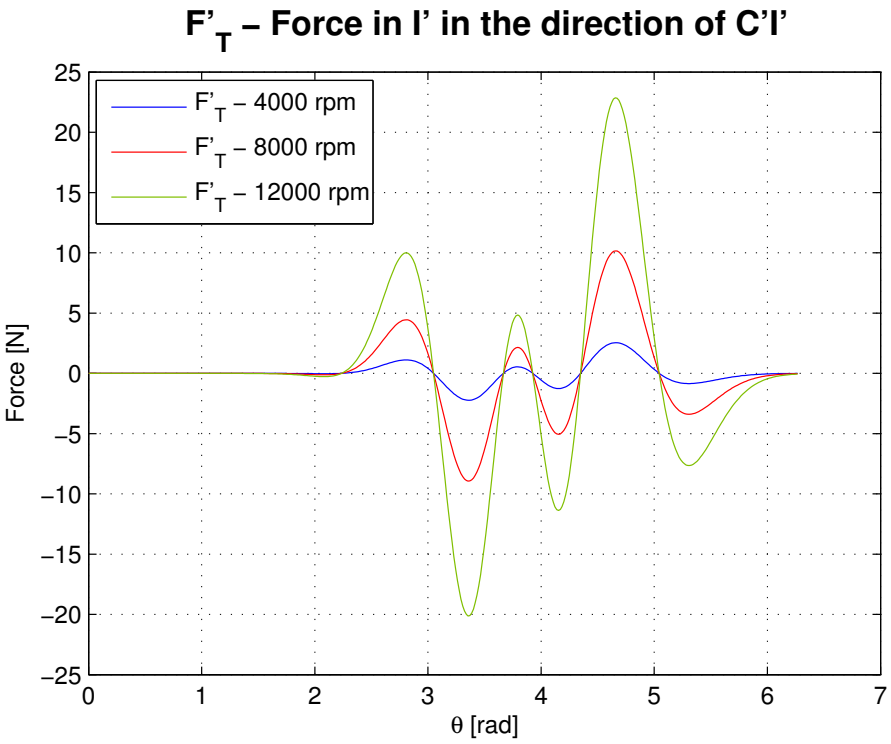

Figure 4.47: $\overrightarrow{F_T}$ profile for the intake sub-system at various engine speeds

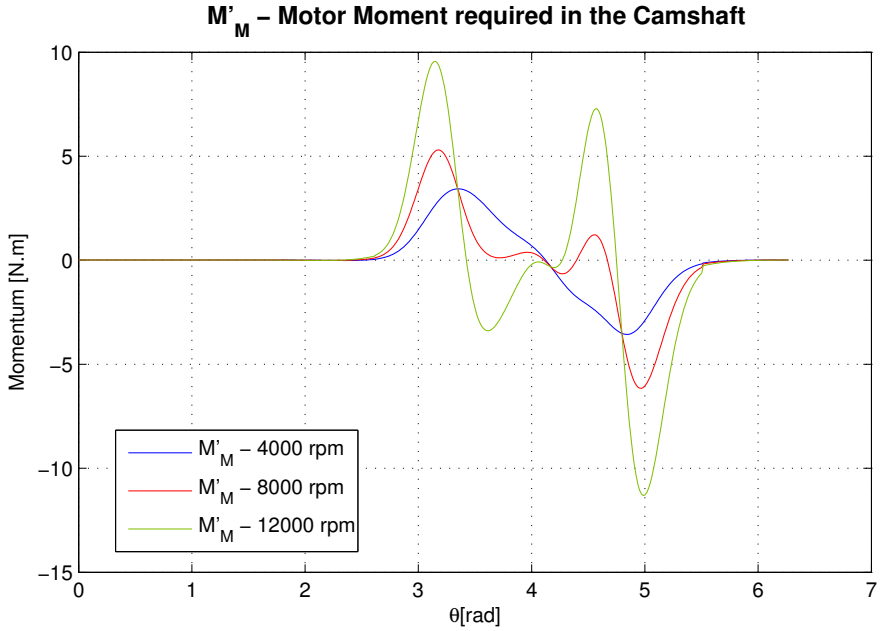

Figure 4.48: $\overrightarrow{M_m}$ profile for the intake sub-system at various engine speeds

The lift profiles (displacement, velocity and acceleration) generated by this system are consistent with the typical or theoretical lift profiles for a common valve train (see figure 4.12). It validates the design and its ability to perform the necessary function. In the following figures 4.13, 4.14, 4.15 and 4.16, the variation of these parameters are presented. This values are necessary in order to calculate the correct displacement, velocity, acceleration, force and momentum profiles that are presented, using the equations proposed above.

It's possible to observe that the lift for the intake system is slightly higher than the lift for the exhaust sub-system (see figure 4.12). This is designed to improve the air intake to the combustion chamber, improving the combustion process.

It's important to notice that the rise of the velocities and accelerations of the various components follows the increase in speed. Some accelerations can reach nearly $10000 m/s^2$. These values will directly influence the forces submitted on the components. The acceleration in the roller (points C and C') is higher in the xx axis than in the yy axis (see figures 4.24, 4.22, 4.36, 4.38). The opposite situation happens regarding points B and B', where the acceleration along the yy axis are significantly greater than the acceleration along the xx axis.

The rise in the speed of the engine also contributes to larger variation of speeds, accelerations and forces in some points, as it can be observed in figures 4.27 and 4.43. This is the result of the increased influence of the inertial forces (generated by the weight and acceleration of the components) that overcome the initial influence of the spring generated forces.

Comparing the intake and exhaust sub-system profiles, there are some differences that are worth mentioning.

The motor moment required for the intake sub-system is fairly different (see figure 4.64), especially in the middle of the intake lift cycle. But it maintains the spike values shown in the exhaust sub-system, as well as the scale of the values. However, it varies significantly in the middle of the cycle.

The tangential forces of contact between the rollers (F_T and F'_T) and the cam, see figures 4.47 and 4.31, only depend on the rotational speed and acceleration of the

rollers. Since the velocity and acceleration of rotation of the rollers ($\dot{\gamma}$ and $\ddot{\gamma}$) were determined considering a perfect rolling between surfaces (which may not occur in practical terms), these profiles might be imperfect.

Despite these differences, the generated profiles are fairly similar, even with the theoretical profiles presented in chapter 2, which helps to validate the constructive solution adopted for the Innercam.

It's also important to notice the profiles for the normal force actuating in the surface of the roller, F_N. Although the calculated profiles show a negative value for the force actuated, in physical terms, this negative value doesn't exists. It only represents the change in the direction of the force as well as the alteration of the contact point between the roller and the cam profile.

Since the contact point has changed, so has the equilibrium equations that need to take into account the different distance between the origin and the point of contact as well as the direction of the forces actuating and the rotation direction of the roller .

4.4 Influence of engine acceleration in the valve train dynamics

Since the engine is not designed to work at a constant speed, the acceleration of the engine (either positive or negative) plays an important role on the dynamics of the motorcycle. Therefore, it's important to test the influence of the engine acceleration on the force and acceleration profiles for the main points of the InnerCam.

Previously, all profiles were generated taking into consideration a constant engine speed. The following graphics will compare those profiles with the ones with the same speed but with an imposed acceleration. To have an idea about the typical acceleration values imposed on the engine, we asked AJP Motos SA about the values that would be appropriate to test these profiles. They suggested the value of 125 rad/s^2 since it allows an engine at 2500 rpm to reach 12000 rpm in about 4 seconds.

The following graphics are presented to compare the profiles generated for a constant speed and the profiles generated for the same speed but with an acceleration present. Specifically, the graphics present profiles for the points C, B and G_3 acceleration at 4000 rpm and 12000 rpm, in order to verify the influence of the acceleration in low and high engine speeds. It's also presented profiles for relevant forces applied in the system.

On figures 4.49, 4.50, 4.51, 4.52, 4.53 and 4.54, the green and black profiles are overlapping the blue and red profiles, respectively. On the force profiles (figures 4.55, 4.56, 4.57, 4.58, 4.59, 4.60) the red profiles overlap the blue profiles. This proves that the engine acceleration has no impact on the components acceleration or on the forces applied in it, since these profiles are identical.

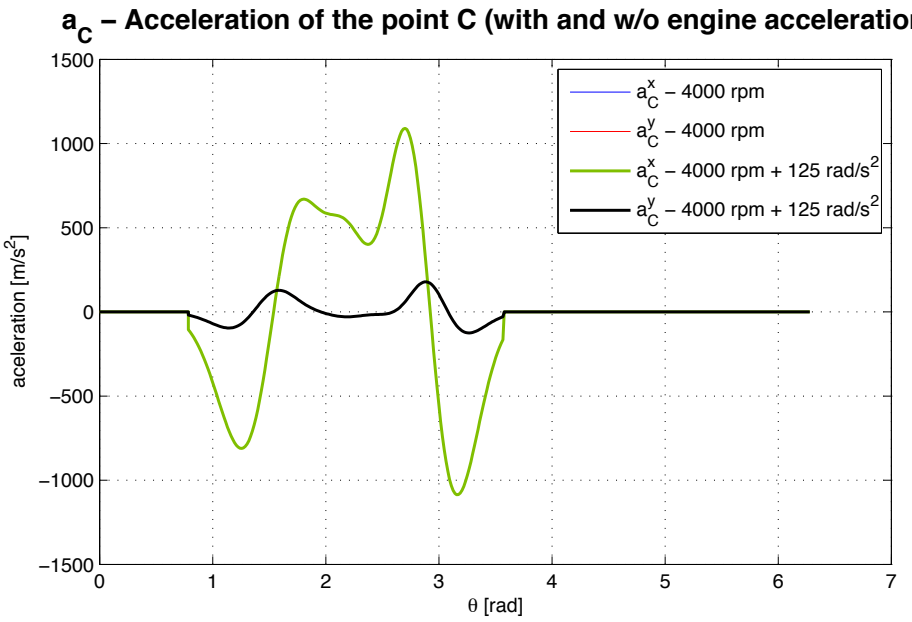

Figure 4.49: $\overrightarrow{a_C}$ profiles comparison of a constant speed vs. speed and acceleration - 4000 rpm

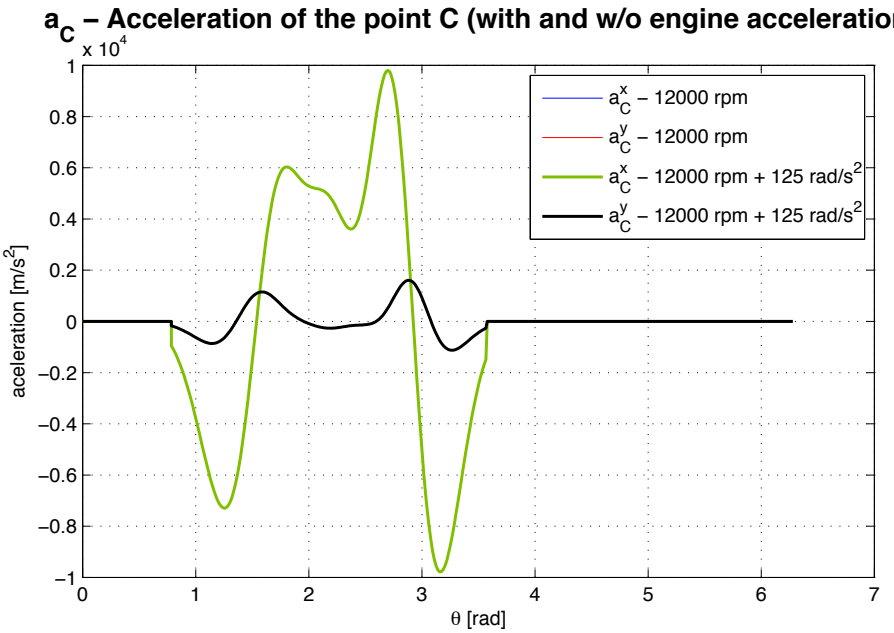

Figure 4.50: $\overrightarrow{a_C}$ profile for the intake sub-system at various engine speeds - 12000 rpm

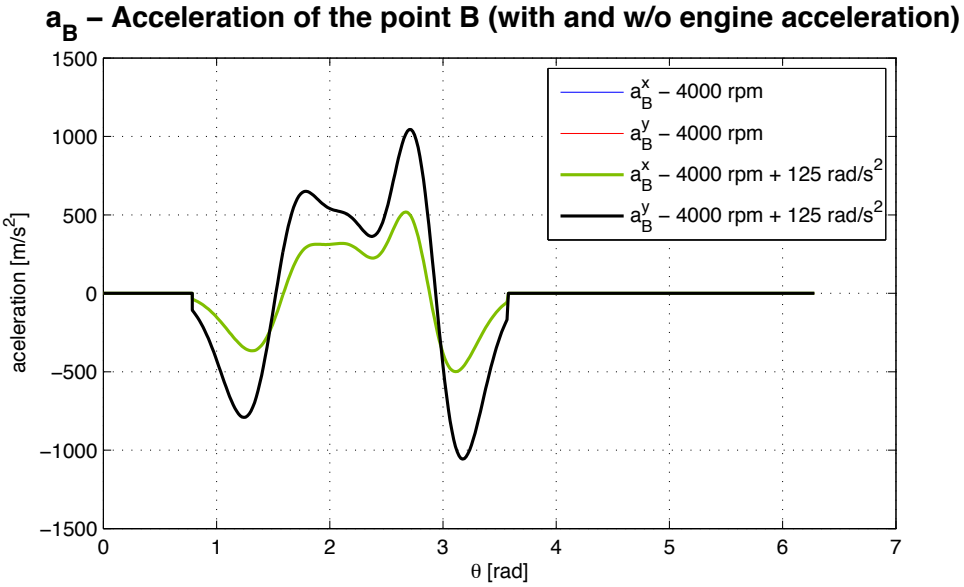

Figure 4.51: $\overrightarrow{a_B}$ profiles comparison of a constant speed vs. speed and acceleration - 4000 rpm

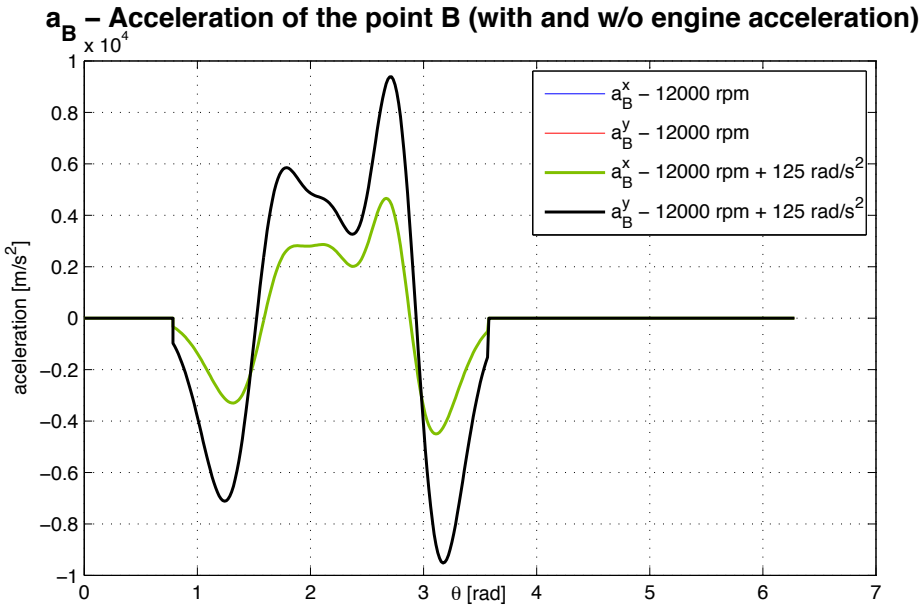

Figure 4.52: $\overrightarrow{a_B}$ profiles comparison of a constant speed vs. speed and acceleration - 12000 rpm

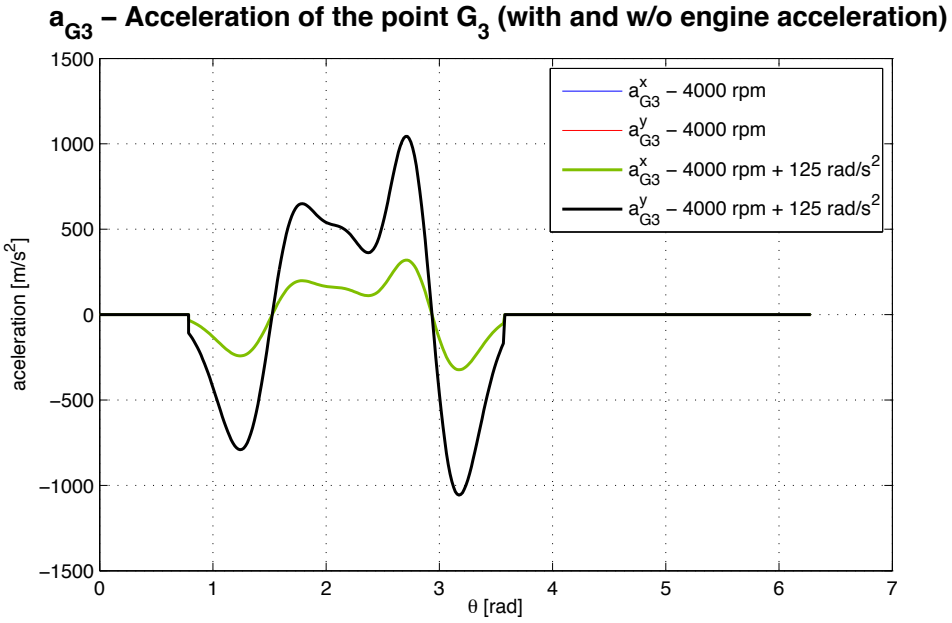

Figure 4.53: $\overrightarrow{a_{G_3}}$ profiles comparison of a constant speed vs. speed and acceleration - 4000 rpm

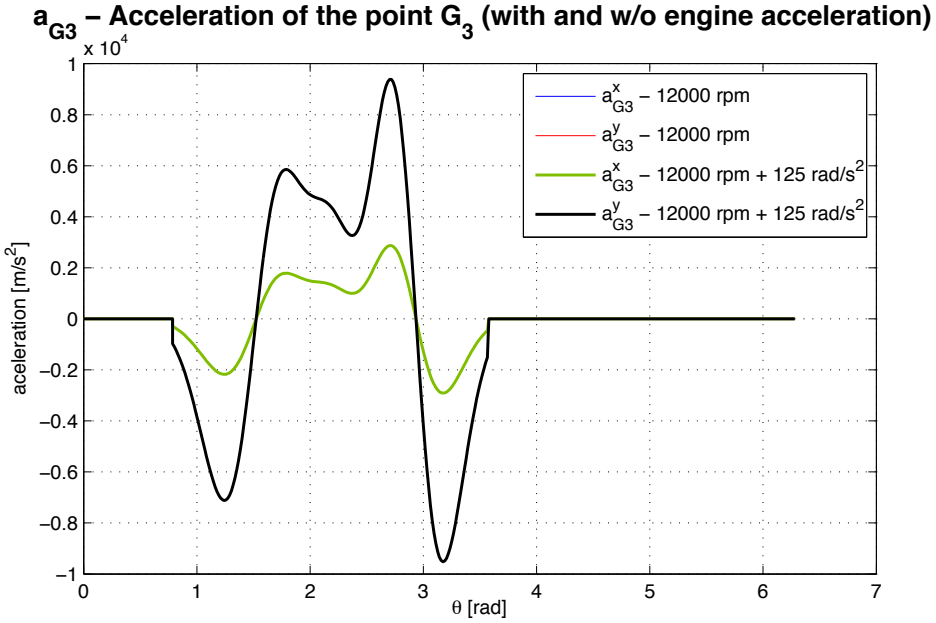

Figure 4.54: $\overrightarrow{a_{G_3}}$ profiles comparison of a constant speed vs. speed and acceleration - 12000 rpm

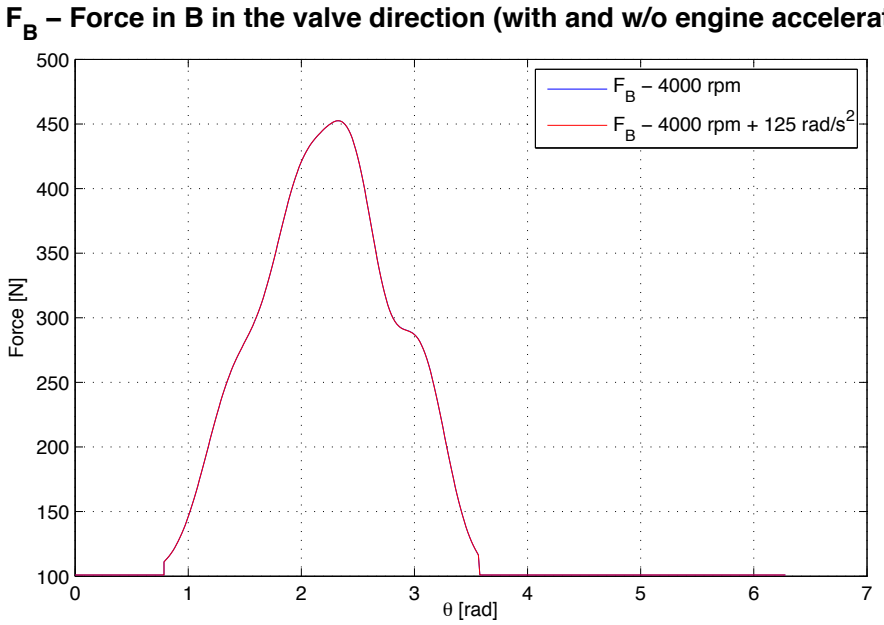

Figure 4.55: $\overrightarrow{F_B}$ profiles comparison of a constant speed vs. speed and acceleration - 4000 rpm

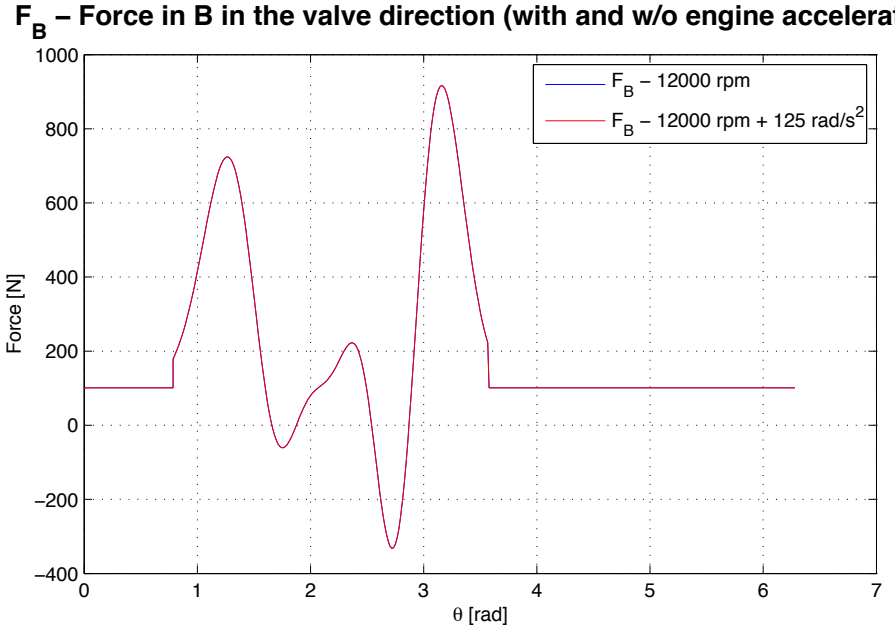

Figure 4.56: $\overrightarrow{F_B}$ profiles comparison of a constant speed vs. speed and acceleration - 12000 rpm

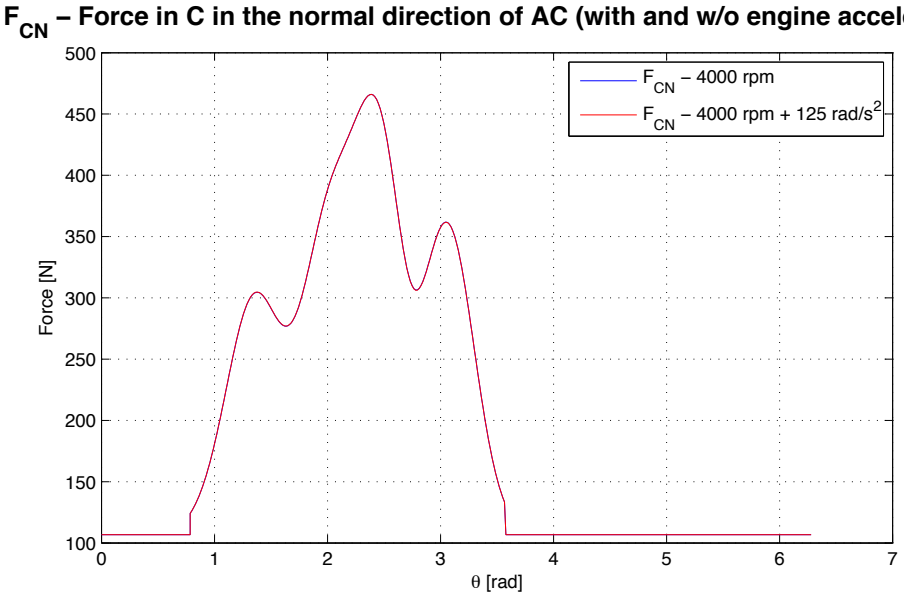

Figure 4.57: $\overrightarrow{F_{CN}}$ profiles comparison of a constant speed vs. speed and acceleration - 4000 rpm

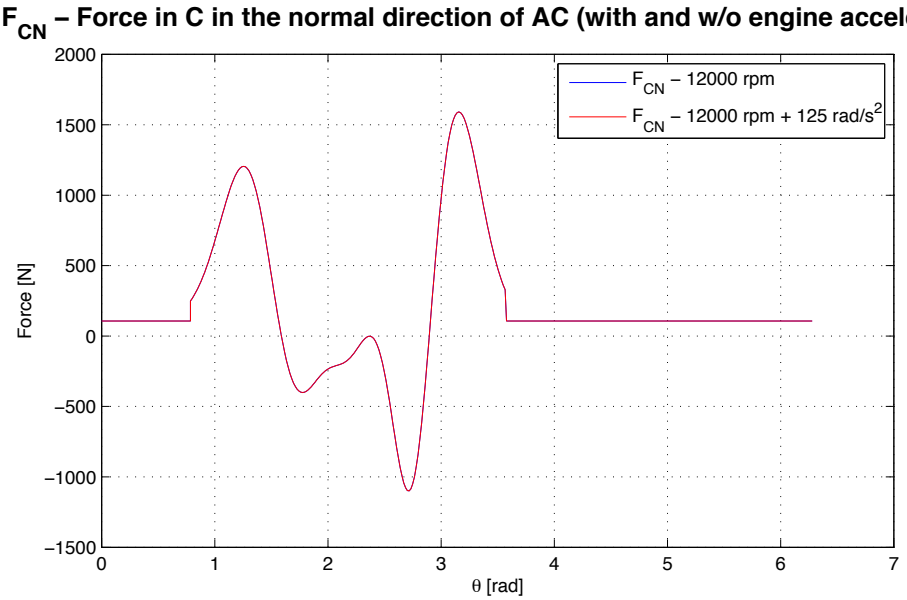

Figure 4.58: $\overrightarrow{F_{CN}}$ profiles comparison of a constant speed vs. speed and acceleration - 12000 rpm

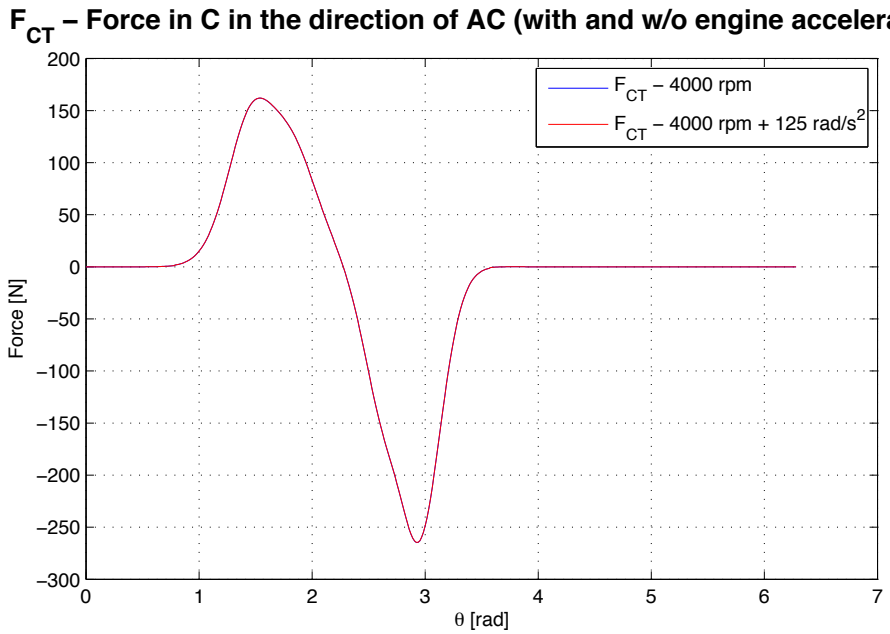

Figure 4.59: $\overrightarrow{F_{CT}}$ profiles comparison of a constant speed vs. speed and acceleration - 4000 rpm

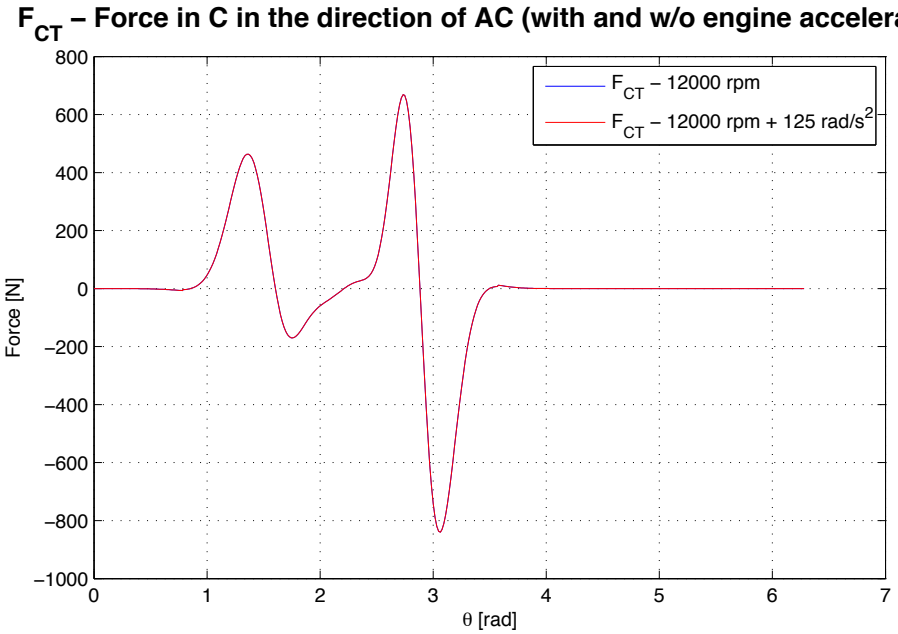

Figure 4.60: $\overrightarrow{F_{CT}}$ profiles comparison of a constant speed vs. speed and acceleration - 12000 rpm

4.5 Influence of variable point of contact between the cam and roller

In order to fully understand the influence of the variation of the point of contact between the roller and the cam, a new set of equilibrium equations were defined for the new dynamic balance. These equations will only be used to calculate the dynamic equilibrium for all the points in the normal cycle of the sub-system in which the value for the contact force F_N is negative or null. Only then it makes sense to use a different set of equations since the dynamic equilibrium has shifted to take into account the changing of the point of contact.

For the purposes of this study, the new equations were only determined for the exhaust sub-system. The behaviour between the two systems will be very similar, so there is no need to repeat the process. The new dynamic equilibrium (described by equations 4.61 and 4.64) will only affect the equations for the cam (body 1) and the roller (body 4) and this new equilibrium can be represented by the following figure and equations:

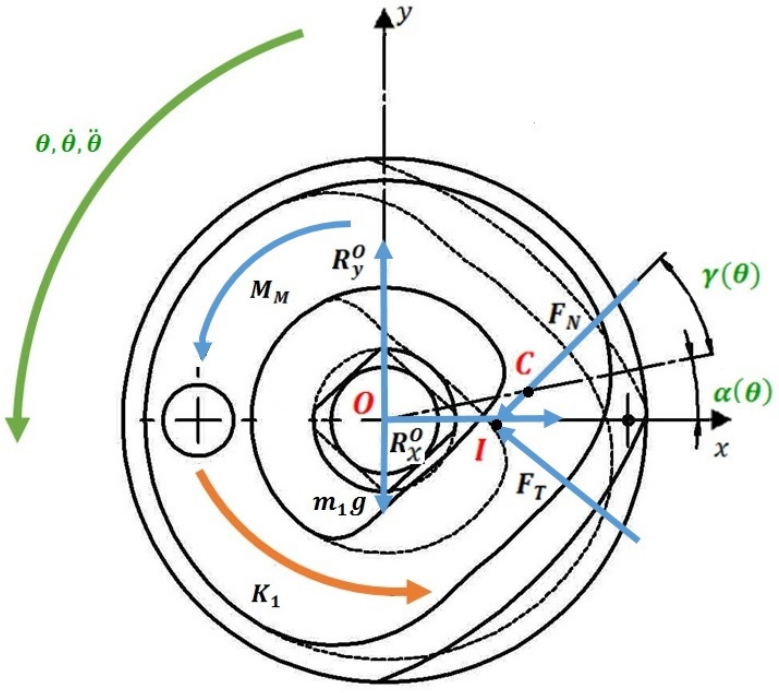

Figure 4.61: Free body diagram of the camshaft

$$\sum \overrightarrow{F_1} = \dot{\overrightarrow{Q_1}} \Leftrightarrow \begin{Bmatrix} 0 \\ -m_1 g \\ 0 \end{Bmatrix} + \begin{Bmatrix} -F_N \cos(\alpha+\gamma) \\ -F_N \sin(\alpha+\gamma) \\ 0 \end{Bmatrix} + \begin{Bmatrix} -F_T \sin(\alpha+\gamma) \\ F_T \cos(\alpha+\gamma) \\ 0 \end{Bmatrix} + \begin{Bmatrix} R_O^x \\ R_O^y \\ 0 \end{Bmatrix} = \overrightarrow{0} \Leftrightarrow \tag{4.61}$$

$$\begin{cases} R_O^x = F_T \sin(\alpha+\gamma) + F_N \cos(\alpha+\gamma) & (4.62) \\ R_O^y = m_1 g - F_T \cos(\alpha) + F_N \sin(\alpha+\gamma) & (4.63) \end{cases}$$

$$\begin{aligned} \sum \overrightarrow{M_1} = \overrightarrow{K_O^1} \Leftrightarrow & \begin{Bmatrix} \overline{OI_x} \\ \overline{OI_y} \\ 0 \end{Bmatrix} \times \begin{Bmatrix} -F_N \cos(\alpha+\gamma) \\ -F_N \sin(\alpha+\gamma) \\ 0 \end{Bmatrix} + \\ + & \begin{Bmatrix} \overline{OI_x} \\ \overline{OI_y} \\ 0 \end{Bmatrix} \times \begin{Bmatrix} -F_T \sin(\alpha+\gamma) \\ F_T \cos(\alpha+\gamma) \\ 0 \end{Bmatrix} + \begin{Bmatrix} 0 \\ 0 \\ Mm \end{Bmatrix} = \dot{\overrightarrow{K_O^1}} \Leftrightarrow \end{aligned} \tag{4.64}$$

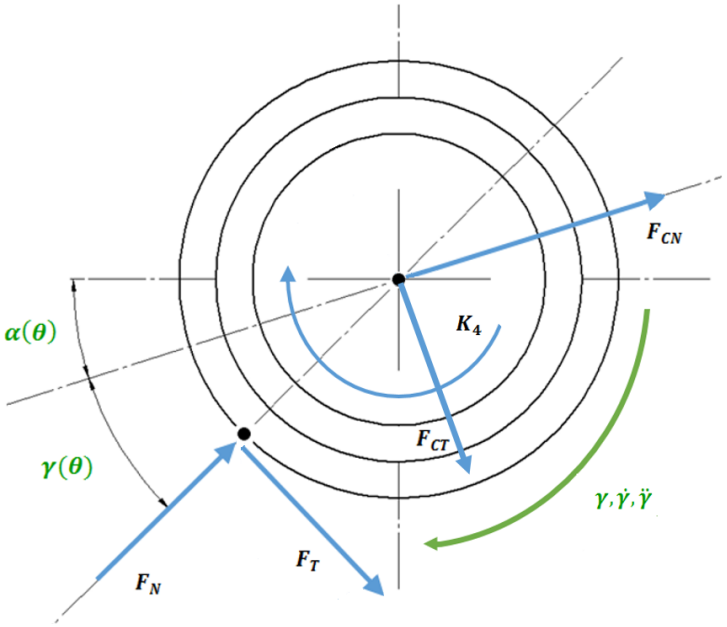

Figure 4.62: Free body diagram of the exhaust cam follower / roller with an internal point of contact

$$\begin{aligned}&\Leftrightarrow Mm = I_{zz}\ddot{\theta} - F_T[OI_x\cos(\alpha+\gamma)+OI_y\sin(\alpha+\gamma)]-\\&-F_N[OI_x\sin(\alpha+\gamma)-OI_y\cos(\alpha+\gamma)];\end{aligned} \tag{4.65}$$

$$\begin{aligned}&\sum\overrightarrow{F_4} = \dot{\overrightarrow{Q_4}} \Leftrightarrow \begin{Bmatrix} F_{CN}\cos(\alpha)\\ F_{CN}\sin(\alpha)\\ 0\end{Bmatrix} + \begin{Bmatrix} F_{CT}\sin(\alpha)\\ -F_{CT}\cos(\alpha)\\ 0\end{Bmatrix} + \begin{Bmatrix} F_N\cos(\alpha+\gamma)\\ F_N\sin(\alpha+\gamma)\\ 0\end{Bmatrix} +\\&+\begin{Bmatrix} F_T\sin(\alpha+\gamma)\\ -F_T\cos(\alpha+\gamma)\\ 0\end{Bmatrix} = m4\begin{Bmatrix} a_C^x\\ a_C^y\\ 0\end{Bmatrix}\end{aligned} \tag{4.66}$$

$$\begin{cases} F_{CN}\cos(\alpha)+F_{CT}\sin(\alpha)+F_N\cos(\alpha+\gamma)+F_T\sin(\alpha+\gamma) = m_4a_c^x & (4.67)\\ F_{CN}\sin(\alpha)-F_{CT}\cos(\alpha)+F_N\sin(\alpha+\gamma)-F_T\cos(\alpha+\gamma) = m_4a_c^y & (4.68)\end{cases}$$

$$\begin{aligned}&\sum\overrightarrow{M_4} = \overrightarrow{K_C^4} \Leftrightarrow \begin{Bmatrix} -\overline{CI}\cos(\alpha+\gamma)\\ -\overline{CI}\cos(\alpha+\gamma)\\ 0\end{Bmatrix} \times \begin{Bmatrix} F_N\cos(\alpha+\gamma)\\ F_N\sin(\alpha+\gamma)\\ 0\end{Bmatrix} +\\&+\begin{Bmatrix} -\overline{CI}\cos(\alpha+\gamma)\\ -\overline{CI}\cos(\alpha+\gamma)\\ 0\end{Bmatrix} \times \begin{Bmatrix} F_T\sin(\alpha+\gamma)\\ -F_T\cos(\alpha+\gamma)\\ 0\end{Bmatrix} = -Izz^4\ddot{\gamma}\end{aligned} \tag{4.69}$$

$$F_T = \frac{-Izz^4\ddot{\gamma}}{\overline{CI}} \tag{4.70}$$

It's possible to observe that the varying point of contact doesn't have a significant influence over the required torque, as it can be observed in figures 4.64 and 4.65 that describe identical profiles for various test conditions. However, it's possible to observe various points in which the point of contact shifts between the outer path and the inner path on the cam, as it can be observed through the change of profile colors in figure 4.63 that mean a different point of contact between surfaces. Each time the point of contact shifts, the rolling direction of the roller inverts.

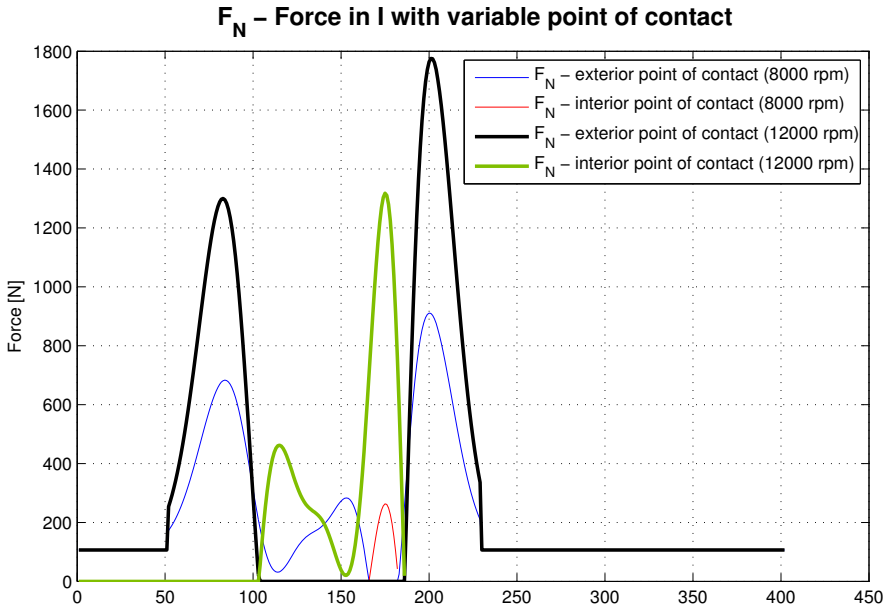

Figure 4.63: F_N profiles with variable point of contact

Each inversion could result in some drag between surfaces, accelerating the wear of the surface of the cam and roller.

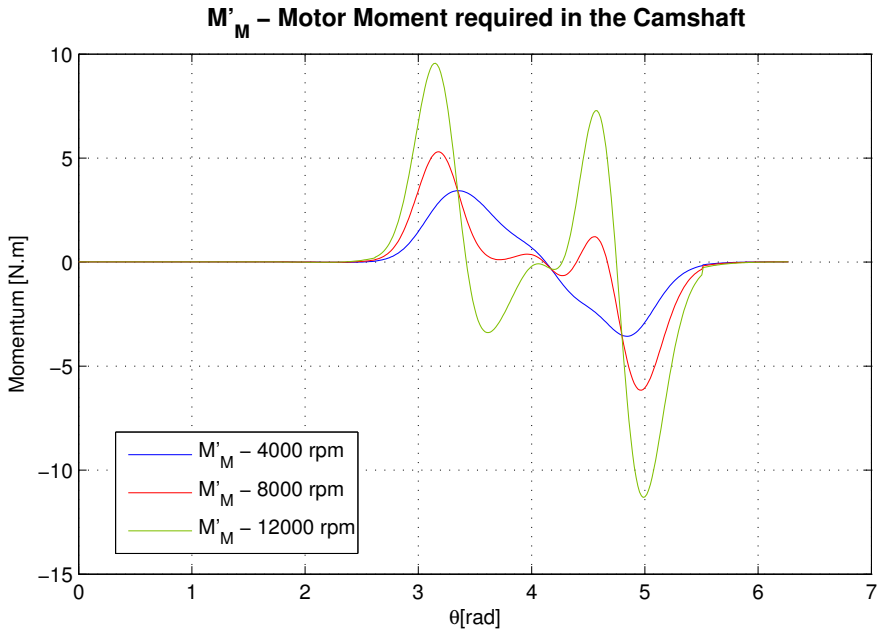

Figure 4.64: M_M profile with variable point of contact (8000 rpm)

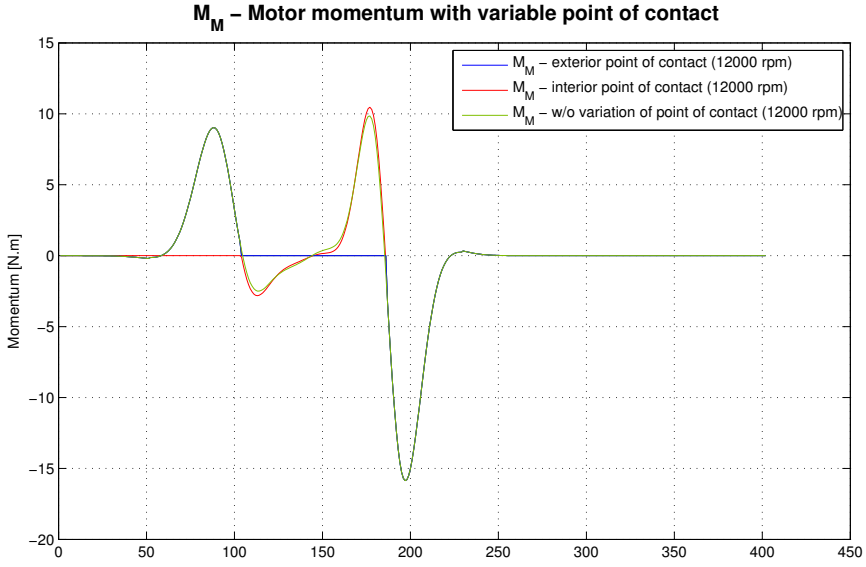

Figure 4.65: M_M profile with variable point of contact (12000 rpm)

Chapter 5

Vibration Analysis

The valve train, because of the functions it performs, is a complex system to analyse from a vibration point of view. The system features rotating bodies, alternate movements and eccentricities during its running time and all of these generate certain responses from the valve train. These vibrations are transmitted to the engine and, consequently, to the chassis. If the vibrations associated with the response of the system are too high, they can put in risk the comfort and security of the rider as well as the durability and reliability of the mechanical components present in a motorcycle.

Therefore, it is extremely important to analyse the system and the response generated by the solicitations applied, as well as the mass/inertia and rigidity properties of the valve train.

In order to analyse the system regarding their vibrational behaviour, we cannot use the same model used so far. The model created and analysed in the previous chapters considers that all components are absolutely rigid. This consideration doesn't allow any response of the system - the system is so rigid that there is no vibrational response. This behaviour is not physically possible since every component has a certain degree of flexibility and therefore generates a vibrational response to outer solicitations. As it was previously done, only the exhaust subsystem will be considered [19] [20] [21].

To properly analyse this valve train in terms of its response to the movements previously determined, it's required to create a new model, one that takes into account the flexibility of the components that make the valve train and, therefore, include a natural vibratory response of the components to the externally applied displacement. Many similar analysis of valve train systems have been conducted, providing some basic information about the correct approach to apply to the InnerCam system (see references [19], [22], [20], [21] and [23]).

The InnerCam can be simplified into a simple mass and springs system, being actuated externally by the camshaft (see figure 5.1). The mass of the new model must be calculated in order to be equivalent to the original system. The first spring of the system has the same rigidity as the equivalent rigidity of the InnerCam components ($k_{eq} = k_1$), except the real spring present in the valve train. That spring corresponds to the second spring in the new model ($k_2 = 25400 \times 2 = 50800 N/m$).

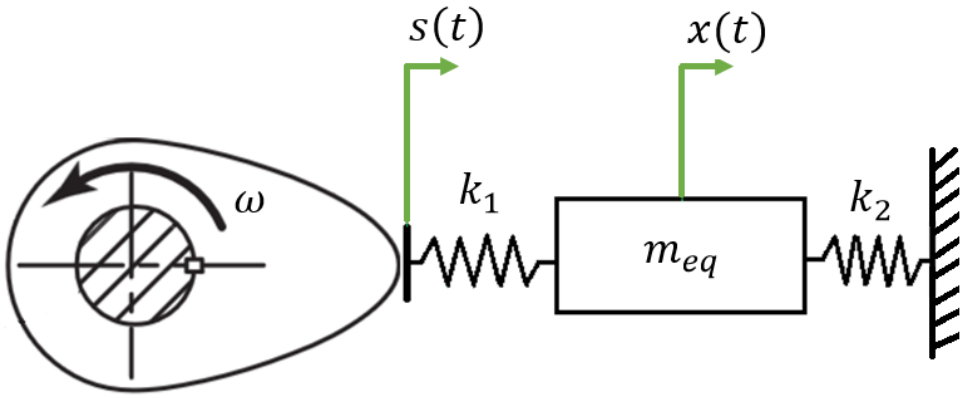

Figure 5.1: New system model created for a vibration analysis

For this new model, we can obtain the following equation of motion, in which $s(t)$ corresponds to the external displacement applied to the system (in this case, the valve lift) and the displacement $x(t)$ corresponds to the natural vibratory response of the valve train (Δ_p corresponds to the pre-deformation of the spring in order to establish the pre-tension of the system):

$$\sum \vec{F} = \dot{\vec{Q}} \Leftrightarrow -k_1(x-s) - k_2(x+\Delta_p) = m_{eq}\ddot{x} \tag{5.1}$$

$$m_{eq}\ddot{x} + (k_2 + k_1)x = k_1 s + k_2 \Delta_p \tag{5.2}$$

Given this equation, it's possible to determine the natural response frequency for the system, by solving the equation of motion 4.34. This equation can be solved with an non-trivial exponential solution ($x(t) = Ce^{st}$) that allows to calculate the natural response frequency [22] [19]:

$$\omega_n = \sqrt{\frac{k_1 + k_2}{m_{eq}}}; \tag{5.3}$$

It is now necessary to determine the equivalent mass and rigidity of the rocker arm and valves of each sub-system. The camshaft is not taken in account since it's the component generating the external displacement ($s(t)$). In order to determine the equivalent mass, one can use the kinetic energy of the original system and equal to the kinetic energy of an equivalent system [22]:

$$T = T_{eq} \tag{5.4}$$

With T being the kinetic energy of the valve train and $T_{eq} = \frac{1}{2} m_{eq} \dot{x}_{eq}^2$ representing the equivalent kinetic energy to be used in the new model. Since the model takes in account the translational movement of the valves and the rigidity of the spring of the valve train, the equivalent velocity is equal the velocity of point B. Equation 5.4 can now be rewritten:

$$\frac{1}{2} m_{valves+springs} \dot{x}_B^2 + \frac{1}{2} m_{G2} \dot{x}_{G2}^2 + \frac{1}{2} J_{rockerarm} \dot{\beta}^2 + \frac{1}{2} m_{roller} \dot{x}_{roller}^2 + \frac{1}{2} J_{roller} \dot{\gamma}^2 = \frac{1}{2} m_{eq} \dot{x}_{eq}; \tag{5.5}$$

It's possible to replace the various velocities (in equation 5.5) by relating them to the velocity in B, using the geometric properties available:

$$\dot{x}_B = \dot{x}_{eq}; \quad \dot{\beta} = \frac{\dot{x}_{eq}}{b}; \quad \dot{x}_{roller} = a\dot{\beta} = \frac{a\dot{x}_{eq}}{b}; \quad \dot{x}_{G2} = \overline{AG_2}\dot{\beta} = \frac{\overline{AG_2}\dot{x}_{eq}}{b} \tag{5.6}$$

Since the influence of the roller has been very low on all the analysis that were previously done, the rotational energy of the roller has been ignored since there is no geometric relation between the rotational speed of the roller and the valve lift, only a numerical one. By undervaluing this energy component, it's possible to simplify the calculation of the equivalent mass. It's now possible to simplify the equation 5.5 in order to determine the equivalent mass:

$$m_{eq} = m_{valve+spring} + m_{G2}\frac{\overline{AG_2}^2}{b^2} + \frac{J_{rockerarm}}{b^2} + m_{roller}\frac{a^2}{b^2} = 0,134062kg \tag{5.7}$$

It's now necessary to determine an equivalent rigidity of the system that can be used in the model. To this end, it's necessary to examine the system and the components that are more susceptible to elastic deformation in its normal operation.

Examining the various free-body diagrams presented in chapter 4, it's possible to identify the rocker arm as the most prone to elastic deformation from all the components of the vibratory model, although all other components are flexible (however, far less flexible than the rocker arms).

This component is submitted to the forces applied in the interface of the valves and the rocker arm (point B in figure 4.6), causing the elastic flexing of those arms. Since the only fixture for this body is located in the roller (point C in figure 4.6) and, in point B, there's only the rotation of this component, it's possible to simplify this component to the trivial case of a beam flexing for the calculus of the equivalent rigidity.

The valve is only supporting compression forces and its rigidity to compression is very high (as is normal for metal components), so it's possible to ignore the valves' contribution to the equivalent rigidity.

In order to determine the rigidity of a flexing beam, it's necessary to firstly determine the deformation caused by a measured force. After that, the rigidity of that beam can be calculated by the following equation (k is the rigidity of the component, F is the magnitude of the force applied and δ is the elastic deformation caused by the applied force):

$$k = \frac{F}{\delta} \tag{5.8}$$

Since the rocker arm actuates 2 valves at the same time, this component must be equated to a set of 2 springs, working in parallel. Each spring rigidity corresponds to the rigidity against the flexing of each arm (that actuates each valve).

We will use the SolidWorks® software to test the elastic deformation of the rocker arm. To that end, each "arm" from the rocker arm was tested by simulating a force of 1 N being applied on the same point as the forces from the spring and valve are usually applied (see figures 5.2 and 5.3). By taking the max deformation values from the simulation software, it was possible to calculate the following rigidities:

- $k_{11} = 1,4053 \times 10^6 N/m$
- $k_{12} = 3,7258 \times 10^6 N/m$

It's possible to further simplify these model springs into a single one. Since they are parallel to each other, the simplified rigidity can be determined by the following equation [19]:

$$k_1 = k_{11} + k_{12} = 5,1311 \times 10^6 N/m \tag{5.9}$$

With the equivalent rigidity and mass calculated, it's possible to determine the value of the natural response frequency of the system, as previously described (see

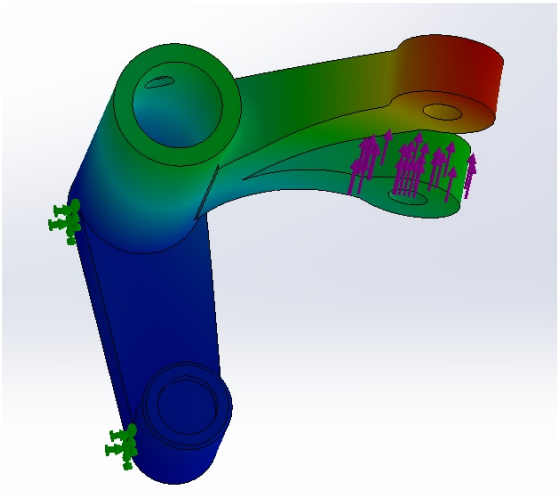

Figure 5.2: Simulation of the deformation of the first "arm" in body 2

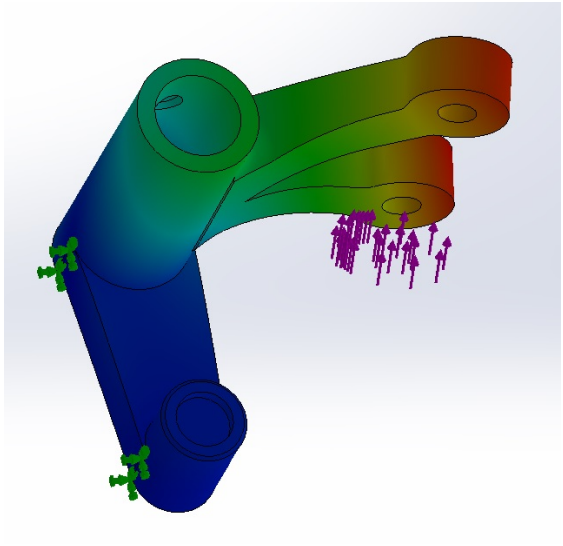

Figure 5.3: Simulation of the deformation of the second "arm" in body 2

eq. 5.3):

$$\omega_n = \sqrt{\frac{k_1 + k_2}{m_{eq}}} = \sqrt{\frac{1,0204 \times 10^6 + 25400}{0,128869}} = 6217,15 rad/s = 59369,5 rpm$$

(on the camshaft)(5.10)

This shows that the sub-systems only resonate at a speed that the engine can't reach, so there are no problems with the current system from a vibrations point of view.

Chapter 6

Conclusions and Future Work

6.1 Conclusions

After completing the dynamic and vibrations analysis, it's possible to reach to some conclusions about the InnerCam system. Firstly, it's important to remind that the models produced and analysed in this document correspond to the perfect functioning of the InnerCam and do not represent the actual operation of the system, since the dynamic equilibriums were made admitting a perfect lift profile. Therefore, these models should be used as a comparison against the actual operation of the system, for a more detailed insight about the best real behaviour that the InnerCam can deliver.

A good example of this disparity between the theoretical and the real operation of the InnerCam is the torque profiles (see figures 4.32 and 4.64) generated by the momentum equilibrium equations (4.34). Although the generated profiles show a variation of the required torque, in the real and normal operation of the engine, the amount of torque given to the valve train is constant and positive. This may alter the dynamic equilibriums of the system, changing the actual force and acceleration profiles for the varied components of the system.

However, there are some important conclusions drawn from this work:

- The InnerCam system is able to generate lift profiles (displacement, velocity and acceleration) similar to the theoretical profiles. It reveals its ability to adequately perform the function of the valve train in the engine,
- The acceleration of the InnerCam components can vary in a significant way, although they maintain the same profile. This variation has a great impact in the calculated force profiles,
- It's possible to observe the rise of influence of the inertia on the forces applied to the valve train. This rising influence reaches a point where the forces are mainly created due to components inertia instead of the elastic force from the springs,
- The profile for the required driving momentum is determined by the force applied in the center of the roller (and extremity of the rocker arm - point C) in the direction of $\overline{CA}$ (see fig. 4.2),
- The influence of the engine acceleration has a negligible effect on the acceleration and force profiles of the InnerCam components. The speed of the engine is the major influence in the dynamic behaviour of the valve train,
- Although the contact between the cam and the roller can vary between the inner and outer cam paths, the dynamic behaviour of the valve train isn't affected. But, since the roller is forced to turn the rolling direction frequently and with high angular accelerations, high wear is expected in both the rollers and the cam,
- The vibration analysis performed on the InnerCam revealed that the natural frequency of the system developed is above the top excitation frequency that the engine can develop (12000 rpm), therefore the system doesn't suffer from resonances on the operating range of the engine,
- The response of the system may influence the sealing of the valves, since it may alter the real lift profile, opposed to the imposed lift to the system,
- The main issue (power loss) afflicting the normal operation of the system (see appendix A) was not explained by the dynamic and vibration analysis

that was performed.

6.2 Future Work

In order to find the reason for the power loss currently happening at around 9000 rpm, the following tasks should be considered as future work:

- A study of the InnerCam system using multi-body dynamics software. It will help validate the results achieved in this work and further understand the dynamic behaviour of the system;
- A dynamic analysis of this system with a constant and given value of driving momentum, in order to observe the profiles generated for this condition instead of admitting a perfect lift profile, as was done in this work;
- Experimental tests to the system in order to compare the real valve train operation with its theoretical and perfect operation (which is described in this work);
- Further studies on the contact between the rocker arm and the valves, in order to fully understand the real response of these components to the varying contact forces that occur.
- Test the balancing of the camshaft. It's an important component on the operation of the InnerCam and, if it's not perfectly balanced, may alter significantly the dynamic behaviour of the entire system;
- Experimental tests on the vibrational response of the system, in order to verify the calculations that were presented in chapter 5;
- Further analyse the thermodynamics of the engine. The main issue afflicting this system may not come from the valve train dynamics but from the combustion cycle.

References

[1] AJP motos S.A. Innercam. **URL:** http://www.ajpmotos.pt/, *Last Accessed:* 16.06.2014, June 2013. http://www.ajpmotos.pt/.

[2] Gordon P. Blair. *Design and simulation of four-stroke engines*. 1999.

[3] N.D. Whitehouse R.S. Benson. *Internal Combustion Engines*. 1979.

[4] Dante Giacosa. *Motori Endotermici*. 1962.

[5] Introduction to the second law of thermodynamics: Heat engines and their efficiency. **URL:** http://cnx.org/content/m42234/latest/?collection=col11406/latest, *Last Accessed:* 15.07.2014, 2012.

[6] V. Arkhangelsky M. Khovakh. *Motor Vehicle Engines*. 1971.

[7] John Lumley. *Engines - An Introduction*. 1999.

[8] Living In The Cebu Forums. Green trail riding in cebu on dual sport motorbike. **URL:** http://www.livingincebuforums.com/ipb/topic/26144-green-trail-riding-in-cebu-on-dual-sport-motorbike/page-51, *Last Accessed:* 07.07.2014.

[9] Nithu Nithish. Mech mecca - internal combustion (ic) engines. **URL:** http://mechmecca.blogspot.pt/2012/06/air-craft-power-producers.html, *Last Accessed:* 10.07.2014, 2012.

[10] Honda. How it works - honda unicam® engines. **URL:** http://powersports.honda.com/experience/articles/090111c0811a9fc2.aspx, *Last Accessed:* 20.06.2014, 2002.

[11] Camshafts: Ohv, sohc, dohc. **URL:** http://users.skynet.be/mercedes-benz/history/SOHC.html, *Last Accessed:* 10.07.2014.

[12] CycleChaos. Honda unicam. **URL:** http://www.cyclechaos.com/wiki/Honda_Unicam, *Last Accessed:* 10.07.2014.

[13] Eric R. Pete C., Steve C. Pent-roof combustion engine. **URL:** http://www.fordscorpio.co.uk/designs.htm, *Last Accessed:* 10.07.2014, 2005.

[14] Seastar Superbikes. Ducati desmodromic (desmo) valve control system - a brief insight. **URL:** http://www.seastarsuperbikes.co.uk/ducatiengines.html, *Last Accessed:* 10.07.2014, 2013.

[15] Spannerhead.com. Technical curiosities: The sleeve valve. **URL:** http://www.spannerhead.com/2012/02/27/technical-curiosities-the-sleeve-valve/, *Last Accessed:* 10.07.2014, 2012.

[16] Dusko Mackoski. A near future where camshafts don't exist and performance is revolutionised! 2001.

[17] Renault. Camless engine, 2008.

[18] Travis Okulski. What it's like to ride in a car with the camless engine of the future. **URL:** http://jalopnik.com/what-its-like-to-ride-in-a-car-with-the-camless-engine-1529865968, *Last Accessed:* 21.06.2014, 2014.

[19] José Dias Rodrigues. *Apontamentos de Vibrações Mecânicas*. 2013.

[20] L. Zhao H. Guo, D. Zhao. Simulation of engina valve train dynamics. 2008.

[21] T. Zhang L. Zhao D. Zhao H. Guo, Q. Wang. Dynamic optimization design of valve train in internal combustion engine. 2008.

[22] Singiresu S. Rao. *Mechanical Vibrations*. 5th edition edition, 2011.

[23] Vasin Paradorn. An impact model for the industrial cam-follower system: simulation and experiment. Master's thesis, 2007.

Appendix A

Benchmarking testes

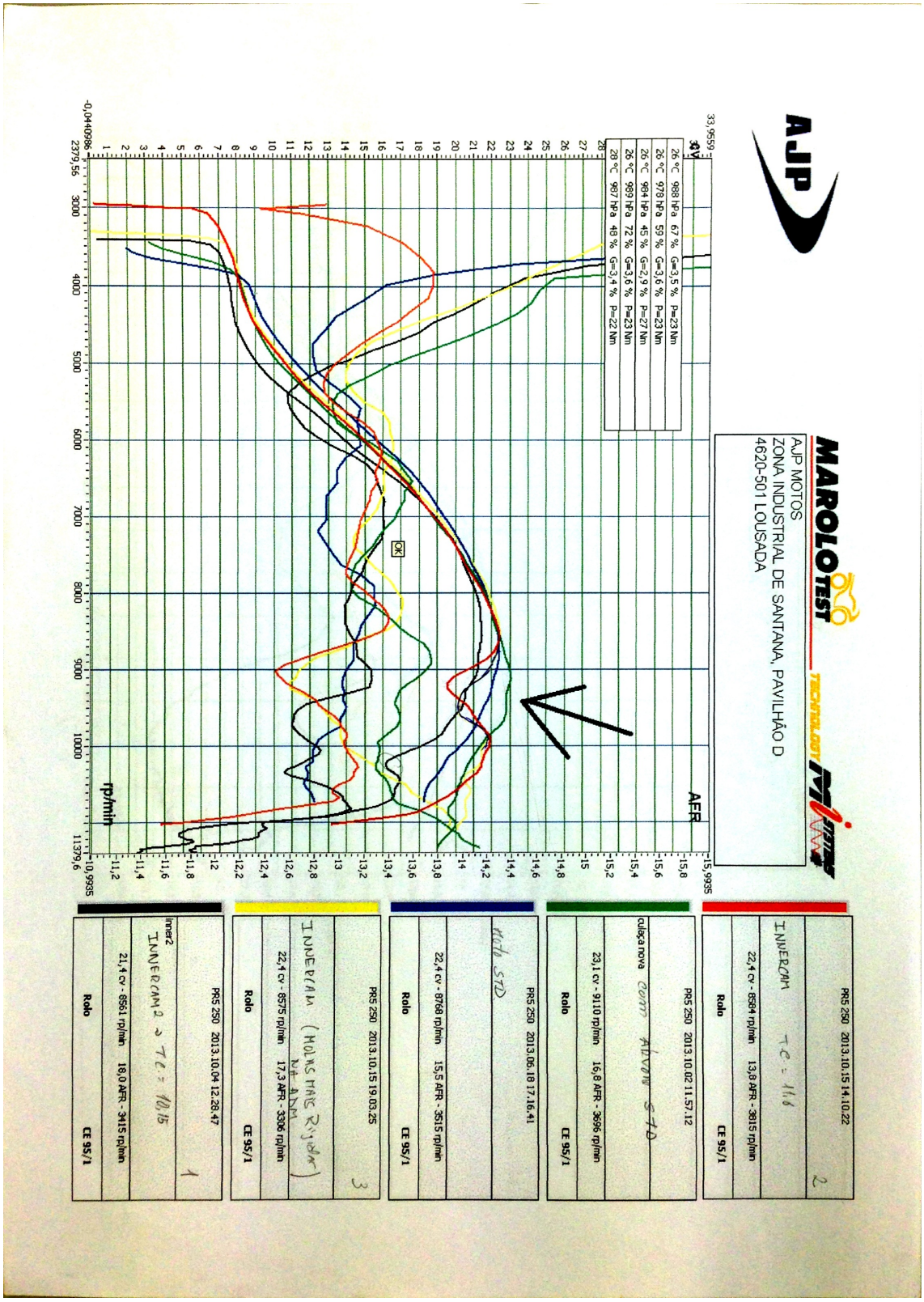
AJP
MAROLO TEST
TECHNOLOGY
AJP MOTOS
ZONA INDUSTRIAL DE SANTANA, PAVILHÃO D
4620-501 LOUSADA
AFR
rpm/min
OK
INNERCAM
Rolo
CE 95/1
PR5 250 2013.10.15 14.10.22
22,4 cv - 8584 rpm/min 13,8 AFR - 3815 rpm/min
PR5 250 2013.10.02 11.57.12
culça nova
23,1 cv - 9110 rpm/min 16,8 AFR - 3696 rpm/min
PR5 250 2013.06.18 17.16.41
22,4 cv - 8768 rpm/min 15,5 AFR - 3515 rpm/min
PR5 250 2013.10.15 19.03.25
INNERCAM (MOLAS MAIS RIJAM)
22,4 cv - 8575 rpm/min 17,3 AFR - 3306 rpm/min
PR5 250 2013.10.04 12.28.47
Inner2
21,4 cv - 8561 rpm/min 18,0 AFR - 3415 rpm/min

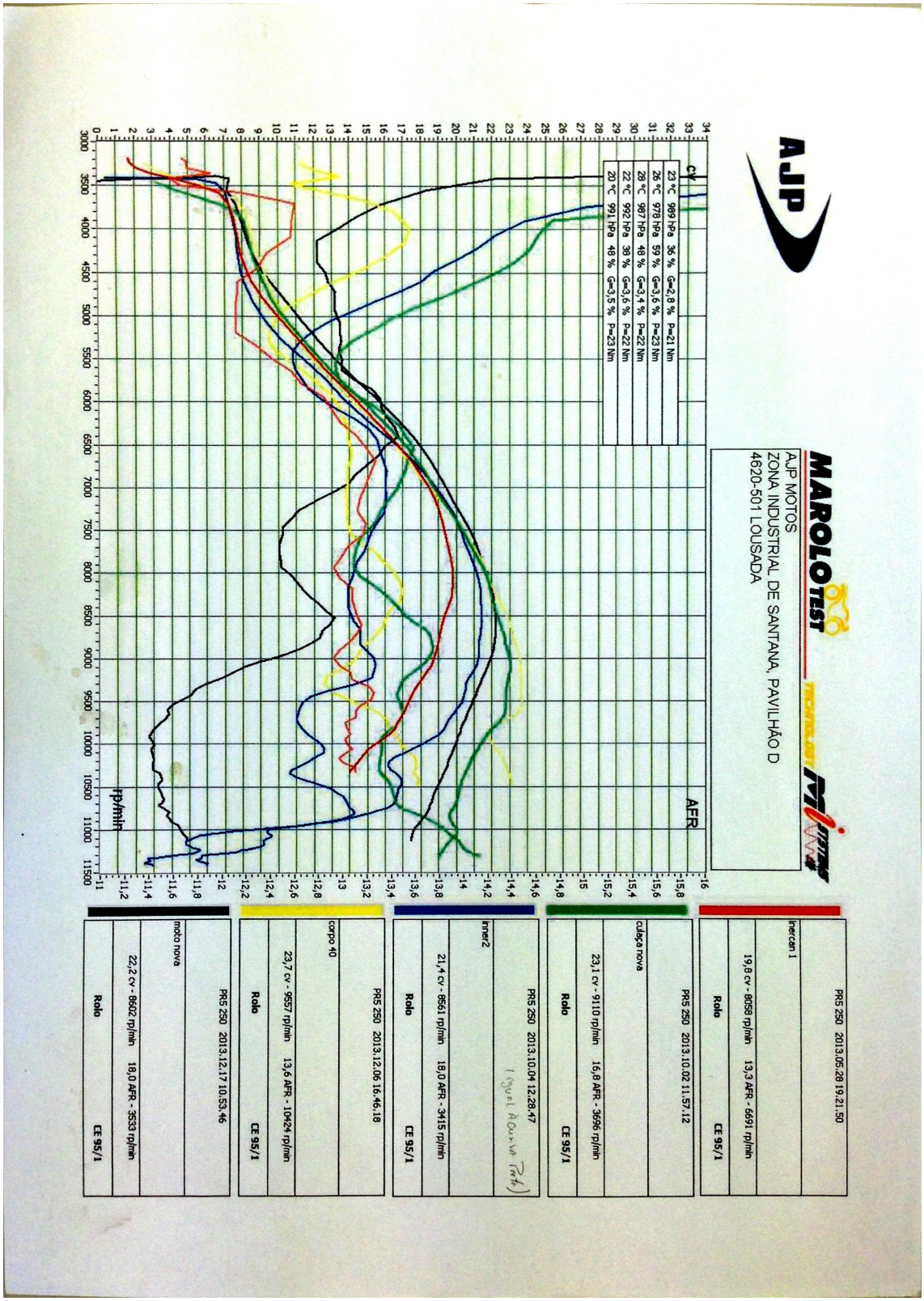
AJP
MAROLO TEST
AJP MOTOS
ZONA INDUSTRIAL DE SANTANA, PAVILHÃO D
4620-501 LOUSADA
CV
AFR
rpm/min
23 °C 989 hPa 36 % G=2,8 % P=21 Nm
26 °C 978 hPa 59 % G=3,6 % P=23 Nm
28 °C 987 hPa 48 % G=3,4 % P=22 Nm
22 °C 992 hPa 38 % G=3,6 % P=22 Nm
20 °C 991 hPa 48 % G=3,5 % P=23 Nm
PR5 250 2013.05.28 19.21.50
linercan 1
19,8 cv - 8058 rpl/min 13,3 AFR - 6691 rpl/min
Rolo CE 95/1
PR5 250 2013.10.02 11.57.12
culaça nova
23,1 cv - 9110 rpl/min 15,8 AFR - 3696 rpl/min
Rolo CE 95/1
PR5 250 2013.10.04 12.28.47
inner2
21,4 cv - 8561 rpl/min 18,0 AFR - 3415 rpl/min
Rolo CE 95/1
PR5 250 2013.12.06 16.46.18
corpo 40
23,7 cv - 9557 rpl/min 13,6 AFR - 10424 rpl/min
Rolo CE 95/1
PR5 250 2013.12.17 10.53.46
moto nova
22,2 cv - 8602 rpl/min 18,0 AFR - 3533 rpl/min
Rolo CE 95/1

Appendix B

Steel's technical sheet

RAMADA
F. RAMADA, AÇOS E INDÚSTRIAS, S.A.

FICHA TÉCNICA DO AÇO

Marca: FR3

Cor: Laranja

Designação: Aço de construção Ligado

Cópia Não Controlada

1 ⇒ QUALIDADE E NORMAS EQUIVALENTES

Num. Do Material	EURONORM	AISI	DIN	AFNOR
1.6582	34 CrNiMo 6	4337	34 CrNiMo 6	35NCD6

2 ⇒ ESTADO DE FORNECIMENTO:

Temperado e Revenido

3 ⇒ CARACTERÍSTICAS MECÂNICAS:

	Rm (MPa)	Rp0,2 (MPa)	% A (l_0=5d_0)
Máximo	1400	-	-
Mínimo	700	490	9

4 ⇒ COMPOSIÇÃO QUÍMICA

Elemento Químico (%)	C	Si	Mn	Cr	Mo	Ni	P	S
Máximo	0,38	0,40	0,80	1,70	0,30	1,70	0,035	0,035
Mínimo	0,30	-	0,50	1,30	0,15	1,30	-	-

5 ⇒ CERTIFICADOS AÇOS (segundo a norma EN 10204:2004)

2.1- Certificado de conformidade	⊙
2.2- Relatório de ensaio	⊙
3.1- Certificado de inspecção (+)	⊙

(+) Em casos especiais quando previamente acordado

Appendix C

Thermal treatment applied to InnerCam components

RAMADA
F. RAMADA, AÇOS E INDÚSTRIAS, S.A.

TRATAMENTO TÉRMICOS

Relatório de Ensaio Não Específico 2.2 NP EN10204

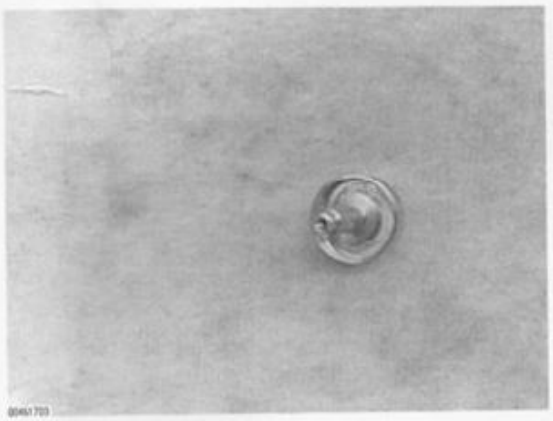

Folha Técnica Nº 00461703

Data de Emissão 2013-05-02 07:40:12

Nº da Requisição S/R

Data Entrada 2013-04-30 14:55:27

Cliente A.J.P. MOTOS, SA

Morada LOUSADA LOUSADA

Aço FR 3

Tratamento NIT.B.P. - ALLNIT ®

Nº Peças	Peso	Referência	Descrição
1	0.34		PEÇA
	0.34		

	Tipo de Dureza	Dureza Min	Dureza Max	Camadas Min	Camadas Max
Valores Pedidos	HV	650.0	900.0	0.10	0.20
Valores Obtidos	HV	717.0	789.0	0.11	0.13

Derrogações Nºs :

Observações:

VALIDADO POR:
Trat. Térmicos - Eng. Paulo Dias

D310.01/03 - Processado e impresso por computador e é válido sem assinatura

1

Sede: OVAR - PORTUGAL
Dique do Poste - Apartado 10
3884-084 OVAR
Tel.: 256 580 400
Fax: 256 580 409 - 256 580 419

LISBOA
Vila Amélia, Lote 268
Cabanas
2650-605 Queluz de Baixo
Tel.: 21 358 89 00 (RGSI)
Fax: 21 435 00 15 / 17

PORTO
Zona Industrial da Maia I SECTOR VII
Trav. Eng. Nobre de Costa, Nº 75
4475-125 MOREIRA MAIA
Tel.: 22 943 03 03
Fax: 22 943 03 04

ÁGUEDA
Lugar do Brejo
3750-711 RECARDÃES
ÁGUEDA
Tel.: 234 600 030
Fax: 234 600 039

MARINHA GRANDE
Estrada Pero Neto
2430-902 MARINHA GRANDE
Tel.: 244 575 680
Fax: 244 575 689

BRAGA
Av.ª Eng.º José Rolo, Lote F1
Parque Industrial de Celeirós
4705-414 CELEIRÓS BRG
Tel.: 253 605 350
Fax: 253 605 352

E-mail: ave.ave@ramada.pt www.ramada.pt Registo na Conservatória de Ovar Nº 101 - Contribuinte Nº PT 500 103 844 - Capital 15.000.000 Euros